University of Liège
Faculty of Applied Sciences
Department of Electrical Engineering
and Computer Science

See, Balance, Exchange

Building an Operational Toolkit for Active Distribution Networks under High DER Penetration

Maurizio Vassallo

Supervisor
Prof. Damien Ernst

This dissertation has been submitted in partial fulfillment of the requirements for the Degree of Doctor of Engineering Sciences.

Jury Members

Prof. Wehenkel Louis	President	University of Liège
Dr. Bahmanyar Alireza	Member	Haulogy
Prof. Capitanescu Florin	Member	Luxembourg Institute of Science and Technology
Prof. Ernst Damien	Member	University of Liège
Dr. Fonteneau Raphaël	Member	University of Liège
Dr. Vandeburie Julien	Member	Resa
Prof. Vergara Pedro P.	Member	Delft University of Technology

Abstract

The energy transition faces a bottleneck at the distribution level, where the rapid integration of distributed energy resources (DERs), such as solar photovoltaics (PVs), electric vehicles (EVs), and heat pumps (HPs), outpaces the capabilities of current distribution networks. Low-voltage (LV) grids, historically designed as passive infrastructure, are now subjected to stress that exceeds their original design. Consequently, distribution system operators (DSOs) must evolve into active managers, requiring new tools to operate the network efficiently. This operational shift is also accelerated by rising regulatory pressure requiring coordination between DSOs and transmission system operators (TSOs) in managing the power systems as whole.

This thesis proposes an operational toolkit built on three core capabilities: seeing the network, balancing its existing capacity, and exchanging access to it. This toolkit view is complemented by a multidimensional analysis of the TSO-DSO coordination literature, which examines why methods of this kind rarely progress to commercial deployment.

First, network observability (**see**) is addressed through a topological path identification (TPI) methodology. Using an integer linear programming (ILP) formulation, this approach assigns a physically feasible path to 88% of customers from incomplete, static geographical data without reliance on advanced metering infrastructure (AMI). When validated on a real-world LV network, the algorithm demonstrated robustness, achieving a fault detection rate exceeding 95% under the tested corruption model.

Second, a phase reconfiguration (**balance**) algorithm is developed. By shifting away from non-linear power-flow models to a linear optimization based on long-term load curves, this method balances the network without the need for physical grid reinforcement. When applied to the topology of a real Belgian network under a synthetic high-DER scenario, the approach successfully reduced load unbalance by 36% and 62% across the two test feeders and decreased total line losses by 4.4%.

Third, a continuous market mechanism (**exchange**) for dynamic operating envelopes (DOEs) is introduced. This framework allows network participants to trade physical network access while guaranteeing operational security under DC power flow assumptions. Results indicate that this limit-exchange mechanism shows the potential to reduce renewable curtailment, incentivize the use of local flexibility, and extract additional value from existing infrastructure without requiring centralized control.

Finally, the thesis evaluates the broader operational landscape through a multidimensional analysis of TSO-DSO coordination. By comparing theoretical literature against real-world pilot projects across five dimensions (modeling, operation, validation, communication, and regulation), this research suggests the gaps blocking commercial deployment are not algorithmic complexity but rather communication infrastructure, validation at scale, and regulatory alignment.

Acknowledgements

I would like to express my gratitude to my co-authors, whose expertise, dedication, and collaboration were essential to the completion of this research.

First, I extend my thanks to my supervisor, Prof. Damien Ernst, for his dedication, guidance, and the time he has invested in me since my master's thesis through the completion of this PhD.

I am honored that Prof. Louis Wehenkel has agreed to preside over this defense. I would also like to thank the members of the jury, Dr. Alireza Bahmanyar, Prof. Florin Capitanescu, Dr. Raphaël Fonteneau, Dr. Julien Vandeburie, and Prof. Pedro P. Vergara, for taking the time to evaluate this work and for their constructive feedback.

It has been a pleasure to collaborate with my colleagues and co-authors at the University of Liège. I extend my thanks to Amina, Adrien, Raphaël, and Anthony for all their work. I also want to acknowledge the collaboration that enriched this research, including Alireza Zabihi, David, Dong, Sania and Sofía.

This research also greatly benefited from the insights and support of our industry partners. My first thanks go to RESA, specifically Simon Gérard, Julien Vandeburie, Thomas Wehenkel, Willy Legros, Christian De Laet, and Luc Warichet, for their practical insights and collaboration. I am also grateful to RTE and Geredis, and in particular to Julien Callec and Dorian Fourniret, for their valuable contributions. Finally, I would like to express my sincere gratitude to the team at Haulogy, in particular Alireza Bahmanyar, Adrien Leerschool, and Laurine Duchesne.

Finally, I would like to thank my family and friends for their endless support, encouragement, and love throughout this journey. This path would not have been the same without you.

Contents

Abstract v

Acknowledgements vii

List of Figures xiii

List of Tables xv

Glossary xvii

1 Introduction 1
- 1.1 Context and motivation . . . 1
- 1.2 From passive to active . . . 2
- 1.3 DSO challenges . . . 3
- 1.4 Research questions . . . 4
- 1.5 Contributions & Outline . . . 5
- 1.6 List of publications . . . 6

2 An Optimization Algorithm for Customer Topological Paths Identification in Electrical Distribution Networks 9
- 2.1 Introduction . . . 9
  - 2.1.1 Literature review . . . 10
  - 2.1.2 Chapter contribution . . . 11
  - 2.1.3 Chapter organization . . . 11
- 2.2 Power distribution modeling . . . 12
  - 2.2.1 Network topological functions . . . 13
- 2.3 Topological paths . . . 13
  - 2.3.1 Paths . . . 14
  - 2.3.2 Hypothetical paths . . . 14
  - 2.3.3 Real paths . . . 14
  - 2.3.4 Estimated paths . . . 14

2.3.5 Paths visualization 15
2.4 Problem statement 16
2.5 Methodology 17
2.5.1 Raw information listing 17
2.5.2 Transformation functions definition 18
2.5.3 Well-defined information 18
2.5.4 Hypothetical paths generation 18
2.5.5 Topological paths estimation 19
2.5.6 Diagnostic function 23
2.5.7 Solution of the TPI problem 23
2.6 Academic example 23
2.6.1 Raw information 24
2.6.2 Transformation functions 24
2.6.3 Well-defined information 24
2.6.4 Hypothetical paths compatible with the well-defined information 25
2.6.5 Results paths estimation 27
2.6.6 Results explanation 27
2.6.7 Example evaluation 31
2.6.8 Diagnostic function 31
2.7 Belgian network 31
2.7.1 Hypothetical paths compatible with the well-defined information 32
2.7.2 Matrix generation 32
2.7.3 Optimization problem results 32
2.7.4 Diagnostic function 33
2.7.5 Parameterization and computational scalability 33
2.7.6 Robustness analysis 35
2.8 Conclusion 37

3 Phase Reconfiguration for Power Distribution Networks with High DERs Penetration 39
3.1 Introduction 39
3.2 Mathematical formalization 41
3.2.1 Network graph 41
3.2.2 Network phases 42
3.2.3 Network feeders 42
3.2.4 Phase matrices 42
3.2.5 Customer power dynamics 44
3.3 Problem statement 45
3.3.1 Objective terms 45

3.3.2 Scaling factors . . . 46
3.3.3 Constraints . . . 47
3.4 Conceptual example . . . 47
3.4.1 Network setup . . . 47
3.4.2 Optimization process . . . 48
3.5 Case study results . . . 49
3.5.1 Cost-benefit analysis . . . 54
3.6 Conclusion . . . 55
3.A TS and phase assignment . . . 56

4 SecuLEx: a Secure Limit Exchange Market for Dynamic Operating Envelopes 59
4.1 Introduction . . . 59
4.2 Grid operation with envelopes . . . 61
4.2.1 Network representation . . . 61
4.2.2 DOEs definition . . . 62
4.2.3 Security verification function . . . 62
4.2.4 DOEs allocation . . . 63
4.3 SecuLEx market organization . . . 63
4.3.1 Limit market temporal operation . . . 63
4.3.2 Orders and order book . . . 64
4.3.3 Clearing function . . . 65
4.3.4 Settlement function . . . 65
4.4 Concrete implementation of SecuLEx . . . 66
4.4.1 Grid operation implementation . . . 66
4.4.2 SecuLEx market implementation . . . 68
4.4.3 Illustrative example . . . 69
4.5 Discussion . . . 74
4.5.1 Technical and computational challenges . . . 74
4.5.2 Economic and market design implications . . . 75
4.6 Conclusion . . . 76
4.A Security function proof . . . 77

5 A Multidimensional Analysis of Existing Limitations for TSO-DSO Coordination 81
5.1 Introduction . . . 81
5.2 Assessment of coordination limitations across five dimensions . 82
5.2.1 Modeling . . . 84
5.2.2 Operation . . . 84
5.2.3 Validation . . . 84
5.2.4 Communication . . . 85

5.2.5 Regulation 85
5.2.6 Summary of research gaps 85
5.3 Pilots & non-pilots results 86
5.4 From Pilot to deployment 87
5.5 Discussion 88
5.6 Conclusion 89
5.A Analysis methodology 90
5.A.1 Literature search and selection process 90
5.A.2 Multidimensional scoring methodology 91

6 Conclusion **95**
6.1 Summary of the contributions 95
6.2 Toolkit limitations 97
6.3 Future directions 97
6.3.1 Toolkit integration and the integrated case study . . . 97
6.3.2 Robustness and uncertainty management 99
6.3.3 Realism and large scale validation 99
6.3.4 Systemic and regulatory barriers 99

Bibliography **101**

List of Figures

1.1 DSO squeezed between DERs and TSO 5

2.1 Visualization of the different sets of paths. 15
2.2 Representation of the different sets and their relationships. . . 16
2.3 TPI flowchart 17
2.4 Illustration of the process of identifying customer paths in the academic network considered. 26
2.5 Part of the digital model of the real network considered. . . . 34
2.6 Sensitivity analysis of the TPI framework 37

3.1 Phase configurations before and after rebalancing 48
3.2 Feeder load distribution and unbalances before optimization. . 50
3.3 Feeder load distribution and unbalances after optimization. . . 51
3.4 Load distribution and unbalances across feeders. 52
3.5 Voltage curves of the phases across feeders. 53
3.6 Flowchart of data availability and assumption processes. . . . 57
3.7 Phase configuration assignment methodology. 58

4.1 Timeline illustrating the sequence from the initial DOE assignment by the DSO 64
4.2 Baseline situation where the reverse power flow exceeds the transformer limit. 70

5.1 Average normalized scores across the five dimensions for pilot and non-pilot studies. 86
5.2 PRISMA diagram of the paper selection process. 91

6.1 Data flow between the three capabilities in the target pipeline. 98

List of Tables

1.1 Future DSO challenges 4

2.1 Algorithm performance, hyperparameters, and execution statistics for the Belgian network 35

3.1 Comparison of the proposed method and literature. 41
3.2 Description of the LV distribution network. 49
3.3 Voltage and line losses comparison before and after the optimization. 54
3.4 Cost-benefit analysis of phase reconfiguration. 54
3.5 Installation sizes and requirements for technology installations 56

4.1 Initial order book. 73
4.2 Updated order book. 73
4.3 Comparison of management approaches. 74

5.1 Papers multidimensional scoring. 83
5.2 Summary of reviewed papers categorized by publication type . 92

Glossary

AC Alternating current
AI Artificial intelligence
AMI Advanced metering infrastructure
ANM Active network management

CapEx Capital expenditure
CI Confidence interval

DC Direct current
DER Distributed energy resource
DOE Dynamic operating envelope
DOY Day of year
DSO Distribution system operator

ES Energy storage
EV Electric vehicle

GDP Gross domestic product
GHG Greenhouse gases
GIS Geographic information system
GPS Global positioning system

HC Hosting capacity
HP Heat pump

ICT Information communication technology
ILP Integer linear programming
IoT Internet of things

LEM Local energy market
LV Low voltage

MILP Mixed-integer linear programming
MIQP Mixed-integer quadratic programming
MV Medium voltage

OpEx Operating expenses

p.u. Per unit
P2P Peer-to-peer
PSD Phase switch device
PV Solar photovoltaic

RQ Research question
RTE Réseau de Transport d'Électricité

SM Smart meter
SOP Soft open point

TPI Topological path identification
TS Time series
TSO Transmission system operator

WT Wind turbine

Chapter 1

Introduction

This chapter establishes the context of the energy transition that motivates this research. It outlines the resulting operational challenges facing modern distribution networks, states the research questions, summarizes the thesis contributions, and provides an outline of the manuscript and the associated publications.

1.1 Context and motivation

Energy is essential to modern society, and its supply directly influences economic development. While the economic impacts vary by country, the role of electricity consumption and the link to gross domestic product (GDP) are documented in the literature [1]. The traditional energy sources, such as oil, coal, and natural gas, are often located far from the regions that consume them. Relying on them for economic growth therefore implied a dependence on external suppliers. Reducing this dependence by substituting imported fuels with generated renewable electricity has, in recent years, become an explicit policy objective in Europe [2].

A second, and increasingly dominant, concern is climate change. There is broad scientific consensus that rising concentrations of greenhouse gases (GHG), which trap heat in the atmosphere, are driving significant warming of the atmosphere and oceans. Under the 2015 Paris Agreement, most nations committed to holding the increase in global average temperature to well below 2 °C above pre-industrial levels, while pursuing efforts to limit it to 1.5 °C [3]. Consistent with this goal, the European Union and many national governments have since pledged to reach net-zero emissions by 2050 [4] [1].

Achieving these targets requires displacing fossil-fuelled generation with low-carbon sources and electrifying sectors such as transport and heating. While a portion of this new renewable generation is supplied by large, transmission-connected wind and solar plants, distributed energy resources (DERs) are increasingly being connected at the distribution level. Solar photovoltaics (PV), electric vehicles (EVs) and heat pumps (HPs) are installed at the low-voltage (LV) network, behind the customer meter.

Therefore, the LV distribution networks are the point where the energy transition physically concentrates its stress. Distribution grids are expected to accommodate around 70% of new renewable generation in Europe by 2030 [5]. This localized stress is made worse by a temporal mismatch between power generation and demand. Rooftop PVs peak around midday when local consumption is at its lowest, whereas EVs charging typically coincides with evening demand peaks. HPs introduce additional unpredictability, as their power draw is dictated by external temperatures.

The result is that LV feeders are seeing large, rapid power variations that were never part of their original design.

1.2 From passive to active distribution networks

Distribution grids were dimensioned under the *fit-and-forget* paradigm, meaning that they were oversized for a worst-case, unidirectional demand and then operated without real-time monitoring or active control. This held as long as demand was predictable and no generation existed at the LV level. Cables and transformers were selected with sufficient margin to accommodate demand peaks, on the assumption that power would always flow downward from the substation to the load.

High DER penetration breaks both assumptions at once, since it introduces uncertainty into demand and drives reverse power flow. The consequences are already visible in several European countries as voltage excursions beyond limits, thermal congestion of lines and transformers, and, increasingly, the rejection of new connection requests. Reinforcing the grid by replacing cables and transformers provides additional margin, but the rate

[1] Net-zero is a condition in which every quantity of GHG emitted is balanced by an equivalent amount removed.

at which DERs are being deployed outpaces the typical times for network reinforcements, which can take several years. Beyond speed, the utilization of new infrastructures may remain low outside of the specific stress periods that triggered the investment, resulting in highly inefficient capital allocation.

This growth makes the passive view unsustainable and pushes the DSO toward more active management of its networks. This is the principle of active network management (ANM): addressing congestion and voltage issues with decision-making policies, generally through dynamic control of network assets or connected resources [6].

1.3 Challenges for the distribution system operator

The distribution system operator (DSO) faces a set of challenges ([7]), which can be grouped into technical, operational, and economic spheres, as summarized in Table 1.1.

From a technical perspective, the bidirectional power flows generated by DERs complicate traditional protection schemes and aggravate local power-quality problems such as voltage fluctuations. As the grid becomes more digitalised, DSOs also face increasing cybersecurity exposure, which calls for specific defensive measures.

Operationally, while DSOs are expected to act as active operators to coordinate these distributed assets, they remain severely constrained by limited visibility within LV feeders. Incomplete topological records, missing or uncertain network parameters, and the absence of interoperable data standards mean that a DSO attempting to run an optimization over its own network may lack the basic inputs that optimization requires.

Finally, the proliferation of DERs raises economic and social questions. Decentralised generation reshapes consumption profiles and changes traditional utility revenue structures, prompting a shift towards new business models. Moreover, when physical limits are reached, the DSO must decide how to allocate grid resources among customers, making fairness and equity an explicit design concern.

At the same time, pressure is mounting from the higher-voltage direction. Recent European regulation calls for closer coordination between the DSO and the transmission system operator (TSO) in operating the system as a whole [8]. This coordination is technically and organisationally non-trivial as the two operators have historically operated on different timescales, with different tools, and with little formal interface. The DSO is thus squeezed

Table 1.1: Future DSOs challenges associated with high penetration of DERs.

Category	Challenges
Technical	Grid stability & power quality
	Integration of advanced ES technologies
	AI-driven operational optimization
	Coordination with TSOs
	Protection coordination
	Cybersecurity risks
Operational & management	Data management & visibility
	Regulatory frameworks
	Operational flexibility & resilience
	DER aggregation & coordination responsibilities
Economic & social	Revenue models & cost recovery
	Fairness & equity in network planning

from two directions simultaneously, as illustrated in Fig. 1.1: from below by DERs reshaping the LV networks, and from above by a growing responsibility to provide services to a transmission system from which it has been insulated.

1.4 Research questions

This work focuses on three operational capabilities, selected to act as the primary building blocks for an active management toolkit. Before any decision can be taken, the operator must know the network it operates (**see**). Given that knowledge, the DSO has to optimize the network, while there may be many possible solutions, the cheapest corrective option is by making better use of existing physical assets (**balance**). However, because capacity optimization cannot entirely absorb the uncertainties of generation and demand introduced by DERs, even a rebalanced network will inevitably experience periods of congestion requiring curtailment. To manage these operational limits, the remaining network capacity must be dynamically allocated among users through a coordinated market framework (**exchange**).

Therefore, this thesis is motivated by the necessity to equip DSOs with an operational toolkit for actively managing high DER penetration. It addresses four research questions (RQs). The first three formalize the *see*, *balance*, and *exchange* capabilities introduced above. The fourth RQ steps back from these specific capabilities: it asks what stands between DSO tools and real-world TSO-DSO coordination at scale.

RQ1 To what extent can customer topological paths in LV networks be identified using incomplete static records without relying on advanced me-

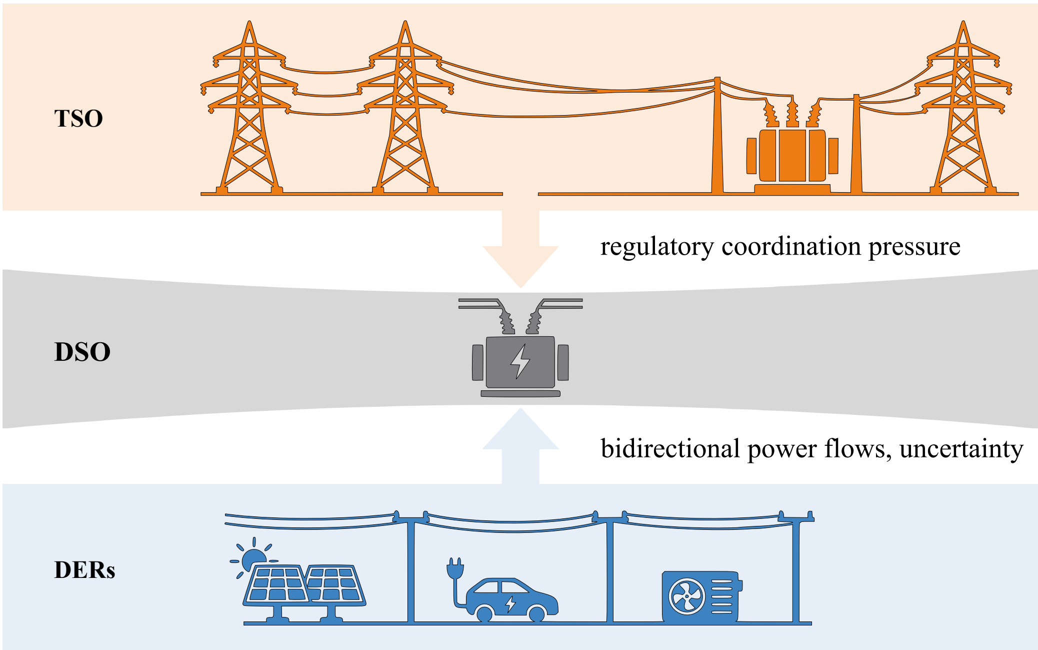

Figure 1.1: The evolving landscape of the distribution network. The DSO is squeezed from two directions: managing bidirectional power flows and load uncertainty from high penetrations of DERs at the LV level, while facing increasing regulatory pressure to coordinate with the upstream TSO.

tering infrastructure (AMI)?

RQ2 How can the customer phase reconfiguration problem be formulated and solved to minimize network unbalance over long temporal horizons without relying on heavy power flow calculations?

RQ3 How can dynamic operating envelopes (DOEs) be translated into tradeable capacity products within a local flexibility market while preserving network security?

RQ4 What are the primary limitations preventing the transition of theoretical TSO-DSO coordination schemes to commercial deployment?

1.5 Contributions and Manuscript Outline

The thesis makes four main contributions, which together trace a path from knowing the network to coordinating its operation. The remainder of this manuscript is organized to reflect this progression:

Chapter 2 addresses the **see** capability (RQ1) through a novel topological path identification (TPI) methodology. By developing an integer linear programming (ILP) formulation, this systematic procedure reconstructs customer connectivity using only incomplete, static records, overcoming the operational blindness of LV networks without relying on advanced metering infrastructure (AMI).

Chapter 3 builds on the established connectivity to address the **balance** capability (RQ2). It formulates customer phase reconfiguration as a linear optimization over long-term load curves, considering phase unbalance, the number of physical reconfigurations required, and the position of each customer along the feeder.

Chapter 4 addresses the **exchange** capability (RQ3), introducing a continuous market mechanism for DOEs. Moving beyond non-transferable capacity limits, this framework enables network participants to trade physical network access while mathematically guaranteeing real-time operational security under the DC approximation.

Chapter 5 steps back from these DSO-level capabilities to contextualize the operational toolkit (RQ4). Through a multidimensional analysis, it evaluates the transition from theoretical transmission and distribution coordination to commercial deployment, suggesting that the primary barriers to large-scale implementation may lie in validation, communication, and regulatory alignment.

Chapter 6 concludes the thesis. It summarizes the findings, reflects on what the toolkit developed in Chapters 2–4 achieves and where its limits lie in light of Chapter 5, and outlines directions for future research.

1.6 List of publications

Publications on which this thesis is based:

[9] **Vassallo, Maurizio**; Benzerga, Amina; Bahmanyar, Alireza; Leerschool, Adrien; Duchesne, Laurine; Gerard, Simon; Vandeburie, Julien; Ernst, Damien; *Phase Reconfiguration for Power Distribution Networks with High DERs Penetration*, IEEE Kiel PowerTech, 2025.
Chapter 3 is based on this paper.

[10] **Vassallo, Maurizio***[2]; Leerschool, Adrien*; Bahmanyar, Alireza; Duchesne, Laurine; Gerard, Simon; Wehenkel, Thomas; Ernst, Damien; *An optimization algorithm for customer topological paths identification in*

[2] Asterisk (*) indicates that authors contributed equally

electrical distribution networks, IET Smart Grids, 2026.
Chapter 2 is based on this paper.

[11] **Vassallo, Maurizio***; Bolland, Adrien*; Bahmanyar, Alireza; Wehenkel, Louis; Duchesne, Laurine; Liu, Dong; Khaskheli, Sania; Thuc, Alexis Ha; Vergara, Pedro P.; Anvari-Moghaddam, Amjad; *SecuLEx: a Secure Limit Exchange Market for Dynamic Operating Envelopes*, Electric Power Systems Research, 2027.
Chapter 4 is based on this paper.

[12] **Vassallo, Maurizio**; Bolland, Adrien; Bahmanyar, Alireza; Fonteneau, Raphaël; Maio, Anthony; Callec, Julien; Fourniret, Dorian; Ernst, Damien. *A Multidimensional Analysis of Existing Limitations for TSO-DSO Coordination.* (Preprint, 2026)
Chapter 5 is based on this paper.

Other publications completed during the PhD that are not part of this manuscript:

[13] **Vassallo, Maurizio**; Benzerga, Amina; Bahmanyar, Alireza; Ernst, Damien; *Fair reinforcement learning algorithm for PV active control in LV distribution networks*, International Conference on Clean Electrical Power (ICCEP), 2023.

[14] **Vassallo, Maurizio**; Bahmanyar, Alireza; Duchesne, Laurine; Leerschool, Adrien; Gerard, Simon; Wehenkel, Thomas; Ernst, Damien; *A systematic procedure for topological path identification with raw data transformation in electrical distribution networks*, 7th International Conference on Energy, Electrical and Power Engineering (CEEPE), 2024.

[15] Benzerga, Amina; **Vassallo, Maurizio**; Gérard, Simon; Vandeburie, Julien; Ernst, Damien; *Combined PV-EV-HP Hosting Capacity Analysis of a Belgian Low-Voltage Distribution Network*, IEEE 34th Australasian Universities Power Engineering Conference (AUPEC), 2024.

[16] Herrero Gómez-Tejedor Yaqin, Sofía; **Vassallo, Maurizio**; & Ernst, Damien; *OffWindFM: A Conceptual Roadmap for Foundation Models in Offshore Wind Energy.* (Preprint, 2026)

[17] Bolland, Adrien; Maio, Anthony; Richard, Thomas; **Vassallo, Maurizio**; Bahmanyar, Alireza; Fonteneau, Raphaël; Callec, Julien; Fourniret, Dorian; Ernst, Damien; *Coordinating Secure and Distributed Operation of Electrical Networks Through Bilateral Agreements on Voltage and Power Envelopes.* (Preprint, 2026)

[18] Zabihi, Alireza; **Vassallo, Maurizio**; Ernst, Damien; Badesa, Luis; Hernandez, Araceli; *Fair Allocation of Operating Envelopes for Distribution Networks Considering Voltage Unbalance.* (Preprint, 2026)

[19] Milambo Kasumba, David, **Vassallo, Maurizio**, Fonteneau, Raphaël, Guy Nkulu Wa Ngoie, Hyacinthe Tungadio Diambomba, Jean-Paul Katond Mbay, Bonaventure Banza WA Banza, & Ernst, Damien; *Power quality and service continuity in a low-voltage urban network in the municipality of Kamalondo in Lubumbashi, DR Congo.* (Preprint, 2026)

Chapter 2

An Optimization Algorithm for Customer Topological Paths Identification in Electrical Distribution Networks

---

Before a network can be physically optimized or its capacity traded, it must first be accurately mapped. Addressing the **see** capability of the thesis, this chapter tackles the TPI problem. Acknowledging that many operators lack advanced metering infrastructure, it proposes an integer linear programming methodology that identifies customer topology connection using only possibly incorrect, static data.

2.1 Introduction

Accurate knowledge of network topologies and the specific routes electricity takes to reach individual customers is often unavailable to DSOs due to incomplete, outdated, or erroneous data records. Accurately reconstructing these customer topological paths remains a challenging task due to several factors. Firstly, DSOs frequently rely on incomplete or inaccurate geographic information system (GIS) data, which may contain errors derived from outdated recordings or limitations in global positioning system GPS technologies

[20]. Secondly, while the integration of AMI in distribution networks has increased, many European countries still lack widespread AMI coverage ([21]), limiting the feasibility of measurement-based methods. Finally, scalability poses a significant obstacle; as networks grow in size and complexity, traditional approaches often fail to provide efficient and scalable solutions.
Despite these challenges, the accurate identification of customer topological paths is fundamental to numerous applications in modern power systems. It serves as a foundation for improving digital representations of distribution networks, supporting DSOs in performing simulations and analyses.

2.1.1 Literature review

In power distribution networks, various methodologies have been proposed to address the network topology identification or the TPI problem specifically. These methods can be characterized into two main categories: techniques that only rely on static data, such as GIS data of the elements in the network, and methods that also rely on AMI data, such as smart meter recordings.
Static data-based methods generally focus on establishing relationships and connections between elements. Relevant studies include: [22, 23, 24, 25, 26, 27, 28, 29, 30, 31]. For example, in [22] and [23] the authors identify the network topology of different networks using publicly available geographical data and connecting the elements based on their distances. In [24], topology identification is performed using Euclidean distances and a breadth-first search algorithm to identify clusters, followed by refinement through connecting nodes to their most probable lines. The chapter [25] presents a kd-tree algorithm for identifying clusters of elements, followed by connecting the elements within each cluster based on a predefined distance. In [26], the authors present a new procedure to exploit graph theory and data structure properties to efficiently detect and correct errors in models of radial secondary systems. The chapter [27] uses knowledge graphs to represent the existing relationships among elements in LV distribution networks. The knowledge graphs are then used to identify the correct network topology.
The main advantage of these methods is that they operate without relying on AMI measurements, making them suitable for DSOs with limited metering infrastructure. However, their major limitation is that GIS data can be incomplete, inaccurate, or missing for certain areas of the networks.
Dynamic data-based solutions rely on AMI measurements from the network. Relevant studies include [32, 33, 34, 35, 36, 37, 38, 39, 40, 41, 42, 43]. For example, in [32], the authors use line current sensor measurements and a mixed-integer linear programming (MILP) optimization algorithm to identify the topology of a power distribution network in California. The authors in [33]

introduce an iterative methodology for reconstructing network topology and cable parameters of LV three-phase networks with limited smart meter coverage. In [34], the authors present a method for topology identification using a combination of knowledge graphs and graph neural networks constructed based on remote signaling and telemetry data. The authors in the chapter [35] propose a similar approach using mixed-integer quadratic programming (MIQP) to identify the topology of power distribution networks using smart sensor recordings. While AMI-based methods can estimate topology and line parameters (e.g., impedance), they often require extensive sensor coverage, limiting their applicability in networks with incomplete AMI deployment, as evidenced by some studies using limited smart meter data [44].

2.1.2 Chapter contribution

This chapter presents an optimization algorithm to assist DSOs in addressing the TPI problem using only static data: GIS coordinates of network elements and customer-to-feeder-terminal-junction assignments as recorded in MV/LV substation databases. While our previous work [14] established the definition of the TPI problem and introduced the raw data transformation process, this chapter introduces and evaluates a concrete computational approach for solving the problem.

Our methodology relies exclusively on GIS data of network elements and customer connections to MV/LV transformers, making it particularly suitable for networks where GIS data is incomplete or inaccurate and AMI coverage is limited. The problem is formulated as an integer linear programming (ILP) optimization algorithm. The objective function of the optimization problem focuses on maximizing the number of customers connected to the correct MV/LV transformer, while some constraints ensure that the solution satisfies the DSO's expectations. The proposed methodology effectively addresses data inaccuracies and incompleteness.
Moreover, a repository with the code of the proposed methodology is released. The repository is publicly available at the following link: github.com/TPIproblem.

2.1.3 Chapter organization

The rest of the chapter is organized as follows: Section 2.2 presents the definition of the power network elements considered in this work. Section 2.3 defines the concept of topological paths. The problem statement is presented in Section 2.4. Section 2.5 defines the methodology used to solve the problem. The methodology is applied to an academic example in Section 2.6 and a real

Belgian power distribution network in Section 2.7. Section 2.8 concludes the chapter and outlines directions for future work.

2.2 Power distribution modeling

The following notation and definitions are consistent with those introduced in our previous paper [14].
Power distribution networks typically encompass a wide range of elements. The set of elements $\mathcal{E}$ is defined as:

$$\mathcal{E} = \{e_1, \ \ldots, \ e_k, \ \ldots, \ e_{|\mathcal{E}|}\} \tag{2.1}$$

where $|\mathcal{E}|$ represents the total number of elements in the set $\mathcal{E}$ and a single element is denoted as e_k, with $k \in \{1, \ \ldots, \ |\mathcal{E}|\}$.

Each element can have some attributes, such as its type and coordinates. The set of all element attributes $\mathcal{A}$ is defined as follows:

$$\mathcal{A} = \{a_1, \ \ldots, \ a_{|\mathcal{A}|}\}. \tag{2.2}$$

A single element $e \in \mathcal{E}$ is defined as a set of attributes. Formally:

$$e = \{e.a_1, \ \ldots, \ e.a_k, \ \ldots, \ e.a_{|e|}\} \tag{2.3}$$

where the dot notation is used to access the attributes of the element e, and a_k represents, for example, the type of the element e, its coordinates, or other relevant properties.

Each element within the network can be categorized based on its type attribute, serving as a characteristic that distinguishes it from other elements. The set of types, denoted as $\mathcal{T}$, includes all the possible types associated with the elements in $\mathcal{E}$:

$$\mathcal{T} = \{t_1, \ \ldots, \ t_{|\mathcal{T}|}\}. \tag{2.4}$$

Among the typical types, there may be *customer* connection elements, MV/LV $transformer$ substations.
Given an element $e \in \mathcal{E}$, its type, $t \in \mathcal{T}$, is accessed as follows:

$$t = e.type. \tag{2.5}$$

2.2.1 Network topological functions

The *Subset*() function is used to identify all elements of a specific type. This function takes two input parameters: the element set, $\mathcal{E}$, and a type $t \in \mathcal{T}$. Formally:

$$Subset(\mathcal{E}, t) = \{e \in \mathcal{E} \,|\, e.type = t\}. \tag{2.6}$$

In particular, three useful subsets are defined:

- $\mathtt{C}$: represents the set of customers in the network, $\mathtt{C} = Subset(\mathcal{E}, customer)$.
- $\mathtt{T}$: represents the set of terminal elements, generally $\mathtt{T} = Subset(\mathcal{E}, transformer)$. In this chapter, the terminal element is the feeder junction in the MV/LV substation, though the methodology supports any network element in this role.
- $\mathtt{R}$: represents the set of all elements, excluding customers and terminal elements, $\mathtt{R} = \mathcal{E} - \mathtt{C} - \mathtt{T}$.

The *Dist*() function takes two elements $e_k, e_m \in \mathcal{E}$ as input, and it outputs a scalar value, d, representing the distance between them. The *Dist*() function is defined as follows:

$$d = Dist(e_k,\, e_m) = ||e_k.coor,\, e_m.coor||_2 \tag{2.7}$$

where $||\bullet||_2$ represents the Euclidean distance and where $e_k.coor$ and $e_m.coor$ give the coordinates of the element e_k and, e_m respectively.

The *Connections*() function identifies all elements in the set $\mathcal{E}$ that can be connected to a given element, $e \in \mathcal{E}$, considering some specific conditions. The conditions for connectivity can depend on the DSOs' requirements such as distance between the elements, the element types, and so on.
Therefore, the *Connections*() function takes three inputs: $\mathcal{E}$, e and some conditions, returning a subset $\mathtt{K} \subseteq \mathcal{E}$. Formally:

$$\begin{aligned} \mathtt{K} = \text{Connections}(\mathcal{E}, e, \text{conditions}) = \\ \{e_m \in \mathcal{E} \,|\, e_m \text{ can be directly connected to } e \text{ if the conditions hold}\}. \end{aligned} \tag{2.8}$$

2.3 Topological paths

This section serves as the foundation for understanding the concepts of hypothetical, real, and estimated paths within the context of this work.

2.3.1 Paths

A customer topological path is represented as an ordered list of elements:

$$p = (p_1,\, p_2,\; \ldots,\, p_k,\; \ldots,\, p_{|p|-1},\, p_{|p|}) \tag{2.9}$$

where p is a generic path, p_1 represents the initial element in the path, which is a customer; p_k represents the k-th element in the path, and $p_{|p|}$ represents the terminal element, generally an MV/LV transformer.
Therefore, $p_1 \in \mathtt{C}$, and $p_k \in \mathtt{R}$ with $k \in \{2,\; \ldots,\; |p| - 1\}$ and $p_{|p|} \in \mathtt{T}$.

2.3.2 Hypothetical paths

Hypothetical paths refer to routes where only the initial elements (the customers) are known, while the connections between intermediate elements up to the terminal point are unknown. These paths represent potential ways that electricity might follow to supply a customer.
The set of hypothetical paths is denoted as $\mathcal{H}$. Each hypothetical path, $h \in \mathcal{H}$, represents a possible supply route for a customer. The number of hypothetical paths, given the set of elements $\mathcal{E}$, is finite, and it is given by:

$$|\mathcal{H}| = |\mathtt{C}| \cdot \sum_{k=1}^{|\mathtt{R}|} {}^{|\mathtt{R}|}P_k \cdot |\mathtt{T}| \tag{2.10}$$

where ${}^{n}P_m$ is the permutation formula, which calculates the number of ways to arrange m items from a set of n items $\left({}^{n}P_m = \frac{n!}{(n-m)!}\right)$.

2.3.3 Real paths

The set of all real paths, denoted as $\mathcal{P}$, is a subset of the hypothetical path set $\mathcal{H}$. Each path $p \in \mathcal{P}$ represents the actual sequence of network elements that connect a customer to an MV/LV transformer.
In distribution power networks, which are generally radial, the number of real paths is equal to the number of customers, since one customer is supplied by only one MV/LV transformer at any given moment. Therefore, the following condition holds $|\mathcal{P}| = |\mathtt{C}|$, where $\mathtt{C}$ represents the set of elements of type customers.

2.3.4 Estimated paths

The estimated paths, denoted by $\hat{\mathcal{P}}$, form a subset of the hypothetical paths, $\mathcal{H}$. This set of estimated paths, $\hat{\mathcal{P}}$, is an approximation to the set of real paths within the network, $\mathcal{P}$.

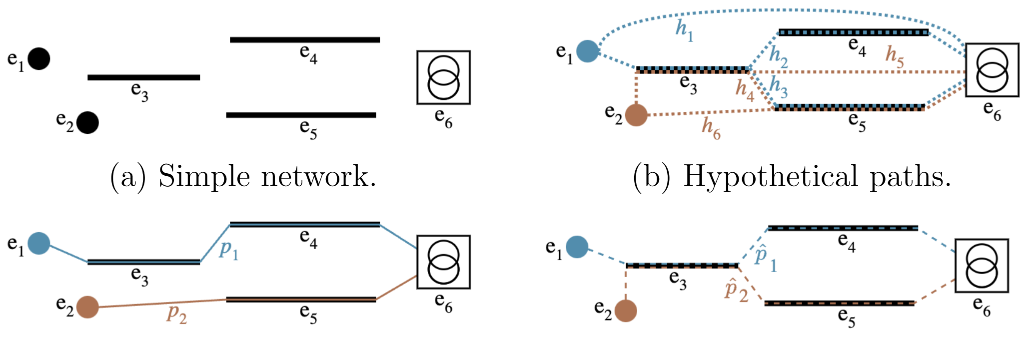

(a) Simple network. (b) Hypothetical paths.

(c) Real paths. (d) Estimated paths.

Figure 2.1: Visualization of the different sets of paths.

The set $\hat{\mathcal{P}}$ satisfies the property that the number of estimated paths in the set is equal to the number of customers considered in the network. Therefore, the following condition holds $|\hat{\mathcal{P}}| = |\mathcal{P}| = |\mathtt{C}|$.

2.3.5 Paths visualization

Figure 2.1 illustrates a simplified network, highlighting hypothetical, real, and estimated paths.
As shown in Fig. 2.1a, the data about network elements are often incomplete, making it difficult to accurately identify the customer paths.
Figure 2.1b shows some of the hypothetical paths. In the absence of prior information, any path could potentially represent the real one.
This highlights the challenge that, with limited information, only limited conclusions can be drawn about whether a hypothetical path corresponds to its real one. Many hypothetical paths for each customer may be available.
Figures 2.1c and 2.1d illustrate the real and estimated paths for each customer, respectively. Each customer is associated with exactly one real path and one estimated path, both of which are subsets of the hypothetical path set. Therefore: $\mathcal{P} \subseteq \mathcal{H}$ and $\hat{\mathcal{P}} \subseteq \mathcal{H}$.
Figure 2.2 presents a Venn diagram illustrating the relationships among the path sets. The set of hypothetical paths, $\mathcal{H}$, encompasses all other sets, representing all possible paths within the network. Notably, the sets of real paths, $\mathcal{P}$, and estimated paths, $\hat{\mathcal{P}}$, overlap to a certain degree, highlighting similarities and discrepancies between the estimation and ground truth. The overlap between $\mathcal{P}$ and $\hat{\mathcal{P}}$ indicates that some estimated paths match the real ones while others do not. For example, the paths $\hat{p}_1$ and p_1 for customer e_1 match perfectly. However, data inaccuracies can result in discrepancies; for example, the estimated path $\hat{p}_2$ deviates from the real path p_2 for the

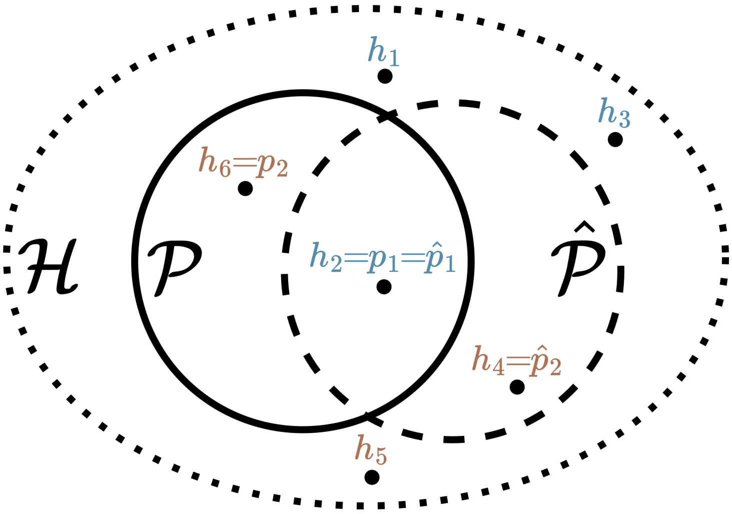

Figure 2.2: Representation of the different sets and their relationships.

customer e_2.

2.4 Problem statement

Generally, DSOs possess different types of information, which we represent formally as the set $\mathcal{I}$. This data can include, for example, files about the GIS data of the network elements, customers' information like annual power consumption, network configuration rules explaining how the elements are connected, and more.
The goal of the DSOs is, given all the raw information available to them, to estimate the customer topological paths that are as close as possible to the real paths. Denoting the set of real paths as the set $\mathcal{P}$ and the set of estimated paths as $\hat{\mathcal{P}}$, the objective is to identify two sets to be as close as possible and in the best case equal resulting in equal sets, which corresponds to a Jaccard index of 1: $J(\hat{\mathcal{P}}, \mathcal{P}) = \frac{|\hat{\mathcal{P}} \cap \mathcal{P}|}{|\hat{\mathcal{P}} \cup \mathcal{P}|} = 1$.
Therefore, the problem is to identify a methodology, $\mathfrak{M}()$, that, starting from the set of raw information, $\mathcal{I}$ can identify the best approximation of the real paths $\mathcal{P}$. Formally:

$$\hat{\mathcal{P}} = \mathfrak{M}(\mathcal{I}) \quad \text{s.t.} \quad \hat{\mathcal{P}} \simeq \mathcal{P}. \tag{2.11}$$

2.5 Methodology

This section provides a detailed description of the sequential procedure of the proposed methodology, $\mathfrak{M}()$, which aims to detect customer topological paths in electrical distribution networks. Figure 2.3 illustrates the methodology graphically.

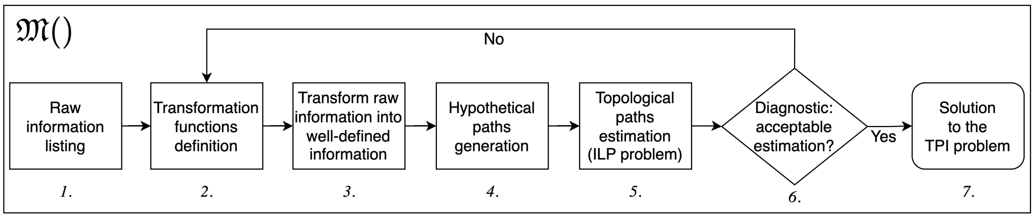

Figure 2.3: Flowchart of the steps proposed by our methodology, $\mathfrak{M}()$, to identify the customer topological paths in electrical distribution networks.

2.5.1 Raw information listing

Raw information refers to available information or data that comes from various sources. The set of raw information is listed as follows: $\mathcal{I} = \{i_1, \ldots, i_k, \ldots, i_{|\mathcal{I}|}\}$, with i_k ($k \in \{1, \ldots, |\mathcal{I}|\}$) denoting a single piece of raw information.

For this chapter, we use only static data, and in particular, the data needed is the GIS coordinates of the different elements in the network, their types, and the feeder terminal junction to which each customer is connected. Generally, this kind of information is available to the DSOs, even if it may be incomplete and/or inaccurate. Formally, the data needed for this chapter is:

- The set of elements, $\mathcal{E}$.
- The set of attributes, $\mathcal{A}$, contains at least the coordinates of the elements, the types, and the feeder terminal junction to which each customer is connected.
- The set of types $\mathcal{T}$ containing at least customer, line, junction, and transformer.

Therefore, *e.coor*, *e.type* must be known for all the elements, $e \in \mathcal{E}$, and *c.junction* is known for all the customers, $c \in \texttt{C}$.
It is important to note that this formulation relies on the assumption that the feeder connection (*c.junction*) provided in the static dataset are correct. A detailed discussion of this assumption, explicitly contrasted with AMI-based methodologies, and the framework's diagnostic behavior when these records are erroneous, is provided in Section 2.7.6.

2.5.2 Transformation functions definition

Transformation functions are responsible for transforming the available raw information into clear knowledge that is relevant within the specific context of a power network. The set of transformation functions is denoted as follows: $\mathcal{F} = \{f_1, \ldots, f_m, \ldots, f_{|\mathcal{F}|}\}$, with f_m ($m \in \{1, \ldots, |\mathcal{F}|\}$) denoting a single transformation function.
Mathematically, the transformation functions take one piece of raw information as input and return the transformed information as output.

2.5.3 Well-defined information

The well-defined information forms the basis for providing a structured foundation to identify customer paths that are as close as possible to reality. The set of well-defined information is denoted as follows: $\mathcal{I}' = \{i'_1, \ldots, i'_n, \ldots, i'_{|\mathcal{I}'|}\}$, with i'_n ($n \in \{1, \ldots, |\mathcal{I}'|\}$) denoting a single piece of well-defined information. Each element in the set $\mathcal{I}'$ is the result of applying a transformation function on a piece of raw information, i.e., $i'_n = f_m(i_k)$.

2.5.4 Hypothetical paths generation

Given the set of well-defined information, $\mathcal{I}'$, the set of hypothetical path compatible with the set $\mathcal{I}'$, denoted as $\mathcal{H}^{\mathcal{I}'}$, is constructed. Each piece of information in $\mathcal{I}'$ allows to reduce the size of the hypothetical path set $\mathcal{H}^{\mathcal{I}'}$. The idea is that the more data is available, the closer to reality the paths inside the set $\mathcal{H}^{\mathcal{I}'}$ are.

Search space reduction

Given the set of well-defined information, $\mathcal{I}'$, the framework constructs the set of compatible hypothetical paths, denoted as $\mathcal{H}^{\mathcal{I}'}$. However, enumerating the complete set $\mathcal{H}$ becomes intractable for large-scale distribution networks due to the combinatorial growth in the number of possible routing configurations.

To ensure computational tractability, we introduce an A^* algorithm as a search space reduction strategy [45]. The algorithm uses information of the starting point (the customer $c \in \mathtt{C}$) and the final point (the feeder terminal junction $t \in \mathtt{T}$) to explore valid paths.
For a given customer c and target junction t, the A^* algorithm evaluates the

potential next element $e \in \mathcal{E}$ by minimizing a cost function:

$$f(e) = g(e) + h(e) \tag{2.12}$$

where $g(e)$ represents the accumulated path length from the customer c to the current element e, defined as:

$$g(e) = \sum_{k=1}^{|p|-1} Dist(p_k,\, p_{k+1}) \tag{2.13}$$

where $p_1 = c$ is the customer, $p_{|p|} = e$ is the current element, and each consecutive pair $(p_k,\, p_{k+1})$ is a directly connected element pair along the explored path.
The heuristic function $h(e)$ is defined as the Euclidean distance from the current element e to the target terminal junction t:

$$h(e) = Dist(e,\, t) \tag{2.14}$$

with $Dist()$ as defined in Eq. 2.7.

During the search process, the paths are discarded by the constraints defined in $\mathcal{I}'$ (e.g., the maximum connection distance D and the maximum overall path length L). Moreover, the algorithm terminates upon identifying a maximum of N valid candidate paths per customer. By applying this search strategy, the framework generates a feasible subset of hypothetical paths ($\mathcal{H}^{\mathcal{I}'}$), enabling the ILP solver to converge efficiently.

2.5.5 Topological paths estimation

After generating the hypothetical paths compatible with the well-defined information, $\mathcal{H}^{\mathcal{I}'}$, the next step of the methodology is to identify the paths in the set $\mathcal{H}^{\mathcal{I}'}$ that are an approximation of the real paths in the actual network, therefore identifying the set of estimated paths $\hat{\mathcal{P}}$.
While various methods can solve the TPI problem, we present an ILP approach designed to find the solution $\hat{\mathcal{P}}$ and to meet the DSO requirements.

Matrices generation

The following sections describe the main components of our ILP formulation, including the matrices and the optimization problem.

- Hypothetical paths matrix:
The set of hypothetical paths, $\mathcal{H}^{\mathcal{I}'}$ can be represented as a binary matrix with as many rows as $|\mathcal{H}^{\mathcal{I}'}|$ and as many columns as $|\mathtt{C}| + |\mathtt{R}| + |\mathtt{T}|$.
Therefore, the hypothetical paths matrix, denoted as $\mathbf{H}$, can be written as follows:

$$\mathbf{H} = \begin{array}{c} \\ h_1 \\ h_2 \\ \vdots \\ h_k \\ \vdots \\ h_{|\mathcal{H}^{\mathcal{I}'}|} \end{array} \begin{array}{c} \begin{array}{cccc|cccc|cccc} c_1 & c_2 & \cdots & c_{|\mathtt{C}|} & r_1 & r_2 & \cdots & r_{|\mathtt{R}|} & t_1 & t_2 & \cdots & t_{|\mathtt{T}|} \end{array} \\ \left(\begin{array}{cccc|cccc|cccc} 0 & 1 & \cdots & 0 & 1 & 0 & \cdots & 1 & 0 & 1 & \cdots & 0 \\ 1 & 0 & \cdots & 0 & 1 & 0 & \cdots & 0 & 0 & 1 & \cdots & 0 \\ \vdots & \vdots & \ddots & \vdots & \vdots & \vdots & \ddots & \vdots & \vdots & \vdots & \ddots & \vdots \\ 0 & 0 & \cdots & 0 & 0 & 0 & \cdots & 0 & 0 & 0 & \cdots & 1 \\ \vdots & \vdots & \ddots & \vdots & \vdots & \vdots & \ddots & \vdots & \vdots & \vdots & \ddots & \vdots \\ 0 & 0 & \cdots & 1 & 0 & 1 & \cdots & 0 & 1 & 0 & \cdots & 0 \end{array} \right) \\ \begin{array}{ccc} \qquad \mathbf{H}_{\mathtt{C}} \qquad & \qquad \mathbf{H}_{\mathtt{R}} \qquad & \qquad \mathbf{H}_{\mathtt{T}} \qquad \end{array} \end{array} \tag{2.15}$$

Each row h_k in the matrix $\mathbf{H}$ represents a hypothetical path compatible with the well-defined information. A value of 1 or 0 in this row indicates whether the corresponding element, $e \in \mathtt{C} \cup \mathtt{R} \cup \mathtt{T}$, is present (1) or not (0) in path h_k. A single element of the matrix is accessed as $\mathbf{H}_{(k,m)}$ where k represents the row ($k \in \{1, \ldots, |\mathcal{H}^{\mathcal{I}'}|\}$) and m represents the column ($m \in \{1, \ldots, |\mathtt{C}| + |\mathtt{R}| + |\mathtt{T}|\}$).

For clarity, we divide the $\mathbf{H}$ matrix into three sub-matrices:

  - The $\mathbf{H}_{\mathtt{C}}$ matrix, denoted as customers' elements matrix, indicates the presence of a customer $c \in \mathtt{C}$ in any path, $h \in \mathcal{H}^{\mathcal{I}'}$. Therefore, the $\mathbf{H}_{\mathtt{C}}$ matrix has dimension $|\mathcal{H}^{\mathcal{I}'}| \times |\mathtt{C}|$.
  Since one and only one customer can be present in one path, the following condition must be satisfied:

$$\sum_{k}^{|\mathtt{C}|} \mathbf{H}_{\mathtt{C}\,(m,k)} = 1, \qquad \forall m \in \{1, \ldots, |\mathcal{H}^{\mathcal{I}'}|\}. \tag{2.16}$$

  - The $\mathbf{H}_{\mathtt{R}}$ matrix, denoted as the remaining elements matrix, indicates the presence of elements $r \in \mathtt{R}$ in the paths, $h \in \mathcal{H}^{\mathcal{I}'}$. Therefore, the $\mathbf{H}_{\mathtt{R}}$ matrix has dimension $|\mathcal{H}^{\mathcal{I}'}| \times |\mathtt{R}|$.
  No particular condition is imposed on the matrix $\mathbf{H}_{\mathtt{R}}$.
  - The $\mathbf{H}_{\mathtt{T}}$ matrix, referred to as the terminal elements matrix, indicates the presence of a terminal node, $t \in \mathtt{T}$, in the paths, $h \in \mathcal{H}^{\mathcal{I}'}$. Therefore, the $\mathbf{H}_{\mathtt{T}}$ matrix has dimension $|\mathcal{H}^{\mathcal{I}'}| \times |\mathtt{T}|$.

Since one and only one terminal element can be present in one path, the following condition must be satisfied:

$$\sum_{k}^{|\mathtt{T}|} \mathbf{H}_{\mathtt{T}\,(m,\,k)} = 1, \qquad \forall m \in \{1,\ \ldots,\ |\mathcal{H}^{\mathcal{I}'}|\}. \tag{2.17}$$

- Terminal association matrix:
  We define a binary matrix, referred to as the terminal association matrix, denoted as $\mathbf{T}_{\mathtt{R}}$, which indicates the association of elements $r \in \mathtt{R}$ to a specific terminal element $t \in \mathtt{T}$.
  The $\mathbf{T}_{\mathtt{R}}$ matrix has dimension $|\mathtt{T}| \times |\mathtt{R}|$ and can be represented as follows:

$$\mathbf{T}_{\mathtt{R}} = \begin{array}{c} \\ t_1 \\ t_2 \\ \vdots \\ t_k \\ \vdots \\ t_{|\mathtt{T}|} \end{array} \begin{array}{c} \begin{array}{ccccccc} r_1 & r_2 & \cdots & r_m & \cdots & r_{|\mathtt{R}|-1} & r_{|\mathtt{R}|} \end{array} \\ \begin{pmatrix} 0 & 1 & \cdots & 0 & \cdots & 0 & 0 \\ 1 & 0 & \cdots & 0 & \cdots & 1 & 0 \\ \vdots & \vdots & \ddots & \vdots & \ddots & \vdots & \vdots \\ 0 & 0 & \cdots & 1 & \cdots & 0 & 0 \\ \vdots & \vdots & \ddots & \vdots & \ddots & \vdots & \vdots \\ 0 & 0 & \cdots & 0 & \cdots & 0 & 1 \end{pmatrix} \end{array} \tag{2.18}$$

  where 0 and 1 represent respectively whether an element $r \in \mathtt{R}$ is assigned to a terminal element $t \in \mathtt{T}$ or not.

- Estimated paths matrix:
  The solution of the TPI problem, the set $\hat{\mathcal{P}}$, can also be conceptualized as a binary matrix that represents the hypothetical paths estimated to be the real paths. This path matrix, denoted as $\hat{\mathbf{P}}$, has dimension $1 \times |\mathcal{H}^{\mathcal{I}'}|$.

$$\hat{\mathbf{P}} = \begin{array}{c} \begin{array}{ccccc} h_1 & \cdots & h_k & \cdots & h_{|\mathcal{H}^{\mathcal{I}'}|} \end{array} \\ \begin{pmatrix} 1 & \cdots & 1 & \cdots & 0 \end{pmatrix} \end{array} \tag{2.19}$$

  where 0 and 1 represent whether the path $h_k \in \mathcal{H}^{\mathcal{I}'}$ is an estimated optimal path or not.

ILP optimization problem

The ILP formulation aims to identify the subset of hypothetical paths that best approximates the real network topology. The optimization problem is presented in Eqs. 2.20a-2.20f.

$$\max_{\hat{\mathbf{P}},\mathbf{T}_{\mathtt{R}}} \quad \omega \cdot \sum_{k}^{|\mathcal{H}^{\mathcal{I}'}|} \hat{\mathbf{P}}_{(k)} - \sum_{m}^{|\mathtt{T}|}\sum_{n}^{|\mathtt{R}|} \mathbf{T}_{\mathtt{R}\,(m,\,n)} \tag{2.20a}$$

$$\text{s.t.} \quad \sum_{k}^{|\mathtt{R}|} \mathbf{H}_{\mathtt{R}\,(m,\,k)} \cdot \hat{\mathbf{P}}_{(m)} \cdot \mathbf{H}_{\mathtt{T}\,(m,\,n)}$$

$$\leq \left(\left(\mathbf{T}_{\mathtt{R}} \times \mathbf{H}_{\mathtt{R}}^{\top}\right) \cdot \mathbf{H}_{\mathtt{T}}^{\top}\right)_{(n,\,m)} \quad \forall m \in \{1, \ldots, |\mathcal{H}^{\mathcal{I}'}|\},\ \forall n \in \{1, \ldots, |\mathtt{T}|\}, \tag{2.20b}$$

$$\left(\hat{\mathbf{P}} \times \mathbf{H}_{\mathtt{C}}\right)_{(k)} \leq 1 \quad \forall k \in \{1, \ldots, |\mathtt{C}|\}, \tag{2.20c}$$

$$\sum_{k}^{|\mathtt{T}|} \mathbf{T}_{\mathtt{R}\,(k,\,m)} \leq 1 \quad \forall m \in \{1, \ldots, |\mathtt{R}|\}, \tag{2.20d}$$

$$\hat{\mathbf{P}}_{(k)} \in \{0, 1\} \quad \forall k \in \{1, \ldots, |\mathcal{H}^{\mathcal{I}'}|\}, \tag{2.20e}$$

$$\mathbf{T}_{\mathtt{R}\,(m,\,n)} \in \{0, 1\} \quad \forall m \in \{1, \ldots, |\mathtt{T}|\},\ \forall n \in \{1, \ldots, |\mathtt{R}|\}. \tag{2.20f}$$

The decision variables are:

- $\hat{\mathbf{P}}_{(k)} \in \{0, 1\}$, indicating whether the hypothetical path $k \in \{1,\ \ldots,\ |\mathcal{H}^{\mathcal{I}'}|\}$ is selected as part of the estimated set $\hat{\mathcal{P}}$.
- $\mathbf{T}_{\mathtt{R}(m,\,n)} \in \{0, 1\}$, representing the assignment of an element $n \in \{1,\ \ldots,\ |\mathtt{R}|\}$ to a terminal element $m \in \{1,\ \ldots,\ |\mathtt{T}|\}$.

The components of the ILP formulation are interpreted as follows:

- **Objective function (Eq. 2.20a).** The objective function is designed to achieve two competing goals. First, it aims to maximize the number of customers correctly connected to their terminal with $\sum_{k}^{\mathcal{H}^{\mathcal{I}'}} \hat{\mathbf{P}}_{(k)}$. Second, it aims to penalize overly complex solutions that assign network elements to feeders without necessity (minimize the number of elements with value 1 in the matrix $\mathbf{T}_{\mathtt{R}}$). The weighting factor ω controls the trade-off between maximizing customer connectivity and minimizing redundant assignments.
- **Path validity constraint (Eq. 2.20b).** This constraint verifies the validity of the paths by enforcing consistency among the elements of each selected path. It ensures that, for every estimated path $h \in \hat{\mathcal{P}}$, all intermediate elements $e \in h$ are assigned to the same terminal element $t \in \mathtt{T}$. In simple terms, it ensures that all intermediate elements belonging to a path are consistently assigned to the same feeder (terminal element).

- **Unique customer-path constraint (Eq. 2.20c).** Each customer $c \in \mathtt{C}$ can be associated with at most one selected path in $\hat{\mathbf{P}}$. This prevents a customer from being linked to multiple estimated paths.

- **Unique element-terminal constraint (Eq. 2.20d).** This guarantees that each element $r \in \mathtt{R}$ is associated with at most one specific terminal element $t \in \mathtt{T}$. Therefore, this constraint is designed to prevent the same elements from being associated with multiple terminal elements.

- **Binary constraints (Eqs. 2.20e-2.20f).** These ensure that the decision variables $\hat{\mathbf{P}}$ and $\mathbf{T}_{\mathtt{R}}$ take only binary values.

In summary, the ILP formulation identifies the optimal set of estimated paths, $\hat{\mathcal{P}}$. It achieves this by ensuring that customers are connected to their transformers, while preventing different feeders from overlapping or sharing lines.

2.5.6 Diagnostic function

The set of estimated paths, $\hat{\mathcal{P}}$, is validated with a *Diagnostic*() function. This abstract function can be customized to implement various validation criteria and methodologies, serving as a critical tool for assessing the quality of the obtained solution. The *Diagnostic*() function evaluates the found paths by checking any possible discrepancies from reality.
If inconsistencies are detected, the corresponding transformation functions can be adjusted to correct the identified issues. The methodology is then re-executed with the updated transformations until satisfactory results are achieved.

2.5.7 Solution of the TPI problem

If no discrepancies are identified or the DSO considers the solution acceptable, the set $\hat{\mathcal{P}}$ is regarded as the final solution to the TPI problem.

2.6 Academic example

To illustrate the methodology used to solve the TPI problem, an academic example of a power distribution network with a limited number of elements is considered.

2.6.1 Raw information

We assume the set of raw information available to the DSO, denoted as $\mathcal{I}$, is provided by some pieces of information:

i_1: Documents containing the DSO's list of elements, their coordinates, and their types. However, some elements may be missing, and some coordinates may be inaccurate.

i_2: MV/LV transformer cabin manuals provide instructions on cabin setup. This includes details about the organization of connection boards and how feeder lines connect to specific terminal elements or feeder terminal junctions on these boards.

i_3: Customers' information about which feeder terminal junction in the MV/LV transformer they are connected to.

i_4: DSO's general practice is to reduce energy losses by minimizing the total path length of each customer.

i_5: Information that LV networks are operated radially.

2.6.2 Transformation functions

The set $\mathcal{F}$ enumerates the transformation functions. Given that there are five pieces of raw information, the number of transformation functions is also five ($|\mathcal{F}| = |\mathcal{I}| = 5$).

2.6.3 Well-defined information

The set of well-defined information is given by:

$i'_1 = f_1(i_1)$: Set of elements, $\mathcal{E}$, and their attributes, $\mathcal{A}$ are known.

$i'_2 = f_2(i_2)$: The elements of two types *junction* and $transformer$ are directly connected with no intermediate element. Since each feeder terminal junction has a known associated transformer, we can simplify the path identification problem by considering the path from the customer to the feeder junction terminal.

$i'_3 = f_3(i_3)$: For each element of type *customer*, $e \in \mathcal{E}$, its attribute $junction$, $c.junction$, where it is connected to is known.

$i'_4 = f_4(i_4)$: An element can be connected to another only if its distance is less than a given distance D. Moreover, the total length of a path must not exceed a maximum length L.

$i'_5 = f_5(i_5)$: Since the network has a radial structure and does not have loops, each element can only appear once in each path.

The set of elements known to the DSO is given by:

$$\mathcal{E} = \{e_1, \ \ldots, e_{18}\}. \tag{2.21}$$

The set of attributes, $\mathcal{A}$, is given by:

$$\mathcal{A} = \{type, \, coordinate, \, junction\}. \tag{2.22}$$

The set of types, $\mathcal{T}$, is given by: *customer* (elements e_1 to e_6), *line* (e_7 to e_{12}), *junction* (e_{13} to e_{16}) and *transformer* (e_{17} and e_{18}) as shown in Fig. 2.4a.

2.6.4 Hypothetical paths compatible with the well-defined information

The first two pieces of information are used to generate an initial set of hypothetical paths, $\mathcal{H}^{i'_1,i'_2}$, containing all the paths from a customer to a terminal junction. Figure 2.4b illustrates the customer-to-feeder terminal junction colors, where matching colors indicate elements that are supposed to be connected to the same terminal junction. Therefore, the size of the set of hypothetical paths, compatible with the first two pieces of the well-defined information, i'_1 and i'_2, is calculated using Eq. 2.10:

$$|\mathcal{H}^{i'_1,i'_2}| = 61607. \tag{2.23}$$

The calculation is performed with the set of elements considered $\mathcal{E}$, the customer set $\mathtt{C} = Subset(\mathcal{E}, customer)$, the terminal points set $\mathtt{T} = Subset(\mathcal{E}, junction)$, the transformer set $\mathtt{F} = Subset(\mathcal{E}, transformer)$ and the remaining elements set $\mathtt{R} = \mathcal{E} - \mathtt{C} - \mathtt{T} - \mathtt{F}$.

Each remaining piece of well-defined information is used to exclude the paths in $\mathcal{H}^{i'_1,i'_2}$ that are not compatible with the well-defined information. Fig. 2.4c highlights some of the hypothetical paths for customer e_3 that satisfy the distance and connectivity constraints defined by i'_1 and i'_2. Therefore, considering all the remaining information, i'_3 to i'_5, the total number of hypothetical paths compatible with the well-defined information is $|\mathcal{H}^{\mathcal{I}'}|$. For example,

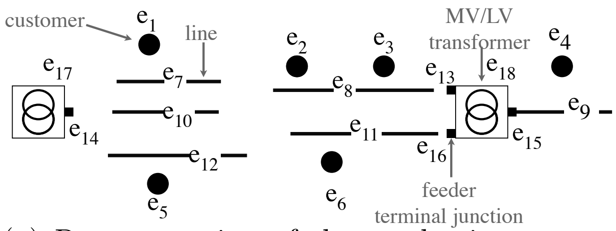

(a) Representation of the academic test network.

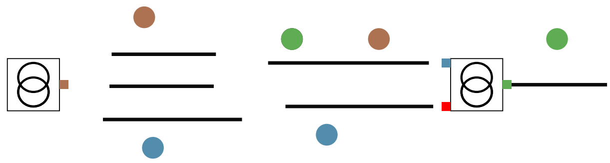

(b) Visualization of customer-to-feeder terminal junction assignments.

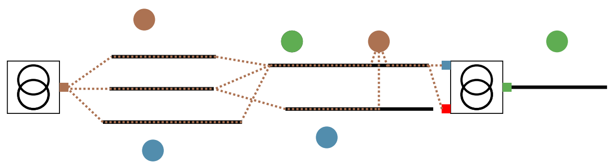

(c) Image showing some hypothetical paths for the customer e_3.

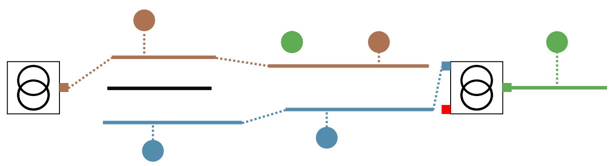

(d) Final network configuration after customer path identification.

Figure 2.4: Illustration of the process of identifying customer paths in the academic network considered.

Fig. 2.4d shows some of the hypothetical paths for customer e_3 that satisfy the distance and connectivity constraints defined by i'_4 and i'_5.
Detailed information about the elements in each hypothetical path can be found in the online repository (see Section 2.1.2).

2.6.5 Results paths estimation

The matrices $\mathbf{H}_{\mathtt{C}}$, $\mathbf{H}_{\mathtt{R}}$, $\mathbf{H}_{\mathtt{T}}$, $\hat{\mathbf{P}}$ and $\mathbf{T}_{\mathtt{R}}$ are used in the optimization problem as shown in Eqs. 2.20a-2.20f.
In particular, the matrices $\mathbf{H}_{\mathtt{C}}$, $\mathbf{H}_{\mathtt{R}}$ and $\mathbf{H}_{\mathtt{T}}$ are used as the parameters of the ILP problem, while $\hat{\mathbf{P}}$ and $\mathbf{T}_{\mathtt{R}}$ are the decision variables and represent a proposed solution to the optimization problem.
The matrix $\hat{\mathbf{P}}$ contains the estimated paths, which are considered as approximations of the real paths; while the matrix $\mathbf{T}_{\mathtt{R}}$ represents which elements belong to each feeder terminal junction.

The estimated optimal paths for this academic network are:

$$\hat{\mathbf{P}} = \begin{array}{c} \begin{array}{cccccccccc} h_1 & h_2 & h_3 & h_4 & h_5 & h_6 & h_7 & h_8 & h_9 & h_{10} \end{array} \\ \begin{pmatrix} 1 & 0 & 0 & 0 & 0 & 0 & 1 & 1 & 1 & 1 \end{pmatrix} \end{array}. \tag{2.24}$$

The matrix $\mathbf{T}_{\mathtt{R}}$ is given by:

$$\mathbf{T}_{\mathtt{R}} = \begin{array}{c c} & \begin{array}{cccccc} e_7 & e_8 & e_9 & e_{10} & e_{11} & e_{12} \end{array} \\ \begin{array}{c} e_{13} \\ e_{14} \\ e_{15} \\ e_{16} \end{array} & \begin{pmatrix} 0 & 0 & 0 & 0 & 1 & 1 \\ 1 & 1 & 0 & 0 & 0 & 0 \\ 0 & 0 & 1 & 0 & 0 & 0 \\ 0 & 0 & 0 & 0 & 0 & 0 \end{pmatrix} \end{array}. \tag{2.25}$$

2.6.6 Results explanation

We will now examine the results obtained from applying the optimization method to the academic example. This analysis will clarify the meaning and role of each component in Eqs. 2.20a-2.20f.

Maximization term

The maximization term, Eq. 2.20a, contains two operations:

- Maximizing estimated paths: the first term, $\sum_{k}^{|\mathcal{H}^{\mathcal{I}'}|} \hat{\mathbf{P}}_{(k)}$, focuses on maximizing the number of estimated optimal paths, therefore paths whose have a value of 1.
- Penalty for unnecessary assignments: the second term, $\sum_{m}^{|\mathtt{T}|} \sum_{n}^{|\mathtt{R}|} \mathbf{T}_{\mathtt{R}\,(m,n)}$, introduces a penalty term related to the terminal association matrix.

This term discourages assigning elements to a feeder terminal junction when unnecessary.

The value of ω is important to determine the relative importance of finding more valid paths over minimizing the number of elements assigned to the path. A larger value of ω encourages the optimization to find more valid paths, while a smaller value puts more emphasis on minimizing the elements used. In this case, ω is set to 10.

Validity path constraint

The left-hand side of the constraint term in Eq. 2.20b is calculated in three operations:

(i) $\sum_k^{|\mathtt{R}|} \mathbf{H}_{\mathtt{R}\,(\bullet,\,k)}$. This operation counts the number of elements present in each hypothetical path, $h \in \mathcal{H}^{\mathcal{I}'}$. The resulting matrix, of dimensions $|\mathcal{H}^{\mathcal{I}'}| \times 1$, is presented in transposed form for space efficiency as follows:

$$\begin{array}{cccccccccc} h_1 & h_2 & h_3 & h_4 & h_5 & h_6 & h_7 & h_8 & h_9 & h_{10} \end{array}$$
$$\begin{pmatrix} 1 & 2 & 2 & 2 & 3 & 3 & 2 & 1 & 2 & 1 \end{pmatrix}. \tag{2.26}$$

(ii) The result, Eq. 2.26, is multiplied element-wise by $\hat{\mathbf{P}}$. This operation assures the verification of the constraint only for the estimated optimal paths. The resulting matrix, still of dimensions $|\mathcal{H}^{\mathcal{I}'}| \times 1$, is transposed and presented as follows:

$$\begin{array}{cccccccccc} h_1 & h_2 & h_3 & h_4 & h_5 & h_6 & h_7 & h_8 & h_9 & h_{10} \end{array}$$
$$\begin{pmatrix} 1 & 0 & 0 & 0 & 0 & 0 & 2 & 1 & 2 & 1 \end{pmatrix}. \tag{2.27}$$

(iii) Finally, the result, Eq. 2.27 is multiplied by the matrix $\mathbf{H}^\top$. The result of this operation still has dimensions $|\mathcal{H}^{\mathcal{I}'}| \times |\mathtt{T}|$ and the transposed form is shown as follows:

$$\begin{array}{c} \\ e_{13} \\ e_{14} \\ e_{15} \\ e_{16} \end{array} \begin{array}{c} \begin{array}{cccccccccc} h_1 & h_2 & h_3 & h_4 & h_5 & h_6 & h_7 & h_8 & h_9 & h_{10} \end{array} \\ \begin{pmatrix} 0 & 0 & 0 & 0 & 0 & 0 & 0 & 0 & 2 & 1 \\ 1 & 0 & 0 & 0 & 0 & 0 & 2 & 0 & 0 & 0 \\ 0 & 0 & 0 & 0 & 0 & 0 & 0 & 1 & 0 & 0 \\ 0 & 0 & 0 & 0 & 0 & 0 & 0 & 0 & 0 & 0 \end{pmatrix} \end{array}. \tag{2.28}$$

The element-wise multiplication of matrices in Eq. 2.27 and $\mathbf{H}^\top$ can be formally represented using diagonal matrix multiplication, ensuring dimensional consistency between the operands. Let $\mathbf{A} \subseteq \mathbb{R}^{M\times 1}$ denote the column vector obtained from Eq. 2.27, and let $\mathbf{B} = \mathbf{H}^\top \subseteq \mathbb{R}^{M\times N}$, with $M, N \in \mathbb{N}^+$. The resulting matrix $\mathbf{C} \subseteq \mathbb{R}^{M\times N}$ is computed as:

$$\mathbf{C} = \mathrm{diag}(\mathbf{A}) \cdot \mathbf{B}, \tag{2.29}$$

where $\mathrm{diag}(\mathbf{A})$ is a diagonal matrix whose diagonal entries correspond to the elements of $\mathbf{A}$.
Therefore, the resulting matrix in Eq. 2.28 has dimensions $|\mathcal{H}^{\mathcal{I}'}| \times |\mathtt{T}|$.

Similarly, the right-hand side of the constraint term in Eq. 2.20b is calculated in two operations:

(i) The matrix multiplication of $\mathbf{T}_{\mathtt{R}}$ and $\mathbf{H}_{\mathtt{R}}^\top$. This operation calculates the number of elements that are present at the same time in a feeder terminal junction $t \in \mathtt{T}$ and in a path $h \in \mathcal{H}^{\mathcal{I}'}$. The resulting matrix has dimensions $|\mathtt{T}| \times |\mathcal{H}^{\mathcal{I}'}|$ and is given as follows:

$$\begin{array}{c} \\ e_{13} \\ e_{14} \\ e_{15} \\ e_{16} \end{array} \begin{array}{c} \begin{array}{cccccccccc} h_1 & h_2 & h_3 & h_4 & h_5 & h_6 & h_7 & h_8 & h_9 & h_{10} \end{array} \\ \begin{pmatrix} 0 & 0 & 1 & 0 & 0 & 1 & 0 & 0 & 2 & 1 \\ 1 & 1 & 1 & 1 & 2 & 1 & 2 & 0 & 0 & 0 \\ 0 & 0 & 0 & 0 & 0 & 0 & 0 & 1 & 0 & 0 \\ 0 & 0 & 0 & 0 & 0 & 0 & 0 & 0 & 0 & 0 \end{pmatrix} \end{array}. \tag{2.30}$$

For example, considering the value at position (e_{14}, h_7) of the matrix in Eq. 2.30. The value is 2 since the same elements e_7 and e_8 are at the same time assigned to the feeder terminal junction e_{14} (second row of the junction association matrix in Eq. 2.25) and are present in the path h_7 $\big(h_7 = (e_3,\, e_7,\, e_8,\, e_{14})\big)$.

(ii) Similarly, for the left-hand side, the result of Eq. 2.30 is multiplied by the matrix $\mathbf{H}_{\mathtt{T}}$. This ensures that the comparison on both sides of the inequality is performed only on the elements that are assigned to the same feeder terminal junction. The result of this operation has dimensions $|\mathtt{T}| \times |\mathcal{H}^{\mathcal{I}'}|$ and is expressed as follows:

$$\begin{array}{c} \\ e_{13} \\ e_{14} \\ e_{15} \\ e_{16} \end{array} \begin{array}{c} \begin{array}{cccccccccc} h_1 & h_2 & h_3 & h_4 & h_5 & h_6 & h_7 & h_8 & h_9 & h_{10} \end{array} \\ \begin{pmatrix} 0 & 0 & 0 & 0 & 0 & 0 & 0 & 0 & 2 & 1 \\ 1 & 0 & 0 & 0 & 0 & 0 & 2 & 0 & 0 & 0 \\ 0 & 0 & 0 & 0 & 0 & 0 & 0 & 1 & 0 & 0 \\ 0 & 0 & 0 & 0 & 0 & 0 & 0 & 0 & 0 & 0 \end{pmatrix} \end{array}. \tag{2.31}$$

Finally, by comparing Eq. 2.28 and Eq. 2.31, the condition Eq. 2.28 $\leq$ Eq. 2.31 is verified for each corresponding value of the matrices.

In general, the constraint Eq. 2.20b assures that all the elements of an estimated path belong to the same feeder terminal junction. This is guaranteed when the number of elements in each estimated path is less than or equal to the total number of elements in the corresponding feeder terminal junction.

Unique estimated path for customer constraint

The constraint in Eq. 2.20c is given as follows:

$$\left(\hat{\mathbf{P}} \times \mathbf{H}_{\mathtt{C}}\right) = \begin{array}{cccccc} e_1 & e_2 & e_3 & e_4 & e_5 & e_6 \\ (1 & 0 & 1 & 1 & 1 & 1) \end{array}, \tag{2.32}$$

$$\left(\hat{\mathbf{P}} \times \mathbf{H}_{\mathtt{C}}\right)_{(k)} \leq 1, \qquad \forall k \in \{1,\ \ldots,\ |\mathtt{C}|\}. \tag{2.33}$$

Equation 2.32 is a matrix of dimensions $1 \times |\mathtt{C}|$ and in this academic example, all the values are 1 except for e_2 whose value is 0 since no path was identified for that customer.

Elements assigned to a unique feeder terminal junction constraint

The constraint in Eq. 2.20d is given as follows:

$$\sum_{k}^{|\mathtt{T}|} \mathbf{T}_{\mathtt{R}\,(k,\bullet)} = \begin{array}{cccccc} e_7 & e_8 & e_9 & e_{10} & e_{11} & e_{12} \\ (1 & 1 & 1 & 0 & 1 & 1) \end{array}, \tag{2.34}$$

$$\sum_{k}^{|\mathtt{T}|} \mathbf{T}_{\mathtt{R}\,(k,m)} \leq 1, \qquad \forall m \in \{1,\ \ldots,\ |\mathtt{R}|\}. \tag{2.35}$$

Equation 2.34 is a matrix of dimensions $1 \times |\mathtt{R}|$ and in this academic example, all the values are 1 except for e_{10} whose value is 0 since the element e_{10} is not used by any path. Therefore, it is not assigned to any feeder terminal junction.
A possible explanation for why e_{10} is not used is that it is a redundant element in the dataset, or that the optimization algorithm may have chosen that alternative paths provide a better solution.

2.6.7 Example evaluation

Because the academic network is a controlled example, the real paths P are known, allowing a direct quantitative assessment of the estimated paths $\hat{P}$. From Eq. 2.32, $\hat{P} \times H_C = (1\ 0\ 1\ 1\ 1\ 1)$, so a valid path is recovered for five of the six customers: e_1, e_3, e_4, e_5 and e_6, giving a per-customer connection coverage of $5/6 = 83.3\%$ and, using the Jaccard index introduced in Section 2.4, to:

$$J(\hat{P}, P) = \frac{|P \cap \hat{P}|}{|P \cup \hat{P}|} = \frac{5}{6} \approx 0.83\,. \tag{2.36}$$

The single discrepancy, customer e_2, is analysed in the diagnostic evaluation below.

2.6.8 Diagnostic function

The proposed solution, the matrices $\hat{\mathbf{P}}$ and $\mathbf{T}_{\mathtt{R}}$ are then evaluated using the *Diagnostic*() function to detect any possible issues.

For example, the solution proposed does not find the paths for each customer, since it is not possible to find a path for customer e_2 given the data available to the DSO. This issue is reported to the DSO, who can perform some further analysis on the case and understand why no path was found.
For this controlled example the cause can be identified precisely. The A^* search generates candidate paths for e_2, but none can be selected: choosing any of them would require assigning a line element to two different feeder terminal junctions, violating the path-validity constraint (Eq. 2.20b). This behavior is consistent with an erroneous recorded *c.junction* for e_2. The *Diagnostic*() function therefore flags e_2 for verification rather than forcing an inconsistent connection.

2.7 Belgian network

We apply our methodology to a real Belgian LV network characterized by incomplete GIS data and missing customer connections to the network. For this use case, we assume that the set of raw information, $\mathcal{I}$, the transformation functions, $\mathcal{F}$, and the well-defined information, $\mathcal{I}'$, are the same as those described in the academic example in Section 2.6.
For this real case, the set of elements known to the Belgian DSO is given by:

$$\mathcal{E} = \{e_1,\ \ldots,\ e_{1089}\}. \tag{2.37}$$

The set of attributes, $\mathcal{A}$, is given by:

$$\mathcal{A} = \{type,\ coordinate,\ junction\}. \tag{2.38}$$

The number of elements for the different types is given in Table 2.1.

2.7.1 Hypothetical paths compatible with the well-defined information

The total number of hypothetical paths in the set $\mathcal{H}$ is generally determined using Eq. 2.10. Following the methodology $\mathfrak{M}()$, the hypothetical paths not compatible with the well-defined information are excluded, keeping only those compatible with each piece of information, obtaining the set $\mathcal{H}^{\mathcal{I}'}$. For the real Belgian network considered, given the large number of elements in the network, it is impractical to explicitly represent the set $\mathcal{H}$ as a set of all the possible hypothetical paths.
For this reason, to efficiently identify the hypothetical paths that are compatible with the well-defined information, the A^* algorithm mentioned in Section 2.5.4 is used.

The implementation of the $A^*()$ function is available on the online repository (see Section 2.1.2). Below, we present the general concept.
After the execution of the $A^*()$ algorithm, considering a maximum number of paths for each customer of $N = 15$, the total number of hypothetical paths is $|\mathcal{H}^{\mathcal{I}'}| = 17335$. The value of N is selected as a balance between computational efficiency and the likelihood of identifying an optimal solution.

2.7.2 Matrix generation

The set $\mathcal{H}^{\mathcal{I}'}$ is decomposed into the three sub-matrices, $\mathbf{H}_{\mathtt{C}}$, $\mathbf{H}_{\mathtt{R}}$ and $\mathbf{H}_{\mathtt{T}}$, as explained in Section 2.5.5.

These matrices are used as input parameters of the optimization problem. The matrices $\hat{\mathbf{P}}$ and $\mathbf{T}_{\mathtt{R}}$ are used as output decision variables of the optimization algorithm.

2.7.3 Optimization problem results

After executing the optimization algorithm, a solution is obtained in the form of matrices $\hat{\mathbf{P}}$ and $\mathbf{T}_{\mathtt{R}}$.

Displaying the matrices directly might be challenging for visualization and comprehension. Therefore, we summarize and present the results in a more comprehensible way.

Therefore, given the matrix, $\hat{\mathbf{P}}$, it is possible to represent the connections among the elements of the estimated paths graphically. In particular, each element of an estimated optimal path is assigned a specific color, with black reserved for unassigned elements.

The color that is assigned to each element depends on the matrix $\mathbf{T}_{\mathtt{R}}$. In particular, the same color is assigned to the elements that belong to the same feeder terminal junction.

Figure 2.5a shows a part of the Belgian network considered with three MV/LV transformers, some lines, and customers. In Fig. 2.5b, it is possible to see the network after the identification of the paths: colors have been assigned to customers and lines belonging to the same feeder terminal junction. Dashed lines represent the connections between the elements, for example, customer-line connections.

2.7.4 Diagnostic function

Moreover, a few purple squares are present. These are customers for whom no path was identified, and these are discovered with the *Diagnostic*() function.

Possible reasons for failing to identify a path include incorrect or missing data for the feeder terminal junction associated with a customer or the inability to assign a line to its corresponding feeder terminal junction.

These issues are reported to the DSO for further investigation.

One of the main challenges in this TPI problem is the absence of a well-defined ground truth, as no explicit reference data is available. Consequently, quantitative criteria cannot be established to evaluate algorithmic performance. Instead, assessment must rely on qualitative evaluation through human interpretation. For example, in this case, the DSO could access only the schematic images of customer paths, and a human-in-the-loop process was employed to compare the identified paths against the schematics to assess their accuracy.

2.7.5 Parameterization and computational scalability

The performance and scalability of the proposed TPI framework depend on a defined set of hyperparameters, summarized alongside execution metrics in Table 2.1. The spatial threshold $D = 50$ m and maximum path length $L = 500$ m were selected based on the DSO's network characteristics and operational experience, effectively restricting the search space to electrically plausible routes. To control combinatorial growth, candidate paths per customer were capped at $N = 15$, ensuring sufficient routing diversity while maintaining tractability. Within the ILP formulation (Eq. 2.20a), the

(a) Before applying the methodology.

(b) After applying the methodology.

Figure 2.5: Part of the digital model of the real network considered.

weighting factor $\omega = 10$ balances the maximization of identified customer paths against the penalization of too long paths.

The methodology was implemented in Python using the Gurobi optimizer

Table 2.1: Algorithm performance, hyperparameters, and execution statistics for the Belgian network

Category	Metric	Value
Network Profile	Total Elements ($\mathcal{E}$)	1089
	Customers (`C`)	526
	Lines (`R`)	441
	Feeder junctions (`T`)	96
	MV/LV transformers (`F`)	26
Hyperparameters	Max candidate paths per customer (N)	15
	Max connection distance (D)	50 m
	Max path length (L)	500 m
	Objective weighting factor (ω)	10
Statistics	Candidate paths generated ($\lvert\mathcal{H}^{\mathcal{I}'}\rvert$)	17335
	A^* Generation time	264 s
	ILP optimization time	5.8 s
Results	Customers connected	88%

and evaluated on a standard machine (Intel i7, 8GB RAM). Applied to the 1089-element Belgian network, the A^* algorithm evaluated the spatial constraints and generated 17335 candidate paths in 264 seconds. Thanks to the highly pruned search space, the resulting matrix sparsity enabled the ILP solver to subsequently reach global optimality in just 5.8 seconds. As detailed in Table 2.1, this runtime disparity highlights that the candidate-path generation phase is the dominant bottleneck, making it the primary target for future scalability improvements.

2.7.6 Robustness analysis

The proposed framework assumes that customer-to-feeder terminal junction assignments (*c.junction*) provided in DSO records are correct. This separates it from AMI-based identification methods, which can infer or verify such assignments directly from smart meter measurements and are therefore less sensitive to errors in static records. However, AMI-based approaches require sufficient sensor coverage; a condition that many European DSOs cannot yet meet [21].

In data-scarce settings, the accuracy of *c.junction* records therefore becomes the critical input quality concern. To evaluate the robustness of the proposed framework against DSO data inaccuracies, a robustness analysis is performed on a part of a sub-network of the real-world case study (the same area de-

picted in Fig. 2.5). The considered sub-network comprises 211 customers, 3 transformers, and 17 feeder terminal junctions.
We changed the input data by randomly corrupting the customer terminal junction (*c.junction*) assignments for a varying percentage of customers (from 10% up to 100%) among one of the terminal junction of the 2 other transformers. To ensure statistical significance, 10 independent iterations are performed for each corruption level, while the spatial hyperparameters (D and L) and the objective penalty (ω) are kept constant. The objective is to measure the algorithm's ability to correctly connect unchanged customers and avoiding connect corrupted customers. The performance is evaluated across three metrics, illustrated in Fig. 2.6:

- **Fault detection rate:** The percentage of customers with corrupted feeder assignments for which the framework failed to identify a valid path, correctly avoiding a false connection (true positive rate).

- **False connection rate:** The percentage of customers with corrupted feeder assignments for which the framework identified a valid path to the wrong feeder (false positive rate).

- **Network connectivity rate:** The percentage of customers that are assigned a path to their correct feeder terminal junction, where ground truth is defined by the original uncorrupted assignment (accuracy).

The results show that under realistic error levels (between 10% and 30% corrupted customer-feeder assignments), the fault detection rate exceeds 95%, meaning that the framework correctly refuses to assign the vast majority of corrupted customers to an inconsistent feeder, leaving them unconnected for further DSO investigation. At the same time, the false connection rate remains below 5%, showing that wrong connections are rarely accepted. The network connectivity rate decreases approximately linearly with the corruption level, reflecting the expected reduction in the number of customers for which a feasible path can be identified as database inconsistencies increase.
It should be noted that corrupted assignments are drawn from feeder terminal junctions associated with other transformers. As these transformers typically serve different geographic areas, many corrupted assignments are geographically distant, causing violations of the distance (D) or path-length (L) constraints and rejection before the ILP stage. While this is an intended feature of the framework, the reported fault detection rate partly reflects the spatial implausibility of the injected errors. A more challenging scenario is assigning a customer to a nearby but incorrect junction, particularly within

the same MV/LV substation. In such cases, feasible short paths exist, spatial constraints are less effective, and detection becomes harder. Therefore, the reported fault detection rate should be regarded as an upper bound for the studied corruption model; evaluation under spatially adjacent, same-substation corruption is left for future work.
This suggests that the proposed TPI framework prioritizes physical grid realities over data errors, with the potential to act as a reliable anomaly detection filter for DSOs.

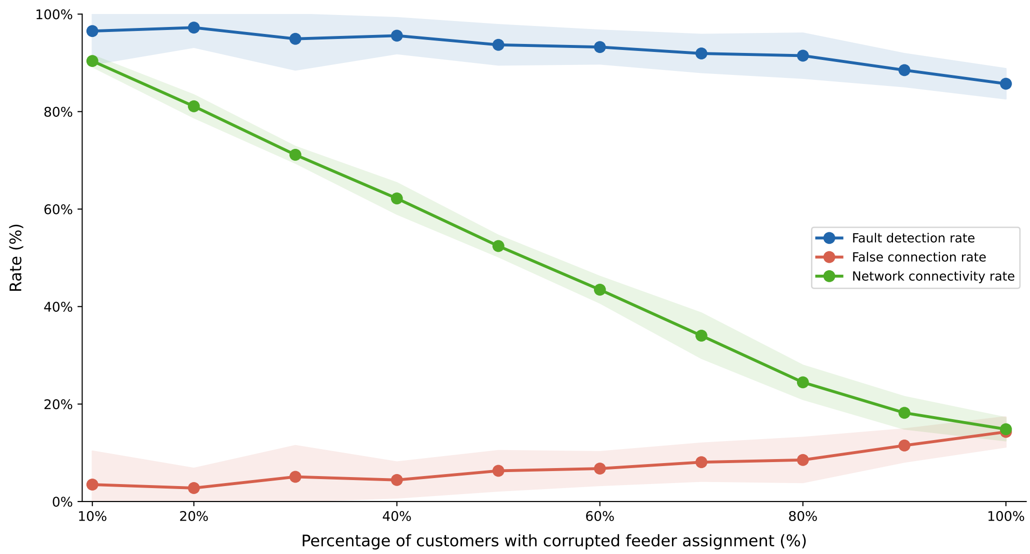

Figure 2.6: Sensitivity analysis of the TPI framework under varying levels of corruption. Shaded regions represent the ± 2 standard deviation interval computed over 10 independent runs per corruption level.

2.8 Conclusion

This chapter addressed the first capability of the toolkit (**see**) by answering RQ1 (*To what extent can customer topological paths in LV networks be identified using incomplete static records without relying on advanced metering infrastructure (AMI)?*) introducing an optimization algorithm to address the TPI problem in LV power distribution networks. Using only static GIS data and customer-to-transformer associations provided by DSOs, the methodology first constructs a set of hypothetical paths via an A^* search strategy, then selects the optimal subset through an ILP formulation that maximizes the number of customers assigned to physically feasible paths. By operating without AMI data such as smart meter recordings, the approach is broadly applicable across distribution networks, including those in regions with limited metering infrastructure, and avoids the cost and complexity of integrating dynamic measurement sources.

The effectiveness of the methodology was validated on both an academic test network and a real Belgian LV network comprising 1089 elements, achieving an 88% customer connection rate. A robustness analysis further demonstrated that, under realistic levels of corrupted customer-feeder assignments (10-30%), the framework achieved a fault detection rate above 95% while maintaining a false connection rate below 5%. This methodology is fundamental for constructing an accurate digital reconstruction of power distribution networks, ultimately aiding DSOs in network management and optimization.

The topological reconstruction developed in this chapter lifts the cover of observability. However, visibility alone does not improve the network's physical capacity. To address this, the next chapter focuses on mitigating the phase unbalance that afflicts LV networks under high DER penetration.

Chapter 3

Phase Reconfiguration for Power Distribution Networks with High DERs Penetration

Assuming connectivity is known (for instance via the method of Chapter 2), the next step for an active operator is to maximize the efficiency of existing infrastructure. Addressing the **balance** capability of the thesis, this chapter focuses on mitigating the phase unbalances caused by high penetrations of DERs. Rather than relying on heavy nonlinear power-flow models, this work introduces a linear optimization to reassign customer phase connections. Results demonstrate improvements, including a reduction in load unbalance, decreased line losses, and improved voltage profiles, particularly in overloaded phases, bringing maximum voltages within acceptable limits.

3.1 Introduction

Managing network phase unbalance has become increasingly important for ensuring stable and efficient grid operation. Phase unbalance arises when the loads across the phases of a network are not evenly distributed, leading to unequal voltage and current between the phases. Both issues can accelerate equipment aging, increase energy losses, and raise operational costs for the DSOs.

Phase unbalance in power distribution networks is influenced by their structural characteristics. Factors such as asymmetrical feeder layouts, differences in line lengths, and impedance often create unbalances. The unbalanced issue is further intensified by uneven customer assignments to phases, variability in load consumption patterns, and the unpredictable behavior of DERs.

There are three main types of solutions for network unbalance: *i)* rephasing, *ii)* phase balancers, and *iii)* ANM [46]. In general, the last two solutions require the deployment of new devices such as phase balancers, storage systems, or other controllable equipment. While effective, the additional equipment represents a significant capital investment and increases operational complexity for DSOs. In contrast, re-phasing focuses on changing customer phase configuration to balance the networks without additional physical equipment.

Re-phasing has been widely studied in the literature, with various strategies addressing the phase unbalance problem. The authors in [47] focus on rephasing single-phase customers to improve the voltage and current unbalance while keeping the number of phase adjustments below a given number established by the DSO. Authors in [48] propose a statistical method to identify the networks that may benefit from re-phasing, considering two consumption scenarios: yearly average and day-by-day consumption. In [49] an optimization problem is built to identify the minimum number of phase connection changes in a network to meet a specific phase unbalance tolerance. In [50] authors apply a Vortex search algorithm to minimize the total power loss of several IEEE networks. The authors in [51] build a strategy to minimize the current unbalance, feeder energy-loss cost, customer-interruption cost, and labor cost. In [52] authors propose the application of devices such as soft open points (SOP) and phase switch devices (PSD) to re-phase the network in real-time and to improve network stability and reduce costs, including the energy curtailment costs of PVs and wind turbines (WTs).

Most studies on network re-phasing focus on short-term scenarios, typically considering only single-day balancing and limited integration of DERs. Table 3.1 provides a summary of the works in the field, categorizing them based on their approaches. Moreover, the table compares these studies with the methodology proposed in this chapter, highlighting the contributions of our approach.

Compared to prior works, which mainly focused on short-term re-phasing under low DER penetration, our method contributes to phase load unbalance mitigation in power distribution networks by proposing an alternative optimization problem without relying on non-linear power flow calculation outputs. The proposed approach formulates a linear optimization problem aimed at minimizing the unbalance between customer load curves across phases while simultaneously reducing the number of required customer reconfigurations. Our methodology focuses on customer connections in single and multi-phase configurations, reflecting the structure of the DSO's network. The optimization is conducted over a year and accommodates different DER technologies such as PVs, EVs, and HPs, providing a robust solution to manage phase unbalance.

Table 3.1: Key features of various phase reconfiguration methods proposed in the literature, compared to our approach.
V = Voltage, I = Current, RC = Reconfiguration count, L = Energy losses, FL = Feeder load, DI = Distance Impact

Feature | paper	[47]	[48]	[49]	[50]	[51]	[52]	ours
1/2/3-phase customer connections	1	3	1, 2	3	1, 2, 3	3	1, 2, 3
Objective function	V, I, RC	I	FL, RC	V	I, L	V, I, L	FL, RC, DI
One year optimization	○	◐	○	○	○	○	●
Real-time reconfiguration	○	○	○	○	○	●	○
DERs	∅	∅	∅	∅	∅	PVs, WTs	PVs, EVs, HPs

The rest of the chapter is organized as follows. Section 3.2 introduces the mathematical formulation of power distribution networks, which serves as the foundation for our method. Section 3.3 presents the definition of the problem. Section 3.4 shows the methodology applied to an example network. The results of the real Belgian network are reported in Section 3.5. Section 3.6 concludes the work and discusses possible future works. Appendix 3.A describes the process of assigning time series data to each customer.

3.2 Network mathematical formalization

3.2.1 Network graph

A power distribution network can be modeled as a directed graph, denoted by $\mathcal{G} = (\mathcal{N}, \mathcal{E})$, where $\mathcal{N}$ represents the set of nodes and $\mathcal{E}$ represents the set of directed edges. Each node corresponds to a network component, such as a transformer or a customer. Each edge $e \in \mathcal{E}$, commonly referred to as lines, establishes a connection between two nodes of the set $\mathcal{N}$.

3.2.2 Network phases

Generally, power distribution networks operate as three-phase systems, where power is distributed across three phases to ensure balanced operation and maximize efficiency. Both nodes and lines are associated with one or more phases. The set of phases in the network is denoted as Φ, with $\Phi = \{A, B, C\}$, representing the three distinct electrical phases.
We define the set of all possible phase configurations, Ψ, as the collection of all customer phase assignments.
For networks with 1-phase, 2-phase, and 3-phase connections, the set Ψ contains 15 distinct possible configurations, representing permutations of the phase without repetition. Here are included some of the possible configurations:

$$\begin{aligned}\Psi = \{&(A), (B), (C),\\ &(A, B), (A, C), (B, A), (B, C), (C, A), (C, B),\\ &(A, B, C), (A, C, B), (B, A, C), ..., (C, B, A)\}.\end{aligned} \tag{3.1}$$

For a given node $n \in \mathcal{N}$ or line $e \in \mathcal{E}$, their respective phase configurations are denoted as n_ψ and e_ψ, with $\psi \in \Psi$. A single phase of a configuration $\psi \in \Psi$ is denoted as $\phi \in \psi$.

3.2.3 Network feeders

In typical power distribution networks, particularly the ones designed in a radial configuration, each feeder radiates outward from a single source, such as a transformer, toward consumption points, such as customers. The set of all feeders is defined by $\mathcal{F}$, where each feeder $f \in \mathcal{F}$ is a subgraph of $\mathcal{G}$, $f \subset \mathcal{G}$.
Every node and line in the network belongs to a specific feeder. A node of a given feeder is denoted as $n \in \mathcal{N}_f$ with $f \in \mathcal{F}$ and $\mathcal{N}_f \subset \mathcal{N}$. Given a feeder $f \in \mathcal{F}$ and a customer in that feeder $c \in \mathcal{C}_f$, the phase configuration of the customer is indicated as c_ψ with $\psi \in \Psi$.

3.2.4 Phase matrices

Some matrices are used to represent the initial, feasible, and track the phase configurations of the customers in the network.

Initial configuration matrix

the initial phase configuration of each customer is represented by the matrix $\mathbf{B}^{init} \in \{0,1\}^{|\mathcal{C}|\times|\Psi|}$, where a value of 1 indicates a connection to a specific phase configuration, and 0 indicates no connection. An example of the matrix $\mathbf{B}^{init}$ is given hereafter:

$$\mathbf{B}^{init}_{example} = \begin{array}{c} \\ c_1 \\ \vdots \\ c_i \\ \vdots \\ c_{|\mathcal{C}|} \end{array} \begin{array}{c} \begin{array}{cccccc} \psi_1 & \psi_2 & \cdots & \psi_{10} & \cdots & \psi_{|\Psi|} \end{array} \\ \begin{pmatrix} 1 & 0 & \cdots & 0 & \cdots & 0 \\ \vdots & \vdots & \ddots & \vdots & \ddots & \vdots \\ 0 & 0 & \cdots & 0 & \cdots & 0 \\ \vdots & \vdots & \ddots & \vdots & \ddots & \vdots \\ 0 & 0 & \cdots & 1 & \cdots & 0 \end{pmatrix} \end{array}. \tag{3.2}$$

Equation 3.2 shows how each customer $c \in \mathcal{C}$ is connected to a particular phase configuration $\psi \in \Psi$. For example, customer c_1 is connected to a single phase A (configuration $\psi_1 \in \Psi$), while the last customer, $c_{|\mathcal{C}|}$, is connected to the three-phase configuration (A, B, C) (configuration $\psi_{10} \in \Psi$).

Complement configuration matrix

we introduce the matrix $\overline{\mathbf{B}}^{init}$ as the complement of the matrix $\mathbf{B}^{init}$ where each value is inverted. This is expressed as:

$$\overline{\mathbf{B}}^{init} = \mathbb{1} - \mathbf{B}^{init}, \tag{3.3}$$

where $\mathbb{1}$ is a matrix of ones with the same dimensions as $\mathbf{B}^{init}$. The operation results in swapping the values of 0 and 1 in $\mathbf{B}^{init}$. The matrix $\overline{\mathbf{B}}^{init}$ is used later in Eq. 3.10 to count the number of reconfigurations of customer phases.

Solution configuration matrix

DSOs can change the phase configuration of each customer to achieve a more balanced network. The matrix $\mathbf{B}$ represents the final phase configuration matrix obtained after solving the optimization problem, as described in Section 3.3. Each element of $\mathbf{B}$ indicates the assigned phase configuration for a customer.

Feasible configuration matrix

not all phase configuration changes are allowed, as there are constraints on customer connections. Specifically, a customer must maintain a configuration with the same number of phases as their initial setup, meaning a customer assigned to a single-phase connection cannot be switched to a multi-phase configuration, and vice versa. For instance, a customer connected to the single phase A (e.g., $\mathbf{B}^{init}_{c1,\psi_1} = 1$) can therefore only be switched to another single phase, but cannot be connected to a multi-phase configuration, such as (A, B, C).
The matrix $\mathbf{B}^{feas}$ represents the set of feasible phase configuration changes. Considering the example matrix $\mathbf{B}^{init}_{example}$ in Eq. 3.2, $\mathbf{B}^{feas}_{example}$ is given as follows:

$$\mathbf{B}^{feas}_{example} = \begin{array}{c} \\ c_1 \\ \vdots \\ c_{|\mathcal{C}|} \end{array} \begin{array}{c} \begin{array}{cccccccc} \psi_1 & \psi_2 & \psi_3 & \psi_4 & \cdots & \psi_{10} & \cdots & \psi_{|\Psi|} \end{array} \\ \begin{pmatrix} 1 & 1 & 1 & 0 & \cdots & 0 & \cdots & 0 \\ \vdots & \vdots & \vdots & \vdots & \cdots & \vdots & \ddots & \vdots \\ 0 & 0 & 0 & 0 & \cdots & 1 & \cdots & 1 \end{pmatrix} \end{array} \tag{3.4}$$

Equation 3.4 shows the feasible configuration matrix $\mathbf{B}^{feas}$. Customer c_1 has a one-phase connection and the only feasible configurations are A, B, or C ($\mathbf{B}^{feas}_{c_1,\psi_1} = \mathbf{B}^{feas}_{c_1,\psi_2} = \mathbf{B}^{feas}_{c_1,\psi_3} = 1$). For all other phase configurations, the corresponding values are 0.

3.2.5 Customer power dynamics

The DSO evaluates the behavior of the network over a finite number of time steps. The set of all time steps is denoted as $\mathcal{T}$, and a single time step is denoted as t, with $t \in \mathcal{T}$.
At any time step t, customers can consume or produce a given amount of power. The term $P^{+}_{\phi,c,t}$ represents the power consumed on the phase $\phi \in c_\psi$ by the customer $c \in \mathcal{C}_f$ of the feeder $f \in \mathcal{F}$ during the time step $t \in \mathcal{T}$. This power consumption includes miscellaneous loads, EVs, and HPs consumption (with $P^{+}_{\phi,c,t} \geq 0$). Similarly, $P^{-}_{\phi,c,t}$ represents the power produced by PVs (with $P^{-}_{\phi,c,t} \leq 0$). The total power for each phase of each customer at any given time step is calculated as the sum of the power consumed and the power produced, expressed as:

$$P_{\phi,c,t} = P^{+}_{\phi,c,t} + P^{-}_{\phi,c,t}. \tag{3.5}$$

The matrix $P_{\phi,c,t}$ captures the net power flow for each customer, phase, and time step, providing a representation of the network dynamic behavior. The values in the matrix can be positive or negative, depending on whether consumption exceeds production or vice versa.

3.3 Problem statement

The DSO aims to determine optimal customer phase configurations in the distribution network, balancing consumption across phases while minimizing the associated reconfiguration costs. The optimization problem is defined as follows:

$$\min_{\mathbf{B}} \ \lambda^P \cdot P^{unb} + \lambda^\Psi \cdot \Psi^{chg} + \lambda^D \cdot D^{wgt} \tag{3.6a}$$

$s.t.$

$$\sum_{\psi}^{\Psi} \mathbf{B}_{c,\psi} = 1 \qquad \forall c \in \mathcal{C} \tag{3.6b}$$

$$\mathbf{B}_{c,\psi} \leq \mathbf{B}^{feas}_{c,\psi} \qquad \forall c \in \mathcal{C}, \forall \psi \in \Psi \tag{3.6c}$$

$$\mathbf{B}_{c,\psi} \in \{0,1\} \qquad \forall c \in \mathcal{C}, \forall \psi \in \Psi \tag{3.6d}$$

3.3.1 Objective terms

- **Phase unbalance impact**: represents the sum over time of the deviations of the load in each phase from the average load across the three phases. Minimizing the term in Eq. 3.7 aims to achieve a more balanced load distribution across the phases.

$$P^{unb} = \sum_{t}^{\mathcal{T}} \sum_{f}^{\mathcal{F}} \sum_{\phi}^{\Phi} |\mathcal{A}_{\phi,f,t} - \mu^{\mathcal{A}}_{f,t}|, \tag{3.7}$$

  where:

  - $\mathcal{A}_{\phi,f,t}$ represents the aggregate load of the customers connected to phase ϕ of feeder f at time t:

$$\mathcal{A}_{\phi,f,t} = \sum_{c}^{\mathcal{C}_f} P_{\phi,c,t}\,; \tag{3.8}$$

  - and $\mu^{\mathcal{A}}_{f,t}$ is the average load across phases of feeder f at time t:

$$\mu^{\mathcal{A}}_{f,t} = \frac{\sum_{\phi}^{\Phi} \mathcal{A}_{\phi,f,t}}{|\Phi|}\,. \tag{3.9}$$

- **Reconfiguration impact**: counts the number of customer phase reconfigurations:

$$\Psi^{chg} = \sum_{c}^{\mathcal{C}} \sum_{\psi}^{\Psi} \mathbf{B}_{c,\psi} \cdot \overline{\mathbf{B}}^{init}_{c,\psi} . \tag{3.10}$$

- **Customer distance impact**: considers the influence of customer distance from the transformer on the network performance:

$$D^{wgt} = \sum_{c}^{\mathcal{C}} \frac{1}{c_{dist}} \cdot \sum_{\psi}^{\Psi} \mathbf{B}_{c,\psi} \cdot \overline{\mathbf{B}}^{init}_{c,\psi} , \tag{3.11}$$

  where c_{dist} represents the distance of the customer c from the transformer, with $c_{dist} > 0$.
  Customers farther from the transformer have a greater impact on network performance due to higher voltage drops and line losses. Maximizing Eq. 3.11 prioritizes configuration changes that have the most significant impact on the network, typically those located farther away from the transformer, often at the end of the feeder.

3.3.2 Scaling factors

The factors λ^P, λ^Ψ, and λ^D are scaling parameters:

- λ^P reflects the cost of phase unbalance, including technical losses and operational inefficiencies caused by the uneven load between phases.

- λ^Ψ represents operational costs associated with changing customer phase configurations, including labor and potential downtime.

- λ^D emphasizes the importance of reconfigurations for customers located farther from the transformer.

The choice of optimization scaling parameters (λ^P, λ^Ψ, λ^D) is determined with an iterative process. Initially, weights are assigned based on the relative importance of each objective, with greater priority given to minimizing phase unbalance over reducing customer reconfigurations or addressing distance-based impacts. Posterior adjustments are made to balance trade-offs, correcting for dominant or small terms by increasing or decreasing their corresponding weights.
The final selected values are: $\lambda^P = 0.015$, $\lambda^\Psi = 6$, $\lambda^D = 1$.

3.3.3 Constraints

The optimization problem defined in Eq. 3.6 is subject to some constraints that ensure the phase reconfiguration solution is feasible. These constraints are:

- *Unique configuration assignment* (Eq. 3.6b): This constraint ensures that each customer $c \in \mathcal{C}$ is assigned exactly one phase configuration from the set of possible configurations Ψ.
- *Phase Configuration Feasibility* (Eq. 3.6c): This constraint restricts phase configuration changes to the ones that are feasible. Therefore, it ensures that the number of phases in a customer's assigned configuration matches their initial setup.

3.4 Conceptual example

This section illustrates the methodology for customer phase reconfiguration using a simplified conceptual example of a power distribution network. The example demonstrates the impact of phase configuration optimization on network unbalance.

3.4.1 Network setup

The example network consists of a 3-phase system with main lines configured for 3-phase connections, while customer connections may be single-phase or multi-phase. Figure 3.1 provides a visualization of the network and the phase configurations. The primary components include the transformer, feeders, lines, and customer nodes. Each customer is initially assigned a phase configuration, shown as blocks of different colors. The height of each block corresponds to the phase load relative to its total capacity. Moreover, customers can install DER technologies, including PVs, EVs, and HPs. The penetration rates for these DERs are as follows:

- 83% for PVs (5 out of 6 customers in Fig. 3.1),
- 50% for EVs and,
- 50% for HPs.

Time series for PVs, EVs, and HPs are assigned following the methodology explained in Appendix 3.A.

3.4.2 Optimization process

Figure 3.1 visualizes the network's phase configuration both before (Fig. 3.1a) and after (Fig. 3.1b) applying the proposed optimization. The initial configuration, $\mathbf{B}^{init}_{example}$, is presented in Eq. 3.2, with the feasible configurations specified in Eq. 3.4.

In this scenario, the DSO identified voltage issues on the A phase of the transformer, primarily due to overloading. To address these issues, an optimization process is used to mitigate phase unbalance, following the methodology described in Section 3.3.

The optimization algorithm adjusts customer phase configurations to reduce stress on the overloaded A phase, leading to a more balanced load distribution among the three phases. For instance, Fig. 3.1b shows that the configurations for customers c_1 and c_6 were updated from A and (A, B, C) to C and (C, B, A), respectively.

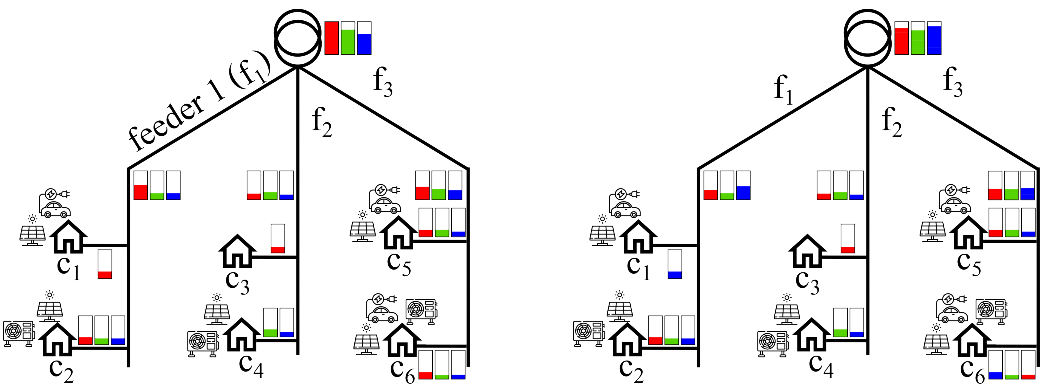

(a) Before optimization (b) After optimization

Figure 3.1: Phase configurations before and after rebalancing. Each color represents a phase: A, B and C.

The resulting solution matrix, $\mathbf{B}_{example}$, is given in Eq. 3.12. This matrix represents the final configuration, reducing voltage stress on the A phase and achieving a more balanced load across all phases.

$$\mathbf{B}_{example} = \begin{array}{c} \\ c_1 \\ \vdots \\ c_3 \\ \vdots \\ c_6 \end{array} \begin{array}{c} \begin{array}{ccccccc} \psi_1 & \psi_2 & \psi_3 & \cdots & \psi_{10} & \cdots & \psi_{|\Psi|} \end{array} \\ \begin{pmatrix} 0 & 0 & 1 & \cdots & 0 & \cdots & 0 \\ \vdots & \vdots & \vdots & \ddots & \vdots & \ddots & \vdots \\ 1 & 0 & 0 & \cdots & 0 & \cdots & 0 \\ \vdots & \vdots & \vdots & \ddots & \vdots & \ddots & \vdots \\ 0 & 0 & 0 & \cdots & 0 & \cdots & 1 \end{pmatrix} \end{array} \tag{3.12}$$

3.5 Case study results

The test network used for this study is a digital representation of a Belgian distribution network [14]. It is a 3-phase network, with 3-phase connections in main lines, while customers are either single-phase or multi-phase.

A specific test scenario is designed to assess the proposed method and to demonstrate the impact of the methodology. In this scenario, the penetration rates for different DERs are set as follows: 90% for PVs, 60% for EVs, and 50% for HPs. Time series for PVs, EVs, and HPs are assigned following the methodology explained in Appendix 3.A.

Table 3.2 shows some details about the considered network and scenario.

Table 3.2: Description of the LV distribution network.

Category	**Number of Elements**	**Details**
Transformer	1	3-phase, 400 kVA
Feeders	2	Radial configuration
Lines	44	3-phase main lines, NAVY 4x50 SE
Customers	23	14 single-phase, 9 multi-phase
DER Types	PV: 21 (91%)	4-16 kWp (62-38%)
	EV: 14 (61%)	3-15 kW (86-14%)
	HP: 12 (52%)	5-14 kW (83-17%)
DER Combinations	PV+EV: 13	56% of customers
	PV+HP: 12	52% of customers
	PV+EV+HP: 7	30% of customers
	None: 1	4% of customers

The optimization is performed over one year with a 15-minute resolution time series, therefore $|\mathcal{T}| = 35040$. For visualization purposes, data from only five days are selected for the figures. These days correspond to the 15th, 40th, 162nd, 241st, and 324th days of the year (DOY).

Figure 3.2 shows the load unbalances for each feeder and phase before the optimization. Figure 3.2a presents the load distribution across feeders and phases, while Fig. 3.2b provides a view of the unbalances for each feeder. The unbalances are calculated using Eq. 3.7. Load peaks can be observed, including high peaks primarily caused by EV charging and HP usage during periods of low PV production, and low peaks resulting during periods of low consumption combined with high PV production.

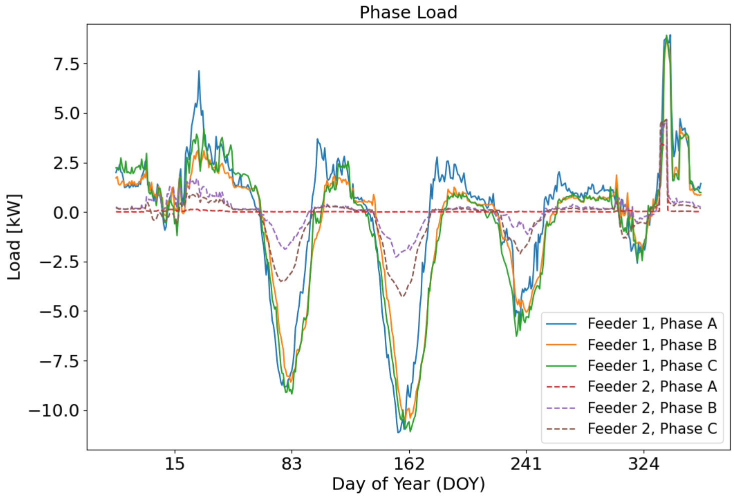

(a)

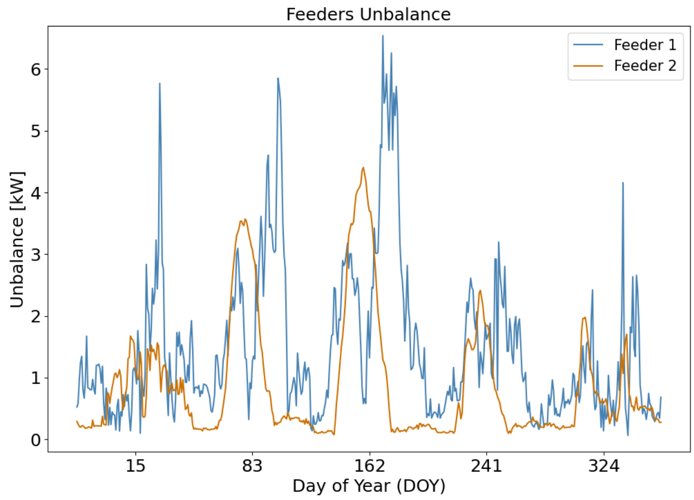

(b)

Figure 3.2: Feeder load distribution and unbalances before optimization.

Figure 3.3 displays the load unbalances in the network after optimization. In particular, Fig. 3.3a shows that the phase load curves within each feeder are now much closer to one another, indicating a reduction in phase deviations compared to before the optimization.

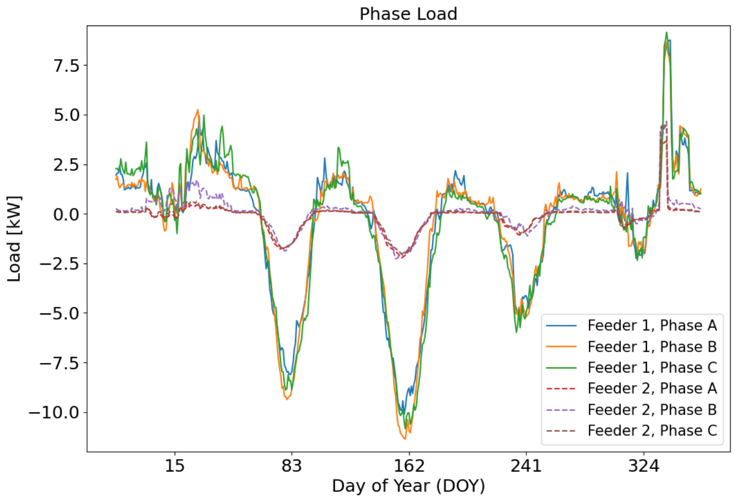

(a)

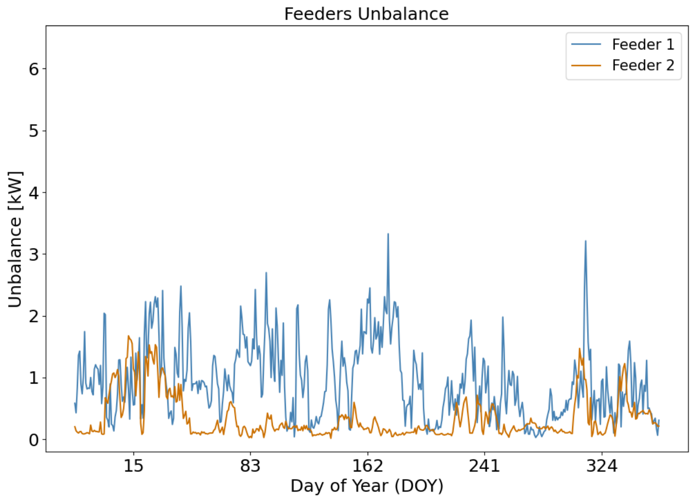

(b)

Figure 3.3: Feeder load distribution and unbalances after optimization.

Figure 3.4 compares the unbalance in the network before and after the optimization for the two feeders. It is possible to see that in both feeders the unbalance was reduced. In particular, the load unbalances were decreased by 36% for feeder 1 and 62% for feeder 2, achieved with 7 and 1 configuration changes, respectively.

A power flow is executed before and after the optimization to test whether

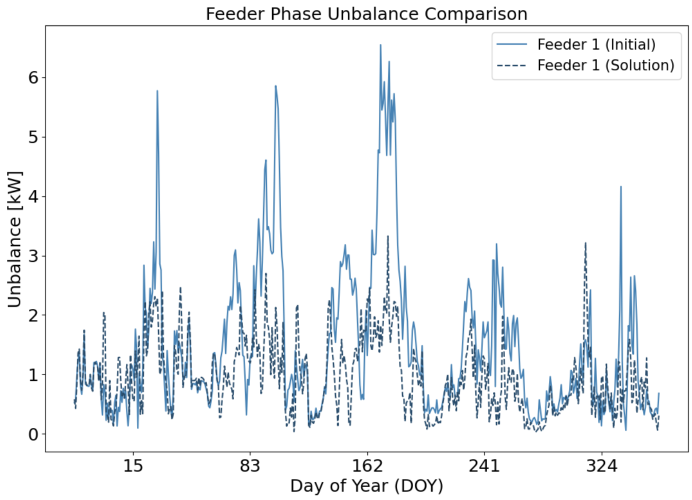

(a)

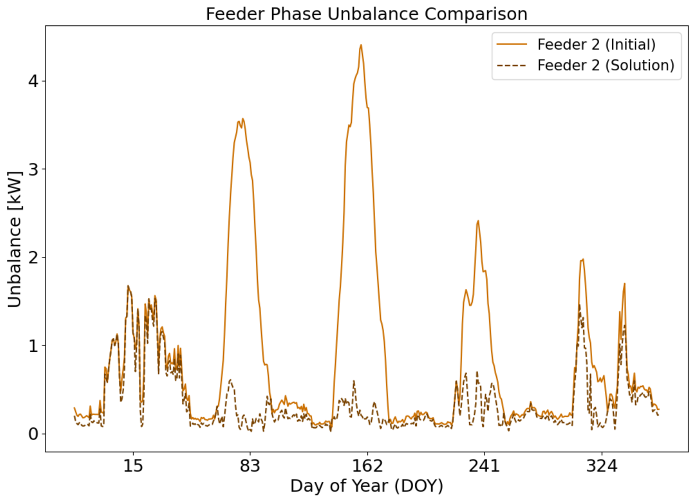

(b)

Figure 3.4: Load distribution and unbalances across feeders.

reducing the load unbalance affects the voltage and losses in the network.

Table 3.3 presents the results of the power flow analysis before and after the optimization. The results show that minimizing the load curve unbalance has a positive effect on the network's voltage profile and line losses. For feeder 1, the identified customer configurations improve voltage conditions in phase A, which was overloaded before optimization. The maximum voltage

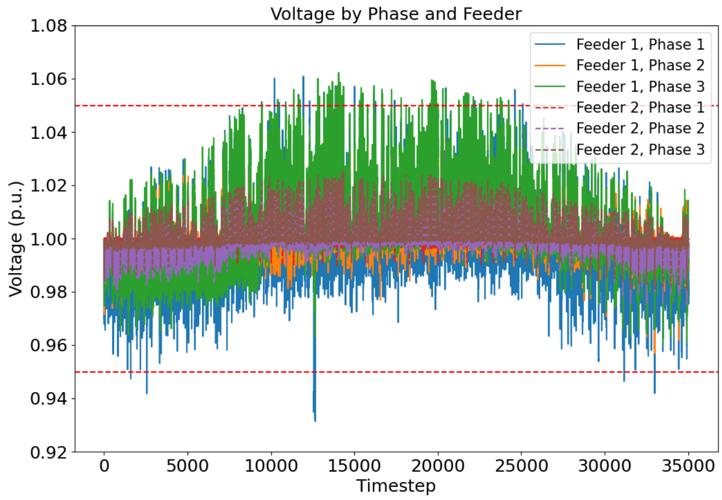

(a)

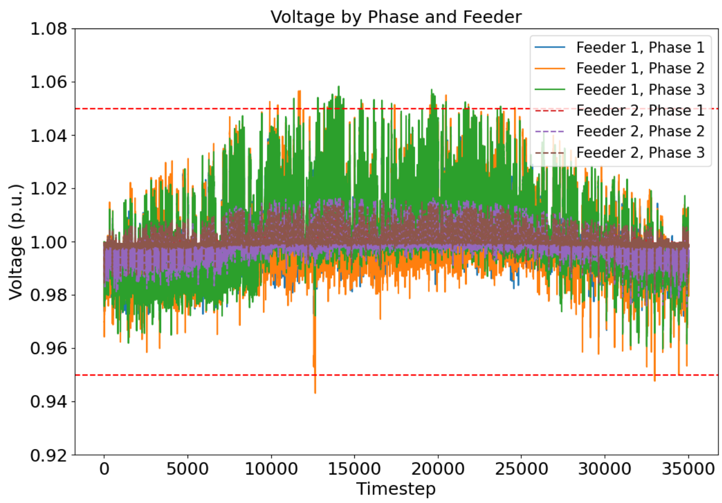

(b)

Figure 3.5: Voltage curves of the phases across feeders.

decreases from 1.0609 p.u. to 1.0482 p.u., bringing it inside the acceptable limits of 1.05, while the minimum voltage increases from 0.9313 p.u. to 0.9505 p.u. However, a side effect is observed in phase B of the same feeder, where the minimum voltage decreases from 0.9568 p.u. to 0.9430 p.u. In terms of line losses, the optimization reduces the total losses across the network by about 4.4%. However, some phases experience slight increases in losses (for

Table 3.3: Voltage and line losses comparison before and after the optimization.

Feeder	Phase	Voltage max [p.u.]		Voltage min [p.u.]		Line Losses [kWh]	
		before	after	before	after	before	after
1	A	1.0609	1.0482	0.9313	0.9505	2784	2122
	B	1.0424	1.0565	0.9568	0.9430	1835	2592
	C	1.0622	1.0582	0.9604	0.9597	2999	2651
2	A	1.0014	1.0085	0.9806	0.9861	14	72
	B	1.0181	1.0163	0.9752	0.9754	313	279
	C	1.0250	1.0154	0.9870	0.9818	258	124

example, phase C in the feeder 2) as a trade-off to achieve better overall balance and operational efficiency.

3.5.1 Cost-benefit analysis

Table 3.4 presents a cost-benefit analysis evaluating the financial and operational impacts of the proposed phase reconfiguration methodology.

The cost of each phase switch is assumed to be €40, based on typical labor and operational expenses, with 8 reconfigurations in the case study, the total switching cost is €320. Technical losses, which DSOs bear as they are not billed to customers, decrease from 8206 kWh/year to 7842 kWh/year after optimization. At an energy price of €0.20/kWh, this reduction yields annual savings of €73, resulting in a break-even period of approximately four years. Beyond loss reduction, phase reconfiguration mitigates voltage problems, reducing them by 58%. These improvements enhance network reliability, potentially decreasing equipment aging.

Table 3.4: Cost-benefit analysis of phase reconfiguration.

Metric	Before Optimization	After Optimization
Network Losses (kWh/year)[a]	8206	7842
Loss Cost (€/year)[b]	1641	1568
Savings (€/year)	-	73
Switching Cost (€)[c]	-	320
Voltage issues	535	227
Net Benefit (€, year 1)	-	-247
Break-even time (year)[d]	-	4.4

[a]Aggregated from Table 3.3. [b]At €0.20/kWh.
[c]8 switches at €40 each. [d]Assumes no additional switches.

3.6 Conclusion

This chapter addressed the second capability (**balance**) by answering RQ2 (*How can the customer phase reconfiguration problem be formulated and solved to minimize network unbalance over long temporal horizons without relying on heavy power flow calculations?*) presenting an optimization problem to address phase unbalance in power distribution networks by reconfiguring customer phase connections without relying on power flow outputs. While detailed power flow-based optimization could provide highly accurate solutions, the computational burden of solving such an optimization for a year-long horizon with 15-minute resolution makes it mostly impractical. This chapter proposes a computationally efficient alternative that delivers robust solutions to improve network conditions.

The optimization reduced phase unbalance by 36% in feeder 1 and 62% in feeder 2, with a total of 8 customer reconfigurations. Voltage profiles improved particularly in overloaded phases, bringing maximum voltages within acceptable limits. However, a slight worsening in voltage and losses was observed in some phases, highlighting the trade-offs in phase balancing.

While the re-phasing solution does not require upfront investments, it is not entirely cost-free, as there may be operational expenses involved in reconfiguring customer connections, such as labor costs. Additionally, it is a temporary solution that may need to be repeated periodically as customer demand patterns evolve. This makes it potentially less efficient than more permanent solutions like phase balancers or ANM. Therefore, future work could explore options that combine re-phasing strategies with strategies requiring more investment.

The phase reconfiguration algorithm presented in this chapter provides a way to improve the network unbalance. Yet even after optimal physical rebalancing, the network remains vulnerable to the daily and hourly variability of DER injections. EVs charge at unpredictable times; cloud cover suddenly reduces PV output; heat pumps cycle on and off. To handle these real-time fluctuations without resorting to costly and inefficient curtailment, the DSO requires a dynamic mechanism that reallocates capacity rather than physical wires. The next chapter therefore shifts to the economic domain, introducing a market-based framework that allows customers to trade their network access limits while preserving real-time security guarantees.

3.A Time series and phases assignment

In this section, we detail the implementation of the optimization problem introduced in Section 3.3. In particular, this section explains how time series (TS) data for load, PV generation, EV charging, and HP usage are assigned to each customer.

Different information is available for each customer. In particular, each *customer's total annual consumption*, *household size*, and *the number of phases* they are connected to are known. For customers equipped with smart meters (SM), additional real-time data is available, including:

- TS information on the customer's load;
- the presence of PVs;
- TS generation profiles for customers with PV installations.

For customers without SMs, detailed information on their connections and consumption/generation is generally unavailable to the DSOs. In such cases, assumptions are made regarding phase configurations and TS curves for load, PVs, EVs, and HPs when the information is missing. The assumption process is summarized in Fig. 3.6.

The assumptions are primarily driven by the annual customer consumption, household size, and the number of phases the customer is connected to, as represented by the red, green, and blue squares in the flowchart.

The installation size of the technologies can be different for the customers. In particular, for each technology, there are two main sizes, summarized in Table 3.5.

Table 3.5: Installation sizes and requirements for technology installations

Technologies	**Small installation**		**Large installation**	
	Size	**Requirements**	**Size**	**Requirements**
PVs	2 kWp	$score_c \leq 3$ & $\lvert c_\psi \rvert \leq 2$	18 kWp	$score_c > 3$ & $\lvert c_\psi \rvert > 2$
EVs	3 kW		15 kW	
HPs	3.5 kW		13 kW	

The score for a single customer $c \in \mathcal{C}$, considered in Table 3.5, is calculated as follows:

$$score_c = \frac{c_{\text{hh\_size}}}{\mu_{\text{hh\_sizes}}} + \frac{|c_\psi|}{\mu_\Phi} \tag{3.13}$$

where:

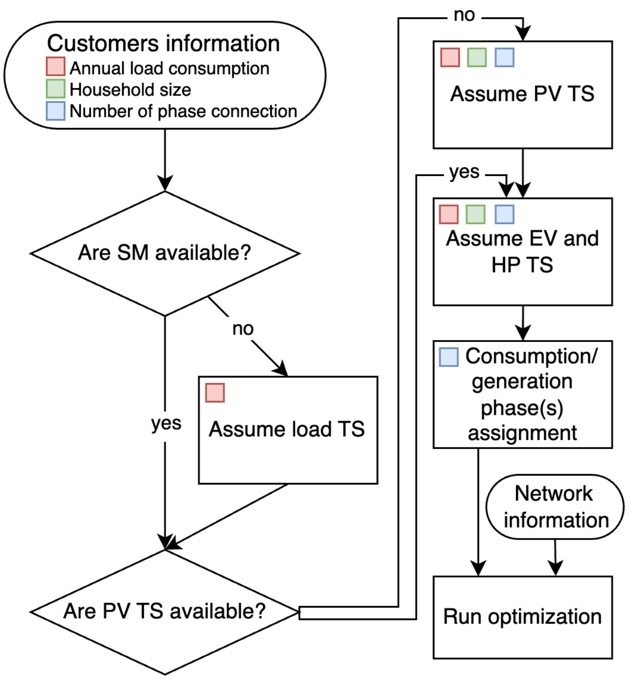

Figure 3.6: Flowchart of data availability and assumption processes.

- $c_{\text{hh\_size}}$ is the customer household size;
- $\mu_{\text{hh\_sizes}}$ is the average of the household group sizes;
- $|c_\psi|$ represents the number of phases the customer is connected to;
- μ_Φ represents the average number of phases available.

The score evaluates how likely a customer is to install a technology of a given size.

After collecting (or assuming) the TS for each customer, a phase configuration is assigned to those without SMs. Figure 3.7 illustrates the methodology used to assign consumption and production for each technology (load, PVs, EVs, and HPs) to the phase(s).

The process for phase assignment follows these steps:

- **Single-phase configuration**: If the customer is connected to only one phase, all technology consumption and generation are assigned to that phase.
- **Multi-phase configuration**: If the customer is connected to more than one phase, the assignment process depends on the size of the installation:

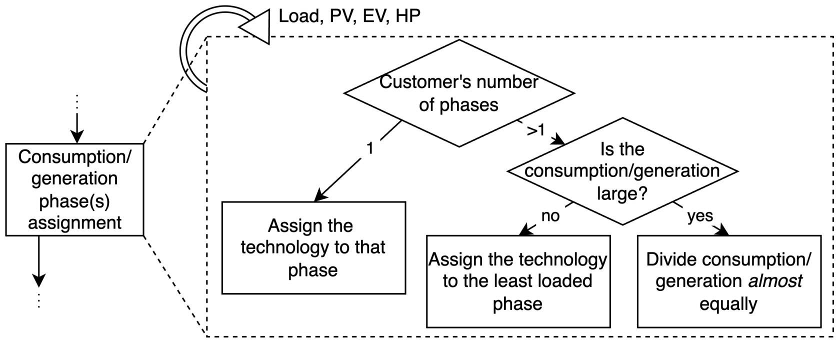

Figure 3.7: Phase configuration assignment methodology.

- If the consumption or generation is large, the load, or generation, is divided *almost equally* across the three phases where *almost equal* means that the phase distribution is based on a random variable drawn from a normal distribution. This randomized approach ensures a realistic division of consumption or generation across the phases, accounting for slight variations occurring in real-world power systems.
- If the consumption or generation is small, it is assigned to the least loaded phase. This scenario reflects the practical reality that distributing small amounts of power across phases often requires specialized equipment (for example, 3-phase inverters for PVs), which may not be cost-effective.

Chapter 4

SecuLEx: a Secure Limit Exchange Market for Dynamic Operating Envelopes

---

> Addressing the **exchange** capability of the thesis, this chapter introduces SecuLEx, a continuous market mechanism for DOEs. Moving beyond rigid, non-transferable capacity limits, this framework allows participants to buy and sell network capacity while mathematically guaranteeing real-time operational security under the direct current approximation. By bridging fair initial capacity allocation with market-driven reallocation, this chapter completes the proposed toolkit for integrating DERs.

4.1 Introduction

Managing real-time power fluctuations in distribution networks is a significant operational challenge, for which different control strategies have been proposed in the literature. ANM allows system operators to dynamically curtail PV injections, coordinate flexible loads, or schedule DERs to reduce the stress on the grid [53]. Building on these ANM principles, specific strategies such as controlled EV charging [54] have been developed to enhance network hosting capacity (HC) and avoid extensive grid reinforcement, complementing traditional approaches like targeted infrastructure upgrades [55].

However, ANM methods face practical limitations in computation scalability and adaptability in networks with high DER penetration and limited observability [56].

To address the computational burden of ANM, the concept of DOEs has emerged as a potential solution. DOEs are power limits on customer injections and withdrawals designed to guarantee network security [57]. By computing these boundaries ahead of time, the DOE framework decouples network optimization from real-time execution. Various methods have been proposed for DOE computation, with a particular focus on fairness. Authors in [58] developed a dynamic approach for assigning export limits to PV devices, explicitly considering network constraints and fairness. Authors in [59] proposed an MILP formulation to compute customer-specific limits that balance network feasibility and fairness. Similarly, [60] proposed a day-ahead stochastic optimization framework for computing fair PV limits using a linear approximation of the AC power flow model. More recent works have considered probabilistic and robust envelope construction to account for the uncertainties in DER generation and load forecasting [61, 62]. While these centralized approaches ensure network security and fair allocation, they treat DOEs as fixed and non-transferable, limiting the ability to fully leverage the network's flexibility under high DER penetration.

In parallel to such control or predictive approaches, market mechanisms have emerged as tools for coordinating DERs in distribution systems. Local energy markets (LEMs) enable peer-to-peer (P2P) trading of energy, facilitating localized balancing and reducing reliance on central infrastructure [63, 64]. Similar works explore market-clearing mechanisms that incorporate voltage and network constraints directly into auction models [65], or game-theoretic frameworks to manage uncertainties in networks with high integration of DERs [66]. Despite these advancements, existing market mechanisms are almost exclusively designed for trading energy (kWh) rather than physical network capacity (kW), and their potential for DOE allocation has found limited application so far. Recent works have begun bridging this gap. Authors in [67] proposed a market-based mechanism to manage injection congestion, and [68] explored DOE-integrated cooperative energy trading with fair allocation. These contributions highlight the potential of market-driven DOE management but stop short of providing a unified framework for secure limit exchange.

This chapter presents SecuLEx, a novel market-based framework that enables customers to trade their DOEs while ensuring network security. Unlike existing static approaches, SecuLEx provides a framework through which customers can reallocate limits according to their needs, offering a possible improvement in the use of existing network capacity. The main contributions of this work are the following:

- We propose an initial DOE allocation mechanism based on lexicographic max–min optimization that maximizes envelope sizes, ensures fairness across customers, and guarantees secure network operation. This allocation provides limits before market exchanges.

- We propose a market mechanism for trading portions of DOEs. The mechanism includes *i)* a definition of orders for buying and selling limits, *ii)* a market-clearing optimization that maximizes social welfare while enforcing network security constraints, and *iii)* a settlement rule determining the limits of transfers between participants.

The rest of the chapter is organized as follows. Section 4.2 presents the mathematical foundation for grid operation using DOEs, including network representation, DOE definitions, security verification mechanisms, and DOE allocation. Section 4.3 introduces the SecuLEx market organization, covering temporal market structure, order specifications, and the clearing and settlement mechanisms. Section 4.4 provides a concrete implementation and illustration of SecuLEx for a radial LV network. Section 4.5 discusses key design choices and limitations of the proposed approach. Section 4.6 concludes the chapter and outlines future research directions.

4.2 Grid operation with envelopes

This section establishes the mathematical foundation for operating distribution networks using DOEs. Section 4.2.1 presents the network model. Section 4.2.2 formalizes the concept of DOEs. Section 4.2.3 introduces the security verification function that checks network security under the given DOEs. Section 4.2.4 formulates the optimization for DOE allocation.

4.2.1 Network representation

An electrical network is modeled as a directed graph, denoted by $\mathfrak{G} = (\mathcal{N}, \mathcal{E})$, where $\mathcal{N}$ represents the set of nodes and $\mathcal{E} \subset \mathcal{N} \times \mathcal{N}$ represents the set of directed edges. Each node $n \in \mathcal{N}$ corresponds to a network component, such as a transformer or a customer. Each edge $e \in \mathcal{E}$ establishes a connection between two nodes of the set $\mathcal{N}$ and is commonly referred to as a line. The orientation is arbitrarily fixed by convention to simplify later modeling.

Network constraints

Each node $n \in \mathcal{N}$ has an associated voltage $V_n \in \mathbb{C}$, and $V \in \mathbb{C}^{|\mathcal{N}|}$ is the voltage vector composed of the voltages at each node $n \in \mathcal{N}$. The voltage magnitude at each node $n \in \mathcal{N}$ must satisfy the voltage magnitude constraint $\underline{V} \leq |V_n| \leq \overline{V}$, where $\underline{V}, \overline{V} \in \mathbb{R}_+$ are the minimum and maximum allowable voltage magnitudes. Similarly, each line $e \in \mathcal{E}$ has an associated current flowing through the line $I_e \in \mathbb{C}$, and $I \in \mathbb{C}^{|\mathcal{E}|}$ is the current vector composed of the current flows at each line $e \in \mathcal{E}$. Each line $e \in \mathcal{E}$ must satisfy the current magnitude constraint $|I_e| \leq \overline{I}$, where $\overline{I} \in \mathbb{R}_+$ is the maximum current allowed through a line.

Customers' power usage

Let $\mathcal{C} \subset \mathcal{N}$ be the set of customer nodes, i.e., nodes where power is withdrawn or injected. Let $S_c = P_c + jQ_c \in \mathbb{C}$ denote the complex power consumption of $c \in \mathcal{C}$, composed of an active part $P_c \in \mathbb{R}$ and a reactive part $Q_c \in \mathbb{R}$. By convention, positive power values correspond to withdrawal and negative values to injection.

4.2.2 DOEs definition

The DSO assigns DOEs, specifying the upper and lower limits of active and reactive power each customer is allowed to consume. These limits are dynamic, meaning that they can change over time, e.g., through trading or through a reallocation imposed by the DSO. When all customers respect their limits, the network is guaranteed to operate within secure voltage and current limits. DOEs are specified by the complex matrix $\mathbf{L}$ of dimension $|\mathcal{C}| \times 2$, defined as:

$$\mathbf{L} = [\underline{S}, \overline{S}] = \begin{bmatrix} \underline{S}_1 & \overline{S}_1 \\ \vdots & \vdots \\ \underline{S}_{|\mathcal{C}|} & \overline{S}_{|\mathcal{C}|} \end{bmatrix}, \tag{4.1}$$

where $\underline{S}_c = \underline{P}_c + j\underline{Q}_c$ and $\overline{S}_c = \overline{P}_c + j\overline{Q}_c$ represent the lower and upper limits for customer $c \in \mathcal{C}$. We write $S = P + jQ \in \mathbf{L}$ when P and Q both respect the bounds defined in the DOE matrix for each customer.

4.2.3 Security verification function

To ensure secure network operations, we introduce a verification function $VerifyLimits$ that determines whether a given DOE allocation preserves network security. The function returns a non-positive value if and only if the limit matrix $\mathbf{L}$ ensures secure operation:

$$\begin{cases} VerifyLimits(\mathfrak{G}, \mathbf{L}) \leq 0 & \forall S \in \mathbf{L} : \mathfrak{G} \text{ is secure}, \\ VerifyLimits(\mathfrak{G}, \mathbf{L}) > 0 & \text{otherwise.} \end{cases} \tag{4.2}$$

Evaluating this function requires solving the power flow:

$$V, I = PowerFlow(\mathfrak{G}, S) \qquad \forall S \in \mathbf{L}, \tag{4.3}$$

and verifying that the voltage limit $\underline{V} \leq |V| \leq \overline{V}$ and current limit $|I| \leq \overline{I}$ are respected $\forall S \in \mathbf{L}$.

4.2.4 DOEs allocation

DOE allocation is formulated as a constrained optimization problem that maximizes network utility while guaranteeing secure operation for any power profile within the assigned limits. This optimization problem is formulated as follows:

$$\max_{\mathbf{L}} \quad U(\mathbf{L}), \tag{4.4a}$$

$$\text{s.t.} \quad VerifyLimits(\mathfrak{G}, \mathbf{L}) \leq 0, \tag{4.4b}$$

where U is a general utility function representing the DSO's objective, such as maximizing customer flexibility, fairness, or system efficiency. The function $VerifyLimits$ ensures that, for all power injections within limits, the network remains within secure operational boundaries.

4.3 SecuLEx market organization

This section presents the market framework that enables customers to exchange their DOEs. Section 4.3.1 defines the temporal organization of trading periods. Section 4.3.2 specifies the order structure and book management for buy and sell requests of envelope portions. Section 4.3.3 introduces the clearing mechanism and Section 4.3.4 the settlement function that determines the money exchanges between customers.

4.3.1 Limit market temporal operation

In SecuLEx, DOEs are assigned in advance for future time periods, called *products*. For example, the DSO may assign limits one day in advance for all hour intervals of the following day. A product is identified by its starting time $t \in \mathcal{T}$ (e.g., $\mathcal{T} = \{00{:}00\,, 01{:}00\,, 02{:}00\,, \dots\,, 23{:}00\}$ for 24-hour intervals in a day). For each product $t \in \mathcal{T}$, the exchange window opens immediately after the DOE assignment and closes shortly before the corresponding time period. This allows participants to adjust their limits to reflect updated forecasts or preferences.

Figure 4.1 illustrates the temporal structure of a single product: the DSO assigns DOEs, the continuous exchange window opens, the order book fills, and trading continues until market closure just before real-time operation.

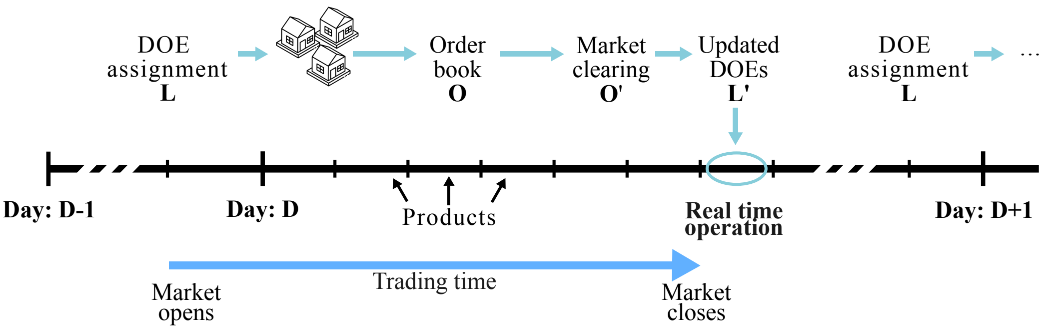

Figure 4.1: Timeline illustrating the sequence from the initial DOE assignment by the DSO to the closing of the continuous exchange window just before the operating period.

4.3.2 Orders and order book

Customers participate in the market by submitting orders to buy or sell portions of their assigned injection and withdrawal limits. A buy order reflects a desire to increase capacity: customers may request additional upper limits to gain withdrawal capacity, or additional lower limits to gain injection capacity. On the contrary, a sell order signals a willingness to sell unused capacity in exchange for financial compensation. Formally, each order o is defined as the tuple:

$$o = (id,\ c,\ type,\ bound,\ power,\ \Delta,\ \pi,\ t), \tag{4.5}$$

where:

- $id \in \mathbb{N}$ is a unique identifier,
- $c \in \mathcal{C}$ is the customer submitting the order,
- $type \in \{\text{buy},\ \text{sell}\}$ distinguishes demand from supply,

- *bound* $\in$ {lower, upper} indicates whether the order concerns the lower or upper limit of the DOE,
- *power* $\in$ {active, reactive} is the nature of the change,
- $\Delta \in \mathbb{R}_+$ is the requested change in limit (kW or kVAR).
- $\pi \in \mathbb{R}$ is the offered price (€/kW or €/kVAR),
- $t \in \mathcal{T}$ is the target time period (i.e., product time),

Orders are stored in the order book $\mathcal{O}$, which we formalize as the set of order identifiers. We define $\mathcal{S}$ and $\mathcal{B}$ as the sets of identifiers for the sell and buy orders. Similarly, $\mathcal{L}$ and $\mathcal{U}$ are the sets of identifiers for orders on lower and upper limits.

4.3.3 Clearing function

Given the limit matrix $\mathbf{L}$ and the order book $\mathcal{O}$, a market operator clears the market by matching buy and sell orders. The clearing process determines which orders are accepted and updates both the DOE limits and the order book accordingly. This process is formalized as:

$$\mathbf{L}', \mathcal{O}' = Clear(\mathbf{L}, \mathcal{O}), \tag{4.6}$$

where $\mathbf{L}'$ is the updated limit matrix reflecting all accepted orders and $\mathcal{O}'$ is the updated order book containing unmatched and partially matched orders.

The updated limit matrix $\mathbf{L}'$ must preserve network security:

$$VerifyLimits(\mathfrak{G}, \mathbf{L}') \leq 0. \tag{4.7}$$

We assume the market operator clears orders instantaneously and publishes updated DOEs immediately, enabling continuous trading and real-time adjustment of operating limits throughout the trading window.

4.3.4 Settlement function

Once orders are executed and limits updated, a settlement process determines the financial compensation for each customer. We define the settlement function as:

$$\Pi = Settlement(\mathbf{L}, \mathbf{L}', \mathcal{O}, \mathcal{O}'), \tag{4.8}$$

where $\Pi \in \mathbb{R}^{|\mathcal{C}|}$ is the resulting payment vector composed of the price compensations Π_c for each customer $c \in \mathcal{C}$. A positive Π_c indicates a payment by the customer $c \in \mathcal{C}$, and a negative Π_c indicates a payment to the customer $c \in \mathcal{C}$.

Similarly to the clearing function, we assume that the settlement is computed instantaneously after clearing and that the payment is due to the market operator.

4.4 Concrete implementation of SecuLEx

This section provides a practical implementation of SecuLEx that achieves computational efficiency while providing limits that maintain network security under DC power flow approximation. Section 4.4.1 describes a fair DOE allocation mechanism. Section 4.4.2 describes a computationally efficient clearing mechanism for maximizing social welfare while ensuring trades preserve network security. Section 4.4.3 provides an illustrative example.

4.4.1 Grid operation implementation

Security verification function

Without additional assumptions, the security verification function in Eq. 4.2 requires solving a power flow for each $S \in \mathbf{L}$ and verifying that the voltages and currents respect the security constraints.

In this implementation, we consider a radial network and adopt a DC power flow approximation of the power flow Eq. 4.3. In this approximation, voltages take constant real values, and the complex parts of currents and powers equal zero. Security is then expressed as constraints on the active power flow through lines, rather than voltage and current constraints. DOEs are also reduced to limits on active power and $\mathbf{L} = [\underline{P}, \overline{P}]$. Under these assumptions, we prove in Appendix 4.A that the security verification function in Eq. 4.2 simplifies to confirming that the network $\mathfrak{G}$ remains secure only for the two boundaries, $\underline{P}$ and $\overline{P}$, of the DOE matrix:

$$\begin{cases} VerifyLimits(\mathfrak{G}, \mathbf{L}) \leq 0 & \text{if } \mathfrak{G} \text{ secure for both } \underline{P} \text{ and } \overline{P}; \\ VerifyLimits(\mathfrak{G}, \mathbf{L}) > 0 & \text{otherwise.} \end{cases} \tag{4.9}$$

DOE allocation

We assume that the DSO wants to maximize the envelope sizes while guaranteeing fairness, in the sense that the size of the smallest envelopes is maximized first. Such a multi-objective function can be formulated as a (complex) maximum utility problem as in Eq. 4.4, which eventually corresponds to solving the following (simpler) lexicographic max-min optimization problem [69]:

$$
\begin{aligned}
\operatorname{lex}\max_{\mathbf{L}} \min \quad & |\underline{P}_c - \overline{P}_c| && \forall c \in \mathcal{C}, && (4.10a)\\
\text{s.t.} \quad & \underline{P}_c^{\text{contr}} \le \underline{P}_c \le \underline{P}_c^{\text{guar}} && \forall c \in \mathcal{C}, && (4.10b)\\
& \overline{P}_c^{\text{guar}} \le \overline{P}_c \le \overline{P}_c^{\text{contr}} && \forall c \in \mathcal{C}, && (4.10c)\\
& \underline{P}_c \le \overline{P}_c && \forall c \in \mathcal{C}, && (4.10d)\\
& \mathbf{L}_c = [\underline{P}_c, \overline{P}_c] && \forall c \in \mathcal{C}, && (4.10e)\\
& VerifyLimits(\mathfrak{G}, \mathbf{L}) \le 0\ . && && (4.10f)
\end{aligned}
$$

The parameters $\underline{P}_c^{\text{guar}}, \overline{P}_c^{\text{guar}}$ denote minimum guaranteed withdrawal/injection limits, while $\underline{P}_c^{\text{contr}}, \overline{P}_c^{\text{contr}}$ denote the contractual extrema based on equipment capacity.

Despite its complex appearance, the problem in Eq. 4.10 can easily be solved by successively maximizing the size of the smallest envelope that can still be enlarged. Let $\mathcal{C}' \subseteq \mathcal{C}$ be the set of customers whose envelopes are already fixed to $[\underline{P}_{c'}^*, \overline{P}_{c'}^*]$, for all $c' \in \mathcal{C}'$. New envelopes are iteratively computed by solving:

$$
\begin{aligned}
\max_{w,\mathbf{L}} \quad & w, && && (4.11a)\\
\text{s.t.} \quad & \underline{P}_c^{\text{contr}} \le \underline{P}_c \le \underline{P}_c^{\text{guar}} && \forall c \notin \mathcal{C}', && (4.11b)\\
& \overline{P}_c^{\text{guar}} \le \overline{P}_c \le \overline{P}_c^{\text{contr}} && \forall c \notin \mathcal{C}', && (4.11c)\\
& \underline{P}_c = \underline{P}_c^* && \forall c \in \mathcal{C}', && (4.11d)\\
& \overline{P}_c = \overline{P}_c^* && \forall c \in \mathcal{C}', && (4.11e)\\
& \underline{P}_c \le \overline{P}_c && \forall c \in \mathcal{C}, && (4.11f)\\
& w \le \overline{P}_c - \underline{P}_c && \forall c \notin \mathcal{C}', && (4.11g)\\
& \mathbf{L}_c = [\underline{P}_c, \overline{P}_c] && \forall c \in \mathcal{C}', && (4.11h)\\
& VerifyLimits(\mathfrak{G}, \mathbf{L}) \le 0. && && (4.11i)
\end{aligned}
$$

The solution to the optimization problem is the DOE matrix $\mathbf{L}^*$ and the width w^*. The customer(s) for which the constraint Eq. 4.11g is tight, i.e., $\overline{P}_c^* - \underline{P}_c^* = w^*$, have their envelopes fixed at the current values $\mathbf{L}_c^* = [\underline{P}_c^*, \overline{P}_c^*]$. These customers are added to $\mathcal{C}'$, and the procedure repeats until all customers have been assigned fixed envelopes.

4.4.2 SecuLEx market implementation

Clearing function

The clearing function implements a centralized market where orders are accepted to maximize the social welfare. Here, accepted orders lead to updated envelopes that are constrained by the security verification function. Assuming orders can be partially cleared, we compute for each order $o \in \mathcal{O} = \mathcal{B} \cup \mathcal{S}$ the accepted quantity a_o by solving:

$$\begin{aligned}
\max_{a,\mathbf{L}'} \quad & \sum_{b\in\mathcal{B}} \pi_b a_b - \sum_{s\in\mathcal{S}} \pi_s a_s, && && (4.12a)\\
\text{s.t.} \quad & 0 \leq a_o \leq \Delta P_o && \forall o \in \mathcal{O}, && (4.12b)\\
& \underline{P}'_c = \underline{P}_c + \sum_{\substack{s\in\mathcal{S}\cap\mathcal{L}:\\ c_s=c}} a_s - \sum_{\substack{b\in\mathcal{B}\cap\mathcal{L}:\\ c_b=c}} a_b && \forall c \in \mathcal{C}, && (4.12c)\\
& \overline{P}'_c = \overline{P}_c - \sum_{\substack{s\in\mathcal{S}\cap\mathcal{U}:\\ c_s=c}} a_s + \sum_{\substack{b\in\mathcal{B}\cap\mathcal{U}:\\ c_b=c}} a_b && \forall c \in \mathcal{C}, && (4.12d)\\
& \underline{P}'_c \leq \overline{P}'_c && \forall c \in \mathcal{C}, && (4.12e)\\
& \mathbf{L}' = [\underline{P}', \overline{P}'], && && (4.12f)\\
& VerifyLimits(\mathfrak{G}, \mathbf{L}') \leq 0. && && (4.12g)
\end{aligned}$$

Solving this optimization problem provides the updated secure limits $\mathbf{L}'$ and the updated order book $\mathcal{O}'$ containing the uncleared quantities.

Settlement function

Orders are settled on a pay-as-bid settlement mechanism. Each customer's total payment equals the sum of their individual order payments, where each order payment is the order price multiplied by the cleared quantity:

$$\Pi_c = \sum_{b\in\mathcal{B}:c_b=c} a_b\pi_b - \sum_{s\in\mathcal{S}:c_s=c} a_s\pi_s. \tag{4.13}$$

The pay-as-bid settlement leads to a surplus that equals the social welfare SW and that is captured by the market operator:

$$SW = \sum_{c\in\mathcal{C}} \Pi_c = \sum_{b\in\mathcal{B}} \pi_b a_b - \sum_{s\in\mathcal{S}} \pi_s a_s. \tag{4.14}$$

4.4.3 Illustrative example

This section illustrates SecuLEx on a simple radial LV distribution network. The illustration follows the temporal structure outlined in Fig. 4.1, considering the DOE assignment on Day $D-1$ for a single period of one hour (12:00-13:00 on Day D), with continuous market operation starting at DOE assignment until real-time (12:00). We present a scenario with congestion and demonstrate the value of SecuLEx compared to alternative management strategies.

The network is represented by the graph $\mathfrak{G} = (\mathcal{N},\ \mathcal{E})$, with nodes $\mathcal{N} = \{T,\ B,\ C_1,\ C_2,\ C_3,\ C_4\}$ corresponding to a transformer T, an intermediate bus B, and four representative customers. Each customer is connected to the bus B that is supplied by the transformer T. The interconnections are represented by the edges $\mathcal{E} = \{(T,B),\ (B,C_1),\ (B,C_2),\ (B,C_3),\ (B,C_4)\}$. The transformer must operate below 60kW, which translates to a security constraint limiting the power flowing through $(T,\ B)$ to 60kW.

Let us consider that during the day, customers have estimations of their future consumption for the midday period. Customers have the following installations, expected consumptions for that period, and known electricity prices:

- C_1 is a load-only: net withdrawal 8kW. They pay 0.15€/kWh.
- C_2 has a PV installation: net injection 21kW. They pay 0.16€/kWh for withdrawal and get paid 0.06€/kWh for injection.
- C_3 has a PV installation: net injection 26kW. They pay 0.15€/kWh for withdrawal and get paid 0.04€/kWh for injection.
- C_4 has a PV-battery installation: PV production of 24kW, battery capacity of $\pm$10kW and discharging by 6kW; net injection 30kW. They pay 0.15€/kWh for withdrawal and get paid 0.02€/kWh for injection.

In this scenario, at midday, there is an expected reverse power flow from the customers to the transformer of 69kW. The magnitude of this power flow exceeds the transformer's 60kW limit, causing congestion, as shown in Fig. 4.2.

Let us compare the outcome depending on the congestion-management scheme of the DSO, assuming that the expected customer consumption is realized at midday.

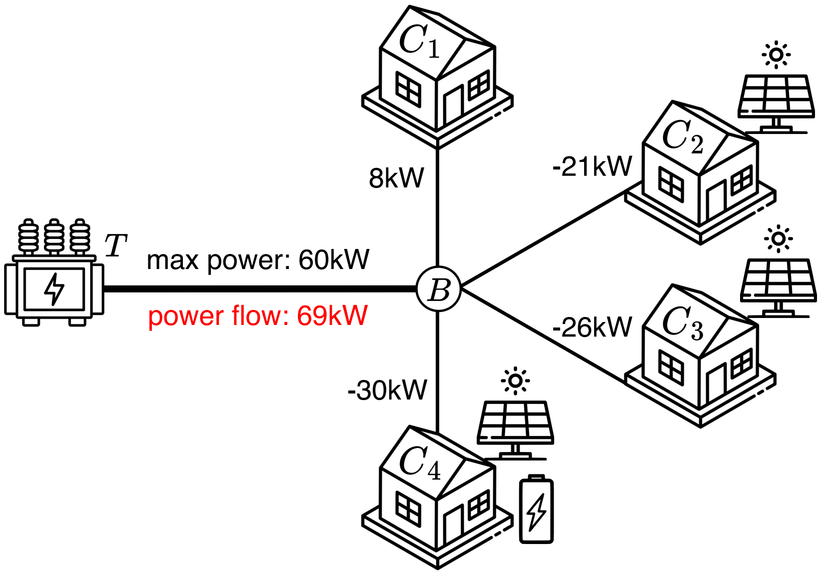

Figure 4.2: Baseline situation where the reverse power flow (69kW) exceeds the transformer limit (60kW), causing congestion.

No control

In this scenario, the DSO takes no action. Without intervention, the line (T, B) is overloaded by 9kW. This causes a security issue; while sustained lower levels of overload accelerate equipment aging, higher levels can activate protective mechanisms, potentially leading to line disconnection and customer disruption at the cost of the DSO.

Centralized ANM

This case represents a traditional management scheme where the DSO reacts in real-time when the problem is emerging. The DSO issues curtailment commands to eliminate the overload, but cannot control customer batteries (no contractual access).

Let us assume that the DSO takes the minimal corrective actions to guarantee security and curtails PV generation equally across C_2, C_3, and C_4 until the limit is respected. Thus, the total curtailed PV is 9kW, equally divided over the three customers injecting power, and the transformer operates securely at 60kW. Curtailment leads to an opportunity loss of $3 \cdot 0.06 + 3 \cdot 0.04 + 3 \cdot 0.02 = 0.36$€.

Static envelope assignment

In this case, the DSO assigns static envelopes one day ahead (Day $D-1$), solving the lexicographic max-min allocation from Eq. 4.10. Here, the security verification function is implemented relying on linearized (DC) power flow equations as discussed previously, leading to the simplified implementation of Eq. 4.9.

An optimal envelope allocation is:

$$\begin{aligned} \mathbf{L}_1 &= [0, 15], & \mathbf{L}_2 &= [-20, 15], \\ \mathbf{L}_3 &= [-20, 15], & \mathbf{L}_4 &= [-20, 15]. \end{aligned}$$

Customers are curtailed in case of envelope violation, guaranteeing secure and distributed real-time operation.

At this stage, customers without flexibility have no alternative to curtailment. Nevertheless, customers with available flexibility may decide to adapt their consumption pattern, knowing the conditions of curtailment. This choice is driven by the balance between the opportunity loss due to curtailment and the cost of changing the schedule, i.e., the expected reduction of the profit from strategically charging and discharging the battery during the day.

We consider two cases, depending on Customer C_4:

- Customer C_4 evaluates that changing the battery schedule may be too expensive, considering their low opportunity loss. The customer maintains their planned discharge, resulting in a net injection of 30kW, which violates their envelope and triggers 10kW of curtailment. Combined with curtailment from other customers, the total curtailment reaches 17kW during one hour, leading to an opportunity loss of $1 \cdot 0.06 + 6 \cdot 0.04 + 10 \cdot 0.02 = 0.50$€.

- Customer C_4 anticipates curtailment and charges their battery with 4kW instead of injecting power, remaining within their assigned limit with a net injection of 20kW. The total curtailment is 7kW during one hour and leads to an opportunity loss of $1 \cdot 0.06 + 6 \cdot 0.04 = 0.30$€.

In this scenario, as customers know their limits, they are incentivized to use their flexibility. Nevertheless, static envelopes are conservative and may result, in this case, in greater curtailment compared to the centralized ANM, which only responds to the actual congestion observed in real-time.

DOE with SecuLEx

Starting from the DOE allocation above, market participants can submit orders to buy/sell portions of their envelopes. In theory, this exchange is driven by their expected future energy usage and corresponding cost.

In an ideal market, each customer should submit orders to maximize their expected future profit. It includes minimizing the expected costs that may result from future curtailment, optimizing the consumption schedules depending on the hourly costs of energy, and maximizing the expected revenues from selling unused parts of their envelopes. In the hypothetical case where customers have known and inflexible future consumptions, they should ask for additional limits to avoid curtailment at the incurred marginal cost and bid unused limits at zero marginal cost. Customers with flexibility furthermore submit orders to also optimize their consumption schedules. In practice, uncertainty about future consumptions, market inefficiencies, and speculation are reflected in prices and volumes.

Let us illustrate the trading incentives in this context:

- Customer C_1 is expecting to withdraw power from the network, and we assume they are not interested in entering the market. It may be considered a market inefficiency or may be due to the need for flexibility within their current envelope.

- Customer C_2 is expecting curtailment of 1kW during one hour, leading to an opportunity loss of 0.06€. The customer thus offers to buy 1kW of lower limits at the price of 0.03€/kW.

- Customer C_3 is expecting curtailment of 6kW during one hour, leading to an opportunity loss of $6 \cdot 0.04 = 0.24$€. The customer offers to buy 6kW of lower limits at the price of 0.02€/kW.

- Customer C_4 is expecting curtailment of 10kW during one hour, leading to an opportunity loss of $10 \cdot 0.02 = 0.20$€, if they discharge their battery. On the one hand, the customer could ask 10kW additional lower limit to avoid curtailment. On the other hand, expecting that lower limits are going to be scarce on the market, they can decide to exploit their battery's flexibility to charge the battery by 10kW. Then, the customer respects its DOE and may even bid 6kW of lower limit. Assuming this situation occurs, the order price should reflect the cost of rescheduling the battery and is assumed to be 0.02€/kW.

All corresponding orders are represented in Table 4.1.

Table 4.1: Initial order book.

ID	Customer	Type	Bound	Price [€/kW]	Quantity [kW]
1	C_2	Buy	Lower	0.03	1
2	C_3	Buy	Lower	0.02	6
3	C_4	Sell	Lower	0.02	6

Providing this order book, the market-clearing algorithm of Eq. 4.12 can be executed and yields the following updated limits:

$$\mathbf{L}_1 = [0, 15], \qquad \mathbf{L}_2 = [-21, 15],$$
$$\mathbf{L}_3 = [-25, 15], \qquad \mathbf{L}_4 = [-14, 15].$$

The exchange between consumers and new envelopes corresponds to a complete clear of orders from Customer C_2 and Customer C_4, and a partial clear of the order from Customer C_3. The updated order book corresponds to the uncleared orders and is represented in Table 4.2.

Under the pay-as-bid principle, Customer C_2 pays $\Pi_{C_2} = 1 \cdot 0.03 = 0.03$€, Customer C_3 pays $\Pi_{C_3} = 5 \cdot 0.02 = 0.10$€, and Customer C_4 is paid $-\Pi_{C_4} = 6 \cdot 0.02 = 0.12$€. The social welfare $SW = 0.01$€is captured by the market operator, as a regulated fee to reduce tariffs or reinvest in the grid.

Table 4.2: Updated order book.

ID	Customer	Type	Bound	Price [€/kW]	Quantity [kW]
2	C_3	Buy	Lower	0.02	1

Customers may submit additional orders as their consumption forecasts evolve, continuing until the market closure, where DOEs are frozen. Let us consider that no additional exchange materializes and that the expected consumptions and injections are realized in real-time. Customer C_3 is the only customer with excess injection and is curtailed by 1kW. The market has created incentives for exploiting flexibility, and Customer C_4 has adapted its behavior to absorb some of the PV production, leading to smaller curtailment.

Summary

Table 4.3 summarizes the performance of the different management schemes. As discussed previously, SecuLEx incentivizes the use of flexibility without requiring real-time centralized operation, leading to the lowest curtailment, highest renewable utilization, and market social welfare.

Table 4.3: Comparison of management approaches.

Metric	**No Control**	**ANM**	**Static envelopes**	**SecuLEx**
Curtailment [kW]	0	9	17 or 7	1
Renewable utilization [%]	100	87	76 or 90	99
Security violation	Yes	No	No	No
Incentivizes flexibility	No	No	Partial	Yes
Market social welfare [€]	/	/	/	0.01

4.5 Discussion

SecuLEx represents a change in network operation in two fundamental respects. First, it moves from operation strategies in reaction to security issues, such as ANM, to forward planning of envelopes that guarantee security under the adopted linear modeling framework. Second, it introduces market-driven coordination that allows responsiveness to real-time system conditions and customer preferences. This section reflects on technical aspects of the implementation and economic implications related to SecuLEx.

4.5.1 Technical and computational challenges

Computational scalability

The initial envelope allocation and order clearing both require solving optimization problems, respectively, problem Eq. 4.10 and Eq. 4.12. In practice, the first problem requires solving one optimization program per customer, where the number of variables and constraints scales linearly with the number of customers. In the second problem, variables and constraints scale linearly with the number of orders. As the number of participants and orders grows, solving these optimization problems may become computationally prohibitive. This could necessitate reconsidering the continuous clearing mechanism or resorting to heuristic approaches that trade optimality for tractability.

Network security verification

In Appendix 4.A, we show that, for radial network topology and DC power flow, the problem reduces to verifying security only at the DOE boundaries.

This simplification may not hold for networks with large losses, in meshed topologies, heavily loaded feeders, or cases with advanced reactive power control. In these cases, ensuring security when solving optimization problems Eq. 4.10 and Eq. 4.12 may become intractable in practice. Possible resolutions include using convex approximations of the AC power flow, where similar simplified resolution techniques exist [70, 71], or evaluating constraints with high probability through sampling-based approaches. Depending on the simplification and approximation used in practice, security guarantees may be lost for some real-time operation conditions [71].

4.5.2 Economic and market design implications

Initial DOE allocation

The initial DOE allocation in SecuLEx is achieved by solving the lexicographic max-min problem in Eq. 4.10. It implements an egalitarian rule, where the sizes of the smallest envelopes are maximized first. Beyond the technical challenges discussed previously, the uniqueness of the solution is not guaranteed, and the fairness requirement may lead to inefficient operation. Typically, envelopes may be small due to blocking consumers, or may be unrelated to the effective energy needs. Alternative allocation rules exist to deal with such problems, including allocation for maximum total network utilization, priority allocation favoring certain customer classes (e.g., critical loads), or market mechanisms that maximize social welfare through an auction for initial DOEs [61, 68]. Similarly, we maximize the size of envelopes, measured in kilowatts. Alternative objectives may account for relative sizes depending on the nominal consumption of nodes or use different metrics to quantify the sizes of DOEs.

Market choices

SecuLEx implements a continuous market. First, by definition, continuous markets clear orders instantaneously and continuously when they arrive. It allows for fast reallocation depending on evolving needs and is thus the best choice when operating close to real time under high uncertainty. It nevertheless requires intensive customer involvement, e.g., compared to single-auction. In addition, fast clearing may be difficult in practice due to computational delays. Second, continuous markets often implement a pay-as-bid settlement. This choice originates as the process does not provide an aggregated market price. It may, in practice, lead to allocation inefficiency and gaming opportunities compared to uniform or Vickrey pricing [72].

Market efficiency and liquidity

In principle, markets allow optimal allocation, but inefficiencies are possible. Typically, too few participants may be involved, resulting in limited liquidity and price volatility. Alternatively, participants with high flexibility could exercise market power through strategic bidding or withholding limits. Moreover, this work assumes zero transaction costs, while in real markets significant overheads (e.g., fees, communication, and administrative costs) exist. These can erode the benefits of small-scale trades and further reduce liquidity.

Regulation and surplus treatment

Implementing SecuLEx in practice requires, on the one hand, guaranteeing independence of the market operation and, on the other hand, guaranteeing non-discriminatory network access [73]. Concerning market independence, it requires introducing a market operator distinct from the DSO, together with clear regulation. This aspect is largely neglected in this work. In addition, we discussed that market inefficiencies may lead to discriminatory network access, which shall be controlled by an independent observer in practice. Finally, in its current form, SecuLEx leads to a market surplus. Regulation should ensure that it is used to reduce tariffs or reinvest in the grid and avoid providing incentives to under-invest in infrastructure.

4.6 Conclusion

This chapter addressed the third and final capability (**exchange**) by answering RQ3 (*How can dynamic operating envelopes (DOEs) be translated into tradeable capacity products within a local flexibility market while preserving network security?*) introducing Secure Limit Exchange (SecuLEx), a market-based paradigm in which DSOs allocate initial DOEs that define limits on power injection and withdrawal. Customers can subsequently exchange these limits through market transactions while preserving network security constraints. We formulated the DOE allocation and market-clearing problems as tractable optimization problems under DC power flow and radial network assumptions, and proved that security can then be efficiently verified. In our illustrative LV network example, DOE trading showed potential for reducing renewable curtailment and improving network utilization and social welfare relative to alternative management schemes. Overall, SecuLEx shows the potential that envelope trading can extract more value from existing infrastructure and provide incentives for flexibility without requiring central control. Scalability to larger and more complex network systems, extending the framework beyond the simplified DC power flow model to a more realistic AC model that can accurately manage voltage levels and reactive power, alternative allocation and pricing rules, and the regulatory treatment of market social welfare, remains an important direction for future work.

The SecuLEx framework complements the proposed set of building blocks for the DSO to see, balance and exchange network capacity. However, shifting from mathematically sound algorithms to commercial solutions presents barriers that lie outside the scope of optimization theory. The next chapter performs a multidimensional analysis of the aspects that currently restrict the real-world adoption of TSO-DSO coordination.

4.A Security function proof

This appendix provides proof that, under radial network and DC assumptions, branch currents are monotone non-decreasing and node voltages are constant as a function of customer consumption. As a result, if the system is secure at the two extreme points of the DOE matrix, it is also secure for every power respecting the limits. We employ a similar strategy to the authors in [74], who proved voltage monotonicity with respect to active and reactive power, and extend it to current.

Network description As described in Section 4.2.1, we model a distribution network as a graph $\mathfrak{G} = (\mathcal{N}, \mathcal{E})$ with nodes $\mathcal{N}$, edges $\mathcal{E}$, and customers $\mathcal{C} \subset \mathcal{N}$. The radial topology ensures the existence of a unique root node $r \in \mathcal{N}$ representing the substation or transformer connecting the feeder to the upstream grid. We subsequently assume that edges are oriented from root to leaves. For each node n, we define the set of downstream nodes $\mathcal{D}_n$ as the set of nodes m for which the unique path from m to r passes through n.

Each edge $e \in \mathcal{E}$ has an associated resistance R_e and reactance X_e. We denote by I_e the line current, by P_e the active power flow, and by Q_e the reactive power flow. To each node $n \in \mathcal{N}$ corresponds an active power consumption P_n, and we denote by V_n the voltage magnitude.

Customer power limits are represented by the matrix $\mathbf{L} = [\underline{P}, \overline{P}] \in \mathbb{R}^{|\mathcal{C}| \times 2}$, where $[\underline{P}_c, \overline{P}_c]$ are the bounds for each customer $c \in \mathcal{C}$. The function $VerifyLimits(\mathfrak{G}, \mathbf{L})$ checks that the network is secure for all $P \in \mathbf{L}$.

Assumptions We make the following assumptions on the network topology and physics linking electrical values.

A1 *Radial topology.* The network graph is a tree.

A2 *DC load flow.* Balanced steady-state, with unity and flat voltages ($\forall n \in \mathcal{N} : V_n = V_r = 1\,\text{p.u.}$), lossless lines ($\forall e \in \mathcal{E} : R_e = 0$), and no reactive power ($\forall e \in \mathcal{E} : Q_e = 0$).

Theorem 4.1 (Monotonicity of current)**.** *Under Assumptions **A1**–**A2**, the branch current I_e is a monotone non-decreasing function of consumption P_c:*

$$\frac{\partial I_e}{\partial P_c} \geq 0, \quad \forall e \in \mathcal{E}, \forall c \in \mathcal{C}.$$

Proof. Under assumptions **A1** and **A2**, the active power flowing in each branch $e \in \mathcal{E}$ respects the balance:

$$P_e = \sum_{k \in \mathcal{D}_e} P_k. \tag{4.15}$$

Furthermore, in each branch $e \in \mathcal{E}$:

$$I_e = \frac{1}{V_r} P_e. \tag{4.16}$$

Combining Eq. 4.15 and Eq. 4.16, we obtain the relationship between the branch current and power consumption:

$$I_e = \frac{1}{V_r} \left(\sum_{k \in \mathcal{D}_e} P_k \right). \tag{4.17}$$

Let us differentiate the current with respect to any downstream node $n \in \mathcal{D}_e$:

$$\frac{\partial I_e}{\partial P_n} = \frac{1}{V_r} \frac{\partial}{\partial P_n} \left(\sum_{k \in \mathcal{D}_e} P_k \right) = \frac{1}{V_r} \geq 0. \tag{4.18}$$

Let us differentiate the current with respect to any other node $n \notin \mathcal{D}_e$ that is not the root r:

$$\frac{\partial I_e}{\partial P_n} = 0. \tag{4.19}$$

The branch currents are therefore monotone non-decreasing with respect to any consumption. □

Theorem 4.2 (Boundary check constraints using monotonicity)**.** *Under Assumptions **A1**–**A2**, for any $\mathbf{L} = [\underline{P}, \overline{P}] \in \mathbb{R}^{|\mathcal{C}| \times 2}$, if both current and voltage security constraints are respected for $\underline{P}$ and $\overline{P}$, then the security constraints are also respected for each $P \in \mathbf{L}$.*

Proof. Under assumptions **A1** and **A2**, the voltage at each node is constant. Therefore, if the voltage security constraints are respected for one power profile, they are respected for each power profile.

Under assumptions **A1** and **A2**, Theorem 4.1 holds, and each branch current I_e is a monotone non-decreasing function of all customer consumptions. This implies that the maximum current and minimum current (i.e., maximum negated current) as a function of P over the domain $P \in \mathbf{L}$ is achieved either at $\underline{P}$ or at $\overline{P}$. Therefore, if the current security constraints are respected for $\underline{P}$ and $\overline{P}$, then they are also respected $\forall P \in \mathbf{L}$. □

According to Theorem 4.2, the $VerifyLimits$ function can be implemented as a function verifying that security is ensured at the two DOE boundary profiles $\underline{P}$ and $\overline{P}$. This makes the verification computationally efficient while guaranteeing security under the DC approximation.

Remark 4.1. The result can be understood geometrically: under Assumptions **A1** and **A2**, branch currents are linear functions of nodal injections. The set of admissible power profiles $\mathbf{L}$ therefore forms a hypercube in $\mathbb{R}^{|\mathcal{C}|}$, and a linear function over a hypercube attains its extremes at the vertices. Theorem 4.2 shows that the current in each branch depends monotonically on each coordinate, so the maximum and minimum are attained at the two vertices $\underline{P}$ and $\overline{P}$ (all customers withdrawing or injecting). Security verification thus reduces to checking these two extreme profiles, rather than all $2^{|\mathcal{C}|}$ vertices.

Chapter 5

A Multidimensional Analysis of Existing Limitations for TSO-DSO Coordination

---

This chapter establishes the broader operational and regulatory context driving the need for an active DSO. By introducing a multidimensional framework, it evaluates existing literature and real-world pilot projects regarding transmission and distribution coordination. The conceptual analysis suggests that while academia focuses heavily on complex modeling, the actual bottlenecks to commercial deployment may lie in communication infrastructure, validation at scale, and regulatory alignment.

5.1 Introduction

The transition to ANM does not end at the DSO's boundary. Regulation increasingly places these capabilities within a coordinated TSO-DSO framework, where the distance between theoretical methods and commercial deployment becomes measurable.

The existing literature proposes a wide range of coordination paradigms (e.g., centralized, decentralized, and hybrid) and technical approaches (e.g., joint planning processes, local markets, aggregators, operational envelopes) to reconcile the differing objectives and operational timescales of TSOs and DSOs [75, 76]. However, despite the several theoretical studies, few implementations have been applied to real-world networks. This discrepancy suggests that the barriers to deployment may not be primarily technical, but that the bottlenecks may lie in non-algorithmic constraints that are overlooked in academic work.

The main contributions of this chapter are the following: *i)* we identify limitations of TSO–DSO coordination across five dimensions: modeling, operation, validation, communication, and regulation; *ii)* we introduce a scoring methodology and apply it to several studies, mapping the current literature; *iii)* we compare pilot and non-pilot studies, highlighting important dimensions in real-world implementations.

The remainder of the chapter is structured as follows. Following this introduction, Section 5.2 describes the multidimensional framework and presents an analysis of the limitations within the current literature. Section 5.3 introduces the pilot and non-pilot categorization and presents an assessment using the proposed scoring methodology. Section 5.4 analyzes why pilot projects have not yet transitioned to commercial deployment. Section 5.5 discusses the limitations of this work. Section 5.6 concludes the work by summarizing key findings and proposing future research directions. Finally, the appendix presents details on the review methodology and the scoring mechanism.

5.2 Assessment of coordination limitations across five dimensions

To analyze deployment barriers, we structure the assessment around five dimensions: modeling, operation, validation, communication, and regulation. This approach extends the classification in [124] by explicitly incorporating modeling assumptions and validation constraints alongside systemic factors. We apply this multidimensional framework to evaluate the limitations of existing TSO-DSO coordination approaches by analyzing 47 selected studies, following the methodology detailed in Appendix 5.A. Table 5.1 details the considered sub-dimensions, associated scoring criteria, and the distribution of characteristics across the analyzed literature, pilot, and non-pilot studies. For each characteristic, the table reports both the number of papers and the corresponding percentage within each category.

Table 5.1: Multidimensional scoring framework and distribution of characteristics across the reviewed literature. Percentages are computed over the papers that propose coordination schemes; reviews, reports, and book chapters are excluded from scoring. Row totals differ slightly across sub-dimensions where a characteristic could not be determined from the paper and the entry was left unscored.

Dimension	Sub-dimension	Characteristic	Score	Total	Non-Pilot	Pilot
Modeling	Transmission network	DC formulation	0	29 (76%)	23 (77%)	5 (63%)
		AC formulation	1	9 (24%)	7 (23%)	3 (37%)
	Distribution network	DC formulation	0	6 (16%)	5 (17%)	1 (13%)
		AC formulation	1	32 (84%)	25 (83%)	7 (87%)
	Phase balance	Balanced system	0	31 (82%)	26 (87%)	5 (63%)
		Unbalanced system	1	7 (18%)	4 (13%)	3 (37%)
	Reactive power	Not considered	0	11 (29%)	9 (30%)	2 (25%)
		Considered	1	27 (71%)	21 (70%)	6 (75%)
Operation	Temporal resolution	Single timestep	0	12 (32%)	10 (33%)	2 (25%)
		Hours	1	18 (47%)	15 (50%)	3 (37%)
		Minutes	2	5 (13%)	3 (10%)	2 (25%)
		Seconds	3	3 (8%)	2 (6%)	1 (13%)
	Uncertainty management	Deterministic	0	20 (53%)	17 (57%)	3 (37%)
		Scenarios	1	15 (40%)	10 (33%)	5 (63%)
		Robust optimization	2	3 (8%)	3 (10%)	0
Validation	Network size	Small	0	18 (47%)	16 (54%)	2 (25%)
		Medium	1	11 (29%)	7 (23%)	4 (50%)
		Large	2	9 (24%)	7 (23%)	2 (25%)
	Network type	Not mentioned	0	1 (3%)	1 (3%)	0
		Standard test-case	1	22 (57%)	22 (74%)	0
		Real network	2	15 (40%)	7 (23%)	8 (100%)
Communication	Infrastructure	Not considered	0	27 (69%)	27 (87%)	0
		Considered	1	12 (31%)	4 (13%)	8 (100%)
	Data standardization	Not considered	0	29 (74%)	29 (94%)	0
		Considered	1	10 (26%)	2 (6%)	8 (100%)
	Privacy	Not considered	0	22 (56%)	22 (71%)	0
		Considered	1	17 (44%)	9 (29%)	8 (100%)
Regulation	Regulation incompatibility	Not considered	0	28 (72%)	28 (90%)	0
		Considered	1	11 (28%)	3 (10%)	8 (100%)
	Objective alignment	Not considered	0	24 (63%)	23 (77%)	1 (13%)
		Considered	1	14 (37%)	7 (23%)	7 (87%)
	Strategic behavior	Not considered	0	30 (83%)	26 (93%)	4 (50%)
		Considered	1	6 (17%)	2 (7%)	4 (50%)

5.2.1 Modeling

This dimension evaluates the mathematical simplifications used to represent power systems. Assessment focuses on network representation (AC or DC), phase imbalance, and reactive power constraints.

The literature favors computational tractability over physical realism. At the transmission level, linear DC formulations dominate, while distribution networks are generally modeled using AC power flow. Beyond power flow equations, the vast majority of studies assume balanced distribution systems, often ignoring local constraints, which may lead to optimistic estimates of available flexibility. The necessity of this computational trade-off is evident in pilot projects. For example, in CoordiNet [112], a hybrid approach based on simplified DC models is used for maintaining tractability during market clearing and is followed by an AC power flow validation to ensure feasibility.

5.2.2 Operation

The operation dimension covers temporal granularity (ranging from a single snapshot to sub-minute resolution) and stochasticity management.

There is a temporal mismatch between theoretical simulations and actual grid operations. Most studies rely on hourly resolution, neglecting intra-hour dynamics such as frequency deviations and rapid voltage variations that are critical to system security. This coarse temporal representation fails to capture the fast-acting nature of DER flexibility, limiting the ability to assess its true operational value. Beyond temporal resolution, uncertainty management remains insufficiently addressed, with most studies relying on deterministic frameworks. Since DER generation and demand are inherently stochastic, deterministic approaches risk producing overly optimistic coordination schemes and potentially being infeasible under real operating conditions.

5.2.3 Validation

Validation reflects the scale of the tested network, categorized as small (<500 nodes), medium (500-2000 nodes), or large (>2000 nodes), and the test network used (e.g., synthetic or real-world networks).

The literature primarily validates coordination schemes on small- or medium-scale synthetic topologies rather than real networks. Real-world experiments, such as the SmartNet project [108], encountered significant computational limits when performing simulations of integrated TSO-DSO topologies at scale, necessitating the development of simplified network representations to maintain tractability without sacrificing important physical characteristics [82, 105].

5.2.4 Communication

This dimension identifies requirements for data exchange, digital protocols, and privacy measures.

Although information and communication technology (ICT) is recognized as the central nervous system of future smart grids, it remains comparatively underexplored in much of the academic literature. Requirements for data standardization and privacy compliance are largely ignored in theoretical studies. Conversely, pilot projects like SmartNet [108] and PLATONE [110] frequently expose the inadequacy of existing data frameworks, often requiring the deployment of supplementary IoT hardware and secure communication protocols.

5.2.5 Regulation

The regulation dimension captures institutional constraints, including misaligned incentives, regulatory incompatibilities, and strategic behavior.

Regulatory and market-related aspects are among the least addressed dimensions, despite their importance for real-world implementation. In particular, TSOs and DSOs may compete for the same DERs, where actions beneficial for transmission-level balancing can conflict with local distribution constraints [125]. Existing frameworks, moreover, lack adequate incentives for DSO participation [112, 117]: regulated tariffs compensate capital expenditures (CapEx) but not the operating expenses (OpEx) required to procure flexibility, which constitutes a structural barrier beyond technical design. Finally, strategic behavior is almost entirely neglected, and the assumption of cooperative actors risks producing mechanisms vulnerable to manipulation.

5.2.6 Summary of research gaps

The multidimensional analysis highlights distinct patterns in how the literature addresses aspects relevant to TSO-DSO coordination deployment. For modeling and operation, the field exhibits relatively low variance: most studies converge toward a common set of assumptions, including DC transmission, AC distribution, balanced systems, reactive power consideration, hourly or single-time-step resolution, and no uncertainty handling. In contrast, validation, communication, and regulation display notably higher variability, with aspects such as large-scale real-network validation, communication infrastructure, interoperability, and regulatory integration frequently omitted.

5.3 Pilots and non-pilots results

To bridge the gap between theory and practice, the analyzed literature is partitioned into pilot projects and non-pilot studies. Following the scoring methodology detailed in Appendix 5.A.2, each paper is evaluated across the five dimensions and normalized to its maximum possible score. Figure 5.1 presents these average normalized results, utilizing 95% confidence intervals (CIs) calculated via a Student's t-distribution to correctly account for the smaller sample size of pilot projects.

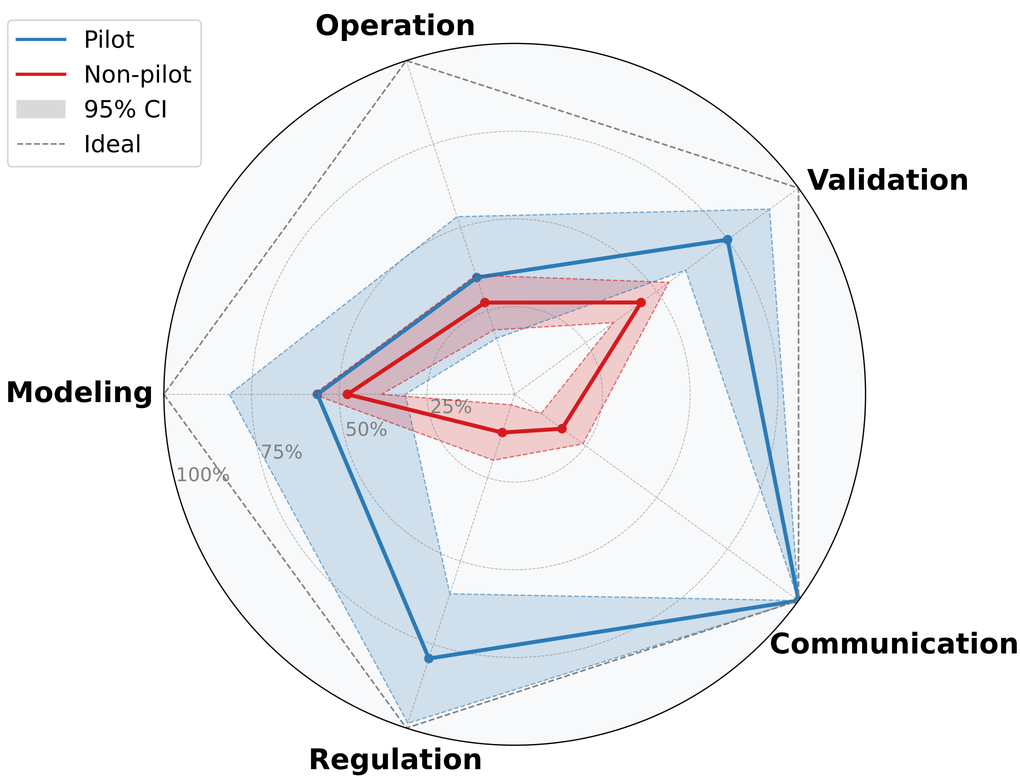

Figure 5.1: Average normalized scores across the five dimensions for pilot and non-pilot studies.

Differences between pilot and non-pilot studies are negligible when considering modeling and operation dimensions. The overlapping CIs indicate that both groups face similar trends in modeling physical systems and managing temporal dynamics. This demonstrates that real-world implementations do not necessarily rely on more advanced mathematical or operational representations; instead, they operate under the same simplifying assumptions and computational trade-offs as theoretical studies. Consequently, while important, modeling complexity has not emerged as a clear metric for differentiating deployable approaches from academic ones. In contrast to these shared technical challenges, substantial differences appear in the validation, communication, and regulation dimensions. As visually pronounced in the radar plot, the gap between pilots and non-pilots across these three axes is significant. While simulation-based studies typically assume idealized information exchange and simplified institutional environments, pilot projects are forced to explicitly navigate data interoperability, stakeholder conflicts, and regulatory misalignment.

This comparative analysis reveals a critical asymmetry in the literature: although modeling and operational complexities are central to algorithmic design, they are not the primary bottlenecks for deployment. Ultimately, transitioning from theory to field implementation requires the research community to recognize these non-algorithmic constraints and shift priorities toward validation at scale, communication infrastructure, and implementable regulatory frameworks.

5.4 From pilot to commercial deployment

Although pilot projects score higher on validation, communication, and regulatory alignment, they still struggle to transition into widely deployed operational systems. In particular, pilot projects exposed a range of frictions that impacted their experiments. These include computational tractability forcing simplified models; low-voltage visibility suffering from weak DSO incentives; communication requiring far more engagement than expected; market design suffering from illiquidity and fragmentation; and forecasting errors undermining operations. Even in dimensions where pilots score reasonably well by our metrics, that level of integration may still be insufficient for robust, commercial deployment. For instance, no pilot in our review has demonstrated long-term stability under high degrees of unbalanced loading, sub-minute volatility, or widespread communication latency.

In summary, pilots demonstrate feasibility under controlled conditions, not robustness against real-world variability. They remain intermediate tests, and the gap to commercial deployment likely requires simultaneous advances across all five dimensions, including those at which current practice may appear mature.

5.5 Discussion

The proposed multidimensional framework is intended as a diagnostic tool, not an absolute metric of deployment readiness, and several limitations must be acknowledged.

First, the analysis relies on peer-reviewed literature subject to publication bias. Successful methodologies are overrepresented, while operational failures, for instance, the scalability limits of AC formulations on large real-world networks, are rarely reported. Consequently, literature may underestimate the severity of practical deployment barriers, producing scores that reflect a best-case scenario rather than the typical reality faced by system operators.

Second, applying equal weights to all sub-dimensions assumes that a technical feature like three-phase unbalance carries the same operational weight as a regulatory constraint. Moreover, the normalized scores are sensitive to the choice and granularity of sub-dimensions, meaning that cross-dimensional comparisons ("modeling is more advanced than communication") are not meaningful. Consequently, the relative scores across dimensions cannot be directly compared without explicitly acknowledging that the current framework captures a curated subset of sub-dimensions, rather than an exhaustive list of all requirements for a commercial solution.

Third, several deployment barriers are not included in the five dimensions. For example, emerging technical threats such as cybersecurity (e.g., false data injection, malicious intrusions) are omitted [126]. Furthermore, experiences from system operators such as RTE and Enedis indicate that effective coordination requires not only technical solutions but also an operational culture shift supported by dispatcher workflow integration [113, 114]. This socio-technical dimension is often overlooked in the literature. As a result, achieving a perfect score in a given dimension (for example, a pilot project that ticks all our communication sub-dimensions) may correspond to fulfilling only a small fraction of actual real-world operational requirements.

Fourth, the five dimensions are not strictly orthogonal: regulatory requirements on data privacy directly constrain communication architectures [124], and modeling assumptions affect the tractability of large-scale validation. Because these dimensions are interconnected, a low score in one area may restrict the progress of another, meaning that achieving real-world deployment requires a coordinated, simultaneous advancement across all dimensions rather than isolated technical fixes.

Despite these limitations, the framework goes beyond a classical literature review by providing a structured, visual, and quantitative analysis through which research assumptions can be compared against deployment conditions. Rather than simply listing existing approaches, it explicitly highlights the gap between theoretical development and real-world readiness, and offers a basis for identifying where future research efforts are most needed.

5.6 Conclusion

This chapter answered RQ4 (*What are the primary limitations preventing the transition of theoretical TSO-DSO coordination schemes to commercial deployment?*) by presenting a multidimensional analysis of existing TSO-DSO coordination literature to identify the primary barriers limiting the transition from theoretical frameworks to real-world deployment. The analysis is performed over five dimensions: modeling, operation, validation, communication, and regulation. The results reveal an imbalance in the literature, highlighting a gap between conceptual research and pilot implementations.

Modeling and operation exhibit relatively low variability across the literature, with most studies converging toward similar assumptions. Validation, communication, and regulation, in contrast, display notably higher variability, with frequent omission of these aspects.

Moreover, the comparison between pilot and non-pilot studies further refines this picture. Pilot projects address validation, communication, and regulatory aspects more explicitly, while relying on modeling and operational assumptions similarly to those adopted in academic studies. However, pilot projects should not be interpreted as deployment-ready solutions. They represent an intermediate step to commercial implementation.

At the same time, the apparent convergence observed in modeling assumptions should not necessarily be interpreted as full maturity of the field. Current approaches rely on tractable formulations and simplified operational settings, which may be limiting as coordination moves toward commercial deployment with higher uncertainty, stronger coupling between transmission and distribution networks, and faster operational timescales.

Overall, the proposed framework provides a structured way to identify where deployment-oriented considerations remain underrepresented and to compare how different studies address operational realism beyond purely algorithmic performance. More broadly, the results suggest that progress toward large-scale TSO-DSO coordination will likely depend on simultaneous advances across all five dimensions.

5.A Analysis methodology

This appendix provides the supporting methodological frameworks for the study. Specifically, Appendix 5.A.1 details the literature review and paper selection process, and Appendix 5.A.2 formalizes the scoring algorithm used for the multidimensional analysis.

5.A.1 Literature search and selection process

This subsection presents the methodology used to evaluate TSO–DSO coordination research papers and documents. The proposed framework is designed to quantify the gap between algorithmic development and real-world implementability.

Literature search strategy

the paper selection process follows a structured methodology, inspired by the approach proposed in [127]. To ensure broad coverage of the multidisciplinary nature of TSO-DSO coordination, multiple scientific databases and publishers are considered. The search process is conducted with the *Publish or Perish* software tool (©1997-2026, Anne-Wil Harzing), using Google Scholar, Scopus, and Semantic Scholar as primary search engines.

The primary search query was designed to capture the intersection of system operators and their coordination mechanisms:

> (power OR electricity OR network OR grid OR DER OR "distributed energy resource") AND
> (TSO OR "transmission system operator" OR "electricity transmission") AND
> (DSO OR "distribution system operator" OR "electricity distribution") AND
> (coordination OR cooperation OR interaction OR interface)

The search is restricted to publications from 2015 onwards, corresponding to the period during which the number of TSO-DSO coordination papers increased.

Inclusion criteria

Papers were included if they met all the following criteria:

- They are peer-reviewed publications or reports from recognized institutions.

- They provide an explicit discussion of TSO-DSO coordination or interaction mechanisms.
- They mention limitation(s) from Section 5.2, either by explicit acknowledgment, methodological choices, or real-world evidence of implementation challenges.

Paper filtering process

The filtering process followed PRISMA guidelines and is fully detailed in Figure 5.2. From an initial pool of 886 records, the papers are progressively filtered: duplicate removal (305), metadata and title screening (172 candidates), abstract and conclusion screening (65 articles), and final eligibility assessment (47 publications). The selected publications are categorized in Table 5.2.

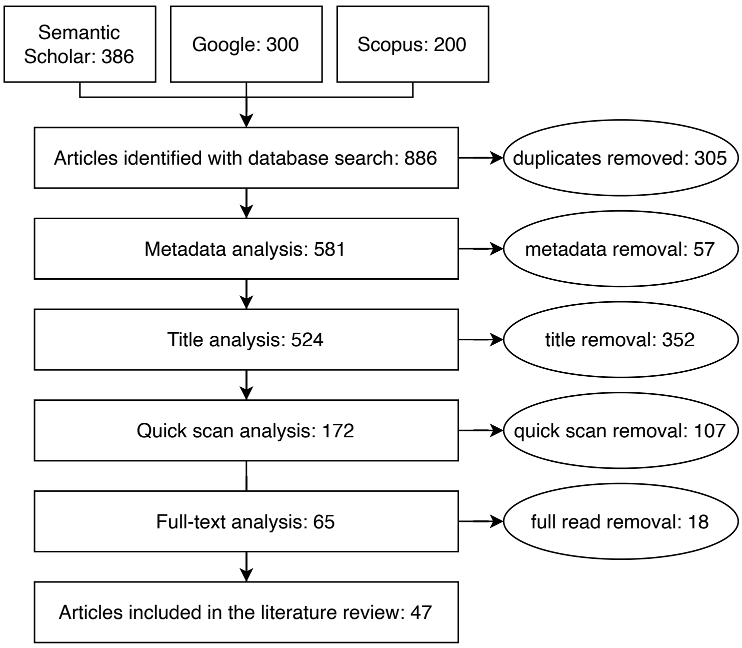

Figure 5.2: PRISMA diagram of the paper selection process.

5.A.2 Multidimensional scoring methodology

To support a structured comparison across the reviewed literature, each paper is evaluated along the five dimensions introduced in Section 5.2 according

Table 5.2: Summary of the 47 reviewed papers categorized by publication type, comprising 23 journal articles, 8 conference papers, 8 pilot projects, 4 technical reports, 3 reviews, and 1 book, with 68% published between 2022 and 2026.

Category	**Articles**
Journal	[77, 78, 79, 80, 81, 82, 83, 84, 85, 86, 87, 88, 89, 90, 91, 92, 93, 94, 95, 96, 97, 98, 99]
Conference	[100, 101, 102, 103, 104, 105, 106, 107]
Pilot	[108, 109, 110, 111, 112, 113, 114, 115]
Reports	[116, 117, 118, 119]
Review	[120, 121, 122]
Book	[123]

to the following scoring system.

For all scientific articles obtained from the process described in Appendix 5.A, we assign an index to each paper (corresponding to its literature review entry) and define the set of indices as $\mathcal{A}$. This set is partitioned into three disjoint subsets: pilots $\mathcal{P} \subseteq \mathcal{A}$, non-pilots $\mathcal{N} \subseteq \mathcal{A}$, and other contributions $\mathcal{O} \subseteq \mathcal{A}$. Only the papers in $\mathcal{P} \cup \mathcal{N}$ propose coordination schemes and are therefore included in the scoring analysis.

Let D denote the set of dimensions along which the papers are compared. For each dimension $d \in D$, we define the set of sub-dimensions I_d. These two sets correspond, respectively, to the first and second columns of Table 5.1 (*Dimension* and *Sub-dimension*).

For each paper $p \in \mathcal{P} \cup \mathcal{N}$, dimension $d \in D$, and sub-dimension $i \in I_d$, we define a discrete score $s_{p,d,i}$ that depends on the characteristics of the paper for that dimension and sub-dimension. Its value corresponds to the entry reported in the fourth column (*Score*) of Table 5.1 for the characteristic associated with the paper.

For each paper p, the scaled per-dimension score $s_{d,p}$ is defined as

$$s_{d,p} = \frac{\sum_{i \in I_d} s_{p,d,i}}{\sum_{i \in I_d} s_{d,i}^{\max}}, \tag{5.1}$$

where $s_{d,i}^{\max}$ is the maximum attainable score for dimension d and sub-dimension i.

Finally, the score of each paper group is given by the average scaled score over pilots and non-pilots:

$$S_{X,d} = \frac{1}{|X|} \sum_{p \in X} s_{d,p}\,, \qquad X \in \{\mathcal{P}, \mathcal{N}\}\,. \tag{5.2}$$

This yields, for each group and dimension, a normalized score in $[0, 1]$ that is directly comparable across the pilot and non-pilot subsets.

Chapter 6

Conclusion

This chapter concludes the thesis. It first summarizes how each chapter answered the RQs, then states what the three capabilities deliver and their limitations. It closes by outlining future research, among which an integrated case study on a single network.

DER integration is reshaping how LV distribution networks must be planned and operated, and it can no longer be treated as a perturbation of an otherwise centralized system. This thesis addressed the resulting problem from the perspective of a DSO confronted with the rapid growth of PV, EV, and HP, proposing to structure the transition to active distribution network management as three capabilities (**see**, **balance**, **exchange**). Taken together, the developed methods trace a path from network observability to exchange of local grid capacity. By extending this perspective to the broader challenge of TSO-DSO coordination, this work suggests that the barriers to commercial deployment lie less in algorithmic complexity but in validation, communication, and regulatory alignment.

6.1 Summary of the contributions

This thesis has developed the structure of a toolkit to transform the passive LV distribution network into an actively managed system, capable of integrating DERs.

Addressing the prerequisite of network observability (**see**), Chapter 2 answered RQ1 presenting a systematic procedure to identify customer topological paths using only static data. This removes the dependency on AMI data. The core contribution is an ILP optimization that maximizes the number of connected customers while minimizing the number of network elements required to establish those connections. The methodology is applied to a real Belgian network of 1089 elements serving 526 customers, to which the method assigned a feasible path for 88% of customers. A robustness analysis under corrupted feeder-assignment data demonstrated a fault detection rate exceeding 95% and a false-connection rate below 5% at realistic error levels, confirming that the method remains reliable even when the underlying operator records are imperfect.

Building on this established connectivity, Chapter 3 answered RQ2 and contributed a computationally efficient customer phase-reconfiguration algorithm (**balance**) to optimize the existing infrastructure. The key innovation is the use of linear optimization that works over long operational horizons (e.g., a full year) without requiring computationally heavy, nonlinear power flows. This is validated on a real Belgian network with high DER penetration and shows improvements: a reduction in phase load unbalance of 36 and 62% across two feeders, and a 4.4% decrease in total line losses.

Chapter 4 answered RQ3 showing how DOEs can be translated into tradeable capacity products while preserving network security (**exchange**). We proposed a market-based paradigm in which the DSO assigns secure DOEs to all customers day-ahead, where security means that, so long as the envelopes are respected, the network is guaranteed to remain within safe operating limits. From that point until real time, customers may trade their limits according to their individual needs through a centralized continuous market, in which every cleared trade preserves the network's security guarantee. An illustrative example on a small test network indicated that this trading mechanism can reduce network curtailment and creates an explicit incentive for flexible customers to reschedule rather than be curtailed; testing on larger network scenarios remains future work.

Chapter 5 answered RQ4 suggesting the bottlenecks to commercial deployment of TSO-DSO coordination schemes. Through a systematic analysis of the literature, we identified five main limitation axes: modeling, operation, validation, communication, and regulatory alignment. The analysis shows that pilot and non-pilot studies are similarly mature in modeling and operational aspects, but diverge sharply on validation, communication, and regulatory alignment. This suggests that the primary bottleneck to deployment is not algorithmic complexity, but the limited integration of non-technical and systemic constraints. The resulting framework highlights key research gaps and proposes directions for coordination methods better suited to real-world adoption.

6.2 Limitations of the developed toolkit

However, while the operations developed in this thesis are important, they may not be enough to make the DSO a fully active player in power system management.

The toolkit relies on deterministic assumptions and mathematical approximations that currently limit its realism. For instance, the balancing methodology introduced in Chapter 3 relies on deterministic time series data. In reality, customer behaviors, DER adoption rates, and weather patterns are highly stochastic. Reconfiguring physical phase connections based on a single deterministic forecast leaves the network vulnerable to future uncertainties; a configuration that is optimal for one simulated year may degrade rapidly if actual consumption profiles or DER installations diverge significantly.

Similarly, the framework proposed in Chapter 4 assumes a balanced network and relies on a DC power flow approximation. In LV networks characterized by high R/X ratios, these linear approximations may fail to capture critical voltage magnitude variations and reactive power flows.

Finally, there are several other necessary aspects required for deployment that lie outside mathematical optimization and are generally ignored in the literature. As explored in Chapter 5, real-world deployment is severely constrained by network size scalability, the lack of standardized communication infrastructures for high-frequency data exchange, and complex regulatory barriers. Without aligning TSO-DSO incentives, establishing robust data privacy protocols, and implementing hardware-level protection schemes, the proposed toolkit remains a highly capable algorithmic foundation rather than a complete operational reality.

6.3 Directions for future research

The limitations identified in this thesis open several paths for future research.

6.3.1 Toolkit integration and the integrated case study

The most direct extension of this thesis is an integrated case study in which the three methods are executed sequentially as a unified pipeline. Figure 6.1 summarizes this target architecture.

Figure 6.1 reconsiders the situation of Figure 1.1. The pressures on the DSO are unchanged: bidirectional flows and uncertainty from the DERs below, regulatory coordination requirements from the TSO above. What the figure adds are the three capabilities developed in this thesis, which now occupy the block that Figure 1.1 left empty, together with the data flow between them. The figure distinguishes two kinds of data flow. Solid arrows are products of the toolkit itself: the **see** block consumes only static operator records (GIS data and customer-junction assignments) and emits the connectivity graph and feeder assignments on which **balance** operates, together with the radial topology and netwok information (such as transformer and line thermal ratings) that **exchange** requires. Dashed arrows are inputs that the toolkit does not itself produce and that must be supplied externally.

Two elements of this architecture are still missing. The first is phase identification. Extending the ILP formulation of Chapter 2 to assign phases alongside topological paths would remove the need to feed **balance** with externally supplied phase connections. The second is a network model shared by **balance** and **exchange**: allocating envelopes on a rebalanced network requires a representation in which unbalance is expressed, which the present DC formulation is not.

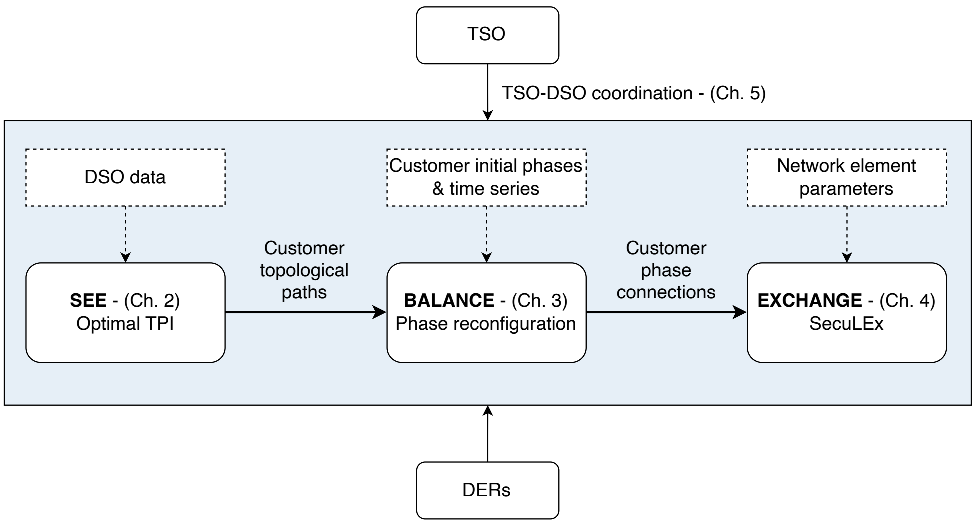

Figure 6.1: Data flow between the three capabilities in the target pipeline.

The Belgian LV network of Chapter 2 is the natural candidate for this integration: its topology is identified by the TPI framework, the resulting connectivity and feeder assignments define the graph on which the phase reconfiguration of Chapter 3 operates, and the rebalanced network provides the grid model for envelope allocation and trading under Chapter 4.

6.3.2 Robustness and uncertainty management

Future work must address the deterministic nature of the phase reconfiguration algorithm by incorporating stochastic or robust optimization techniques. While Chapter 3 demonstrated the computational efficiency of a linear formulation over long temporal horizons, extending this to account for a wide distribution of future DER adoption scenarios and weather uncertainties introduces significant complexity. Therefore, future research must explore tractable stochastic frameworks that allow the DSO to identify resilient phase assignments without sacrificing the ability to optimize over extended, year-long operational horizons.

6.3.3 Realism and large scale validation

Although the SecuLEx market currently demonstrates theoretical viability on small-scale networks, its clearing mechanism must evolve beyond the DC power flow approximation. Validating this limit-exchange mechanism on large-scale, highly asymmetric, real-world distribution networks will require developing computationally tractable convex AC relaxations or multi-phase unbalanced formulations. These advancements are essential to accurately represent voltage limits and reactive power flows during dynamic capacity trading, while simultaneously addressing the non-linear computational scaling challenges associated with securely clearing thousands of simultaneous orders. A first step in this direction is taken in our work [18], where DOEs are computed on three-phase unbalanced AC networks under explicit voltage unbalance constraints, and the lexicographic max-min rule adopted in Chapter 4 is compared against alternative fairness criteria.

6.3.4 Systemic and regulatory barriers

Finally, bridging the deployment gap highlighted in Chapter 5 requires advancing not only in power systems engineering but also into market design and regulatory policy. Future research must investigate mechanisms to mitigate strategic bidding within local flexibility markets, ensuring that participants cannot artificially withhold capacity to manipulate prices. Additionally, research must focus on the design of standardized, low-latency ICT and the establishment of regulatory frameworks that properly incentivize DSOs to utilize operational flexibility over CapEx reinforcements.

Bibliography

[1] Ilhan Ozturk. "A literature survey on energy–growth nexus". In: *Energy Policy* 38.1 (2010), pp. 340–349. ISSN: 0301-4215. DOI: `https://doi.org/10.1016/j.enpol.2009.09.024`.

[2] European Commission. *REPowerEU Plan*. COM(2022) 230 final. 2022. URL: `https://commission.europa.eu/topics/energy/repowereu_en`.

[3] United Nations Framework Convention on Climate Change (UNFCCC). *The Paris Agreement*. UNFCCC, 2015. URL: `https://unfccc.int/process-and-meetings/the-paris-agreement`.

[4] IPCC. *Climate Change 2023: Synthesis Report. Contribution of Working Groups I, II and III to the Sixth Assessment Report*. Tech. rep. Intergovernmental Panel on Climate Change, 2023. URL: `https://www.ipcc.ch/report/ar6/syr/downloads/report/IPCC_AR6_SYR_FullVolume.pdf`.

[5] Eurelectric. *Connecting the Dots: Distribution Grid Connections*. Tech. rep. Eurelectric, 2024. URL: `https://www.eurelectric.org/wp-content/uploads/2024/09/eurelectric-connecting-the-dots-full-study.pdf`.

[6] J.A. Peças Lopes et al. "Integrating distributed generation into electric power systems: A review of drivers, challenges and opportunities". In: *Electric Power Systems Research* 77.9 (2007), pp. 1189–1203. ISSN: 0378-7796. DOI: `https://doi.org/10.1016/j.epsr.2006.08.016`.

[7] Han Pyo Lee. "Integrating Distributed Energy Resources in Power Distribution Systems: A Comprehensive Review of Impacts, Challenges, and Opportunities from a Distribution System Operator's Perspective". In: *Applied Energy* 403 (2026), p. 127052. ISSN: 0306-2619. DOI: `10.1016/j.apenergy.2025.127052`.

[8] *Netzausbaubeschleunigungsgesetz Übertragungsnetz (NABEG) (Grid Expansion Acceleration Act)*. Federal Law Gazette (BGBl). Germany, 2019. URL: `https://www.wind-energie.de/themen/netze/redispatch/`.

[9] Maurizio Vassallo et al. "Phase reconfiguration for power distribution networks with high DERs penetration". In: *2025 IEEE Kiel PowerTech*. IEEE. 2025, p. 7. URL: `https://ieeexplore.ieee.org/stamp/stamp.jsp?tp=%5C&arnumber=11180600`.

[10] Maurizio Vassallo et al. "An optimization algorithm for customer topological paths identification in electrical distribution networks". In: *arXiv preprint arXiv:2409.09073* (2024).

[11] Maurizio Vassallo et al. "SecuLEx: a Secure Limit Exchange Market for Dynamic Operating Envelopes". In: *Electric Power Systems Research* (2026). ISSN: 0378-7796. DOI: 10.1016/j.epsr.2026.113736.

[12] Maurizio Vassallo et al. "A Multidimensional Analysis of Existing Limitations for TSO-DSO Coordination". 2026. eprint: https://orbi.uliege.be/handle/2268/345652.

[13] Maurizio Vassallo et al. "Fair reinforcement learning algorithm for PV active control in LV distribution networks". In: *2023 International Conference on Clean Electrical Power (ICCEP)*. IEEE. 2023, pp. 796–802.

[14] Maurizio Vassallo et al. "A systematic procedure for topological path identification with raw data transformation in electrical distribution networks". In: *Proceedings of international conference on energy, electrical and power engineering (CEEPE)* (2024). DOI: 10.48550/arXiv.2409.09075.

[15] Amina Benzerga et al. "Combined PV-EV-HP hosting capacity analysis of a Belgian low-voltage distribution network". In: *2024 IEEE 34th Australasian Universities Power Engineering Conference (AUPEC)*. IEEE. 2024, p. 6.

[16] Sofía Herrero Gómez-Tejedor Yaqin, Maurizio Vassallo, and Damien Ernst. "OffWindFM: a conceptual roadmap for foundation models in offshore wind energy". In: (2026).

[17] Adrien Bolland et al. *Coordinating Secure and Distributed Operation of Electrical Networks Through Bilateral Agreements on Voltage and Power Envelopes*. 2026. eprint: https://orbi.uliege.be/handle/2268/345742.

[18] Alireza Zabihi et al. *Fair Allocation of Operating Envelopes for Distribution Networks Considering Voltage Unbalance*. 2026. arXiv: 2606.29351 [eess.SY]. URL: https://arxiv.org/abs/2606.29351.

[19] David Milambo Kasumba et al. "Power quality and service continuity in a low-voltage urban network in the municipality of Kamalondo in Lubumbashi, DR Congo". In: (2026).

[20] Frederik Geth, Marta Vanin, and Dirk Van Hertem. "Data quality challenges in existing distribution network datasets". In: *CIRED* (2023). DOI: 10.1049/icp.2023.1175.

[21] Maksymilian Kochański, Katarzyna Korczak, and Tadeusz Skoczkowski. "Technology innovation system analysis of electricity smart metering in the European Union". In: *Energies* (2020). ISSN: 1996-1073. DOI: 10.3390/en13040916.

[22] Carlos Mateo Domingo et al. "A Reference Network Model for Large-Scale Distribution Planning With Automatic Street Map Generation". In: *IEEE Transactions on Power Systems* (2011). DOI: 10.1109/TPWRS.2010.2052077.

[23] Andre Seack, Jan Kays, and Christian Rehtanz. "Generating low voltage grids on the basis of public available map data". In: (2014). URL: https://api.semanticscholar.org/CorpusID:38279545.

[24] Alejandro Navarro-Espinosa and Luis F. Ochoa. "Reconstruction of low voltage distribution networks: From GIS data to power flow models". In: CIRED, 2015, p. 5. URL: https://api.semanticscholar.org/CorpusID:55344363.

[25] Abdenago Guzmán, Jairo Quirós-Tortós, and Gustavo Valverde. "Efficient connectivity identification of large-scale distribution network elements in GIS". In: *Proceedings of IEEE Manchester PowerTech*. 2017, p. 6. DOI: 10.1109/PTC.2017.7981064.

[26] Abdenago Guzmán et al. "Processing and correction of secondary system models in Geographic Information Systems". In: *IEEE Transactions on Industrial Informatics* (2019). DOI: 10.1109/TII.2018.2876356.

[27] Gao Zepu et al. "Knowledge graph-based method for identifying topological structure of low-voltage distribution network". In: *The Journal of Engineering* (2020). DOI: 10.1049/joe.2019.1319.

[28] X. Li et al. "Distribution feeder one-line diagrams automatic generation from geographic diagrams based on GIS". In: *Third International Conference on Electric Utility Deregulation and Restructuring and Power Technologies*. IEEE, 2008. DOI: 10.1109/DRPT.2008.4523781.

[29] L. Wu, Y. Lin, and W. Pang. "Distribution network topology modelling and automatic mapping based on CIM and GIS". In: *IEEE 4th Information Technology and Mechatronics Engineering Conference (ITOEC)*. IEEE. 2018. DOI: 10.1109/ITOEC.2018.8740683.

[30] L. Shang et al. "Automatic generation algorithm of distribution network topology map based on GIS drawing". In: *IOP Conference Series: Earth and Environmental Science*. 2019. DOI: 10.1088/1755-1315/384/1/012231.

[31] Z. Yin et al. "Research on network topology analysis method of distribution management based on GIS". In: *International Conference on Intelligent Transportation, Big Data and Smart City (ICITBS)*. IEEE. 2021. DOI: 10.1109/ICITBS53129.2021.00045.

[32] Mohammad Farajollahi, Alireza Shahsavari, and Hamed Mohsenian-Rad. "Topology identification in distribution systems using line current sensors: An MILP approach". In: *IEEE Transactions on Smart Grid* (2020). DOI: 10.1109/TSG.2019.2933006.

[33] Daniele Marulli et al. "Reconstruction of low-voltage networks with limited observability". In: *IEEE PES Innovative Smart Grid Technologies Europe (ISGT Europe)* (2021). DOI: 10.1109/ISGTEurope52324.2021.9640163.

[34] Changgang Wang, Jun An, and Gang Mu. "Power system network topology identification based on knowledge graph and graph neural network". In: *Frontiers in Energy Research* (2021). DOI: 10.3389/fenrg.2020.613331.

[35] Zahra Soltani and Mojdeh Khorsand. "Real-time topology detection and state estimation in distribution systems using micro-PMU and smart meter data". In: *IEEE Systems Journal* (2022). DOI: 10.1109/JSYST.2022.3153449.

[36] P. A. Parikh and T. D. Nielsen. "Transforming traditional geographic information system to support smart distribution systems". In: *2009 IEEE/PES Power Systems Conference and Exposition* (2009). DOI: 10.1109/PSCE.2009.4839979.

[37] Jouni Peppanen et al. "Distribution system low-voltage circuit topology estimation using smart metering data". In: *IEEE/PES Transmission and Distribution Conference and Exposition* (2016). DOI: 10.1109/TDC.2016.7519985.

[38] Thomas Morrell et al. "Modeling of electric distribution feeder using smart meter data". In: *IEEE/PES Transmission and Distribution Conference and Exposition (T&D)* (2018). DOI: 10.1109/TDC.2018.8440540.

[39] Shijie Cui et al. "Low-voltage distribution network topology identification based on constrained least square and graph theory". In: *Soft Computing* (2022). DOI: 10.1007/s00500-022-07151-3.

[40] Haifeng Li et al. "Topology identification method for residential areas in low-voltage distribution networks based on unsupervised learning and graph theory". In: *Electric Power Systems Research* (2023). DOI: 10.1016/j.epsr.2022.108969.

[41] Xiao Yu et al. "Data-driven distributed grid topology identification using backtracking Jacobian matrix approach". In: *IEEE Transactions on Industrial Informatics* (2024). DOI: 10.1109/TII.2023.3280936.

[42] Abu Bakr Pengwah et al. "Topology identification of distribution networks with partial smart meter coverage". In: *IEEE Transactions on Power Delivery* (2024). DOI: 10.1109/TPWRD.2024.3354292.

[43] Dong Liu et al. "Topology identification and parameters estimation of LV distribution networks using open GIS data". In: *International Journal of Electrical Power & Energy Systems* (2025). ISSN: 0142-0615. DOI: 10.1016/j.ijepes.2024.110395.

[44] Alexander Hoogsteyn et al. "Low voltage customer phase identification methods based on smart meter data". In: *Electric Power Systems Research* (2022). DOI: 10.1016/j.epsr.2022.108524.

[45] Peter E. Hart, Nils J. Nilsson, and Bertram Raphael. "A formal basis for the heuristic determination of minimum cost paths". In: *IEEE Transactions on Systems Science and Cybernetics* (1968). DOI: 10.1109/TSSC.1968.300136.

[46] Kang Ma, Lurui Fang, and Wangwei Kong. "Review of distribution network phase unbalance: scale, causes, consequences, solutions, and future research directions". In: *CSEE Journal of Power and Energy Systems* 6.3 (), pp. 479–488. ISSN: 2096-0042. DOI: 10.17775/CSEEJPES.2019.03280.

[47] Omid Homaee et al. "A practical approach for distribution network load balancing by optimal re-phasing of single phase customers using discrete genetic algorithm". In: *International Transactions on Electrical Energy Systems* 29.5 (2019). ISSN: 2050-7038. DOI: 10.1002/2050-7038.2834.

[48] Lurui Fang, Kang Ma, and Xinsong Zhang. "A Statistical Approach to Guide Phase Swapping for Data-Scarce Low Voltage Networks". In: *IEEE Transactions on Power Systems* 35.1 (Jan. 2020), pp. 751–761. ISSN: 1558-0679. DOI: 10.1109/TPWRS.2019.2931981.

[49] Orlando Pereira, Jairo Quirós-Tortós, and Gustavo Valverde. "Phase Rebalancing of Distribution Circuits Dominated by Single-Phase Loads". In: *IEEE Transactions on Power Systems* 36.6 (Nov. 2021), pp. 5333–5344. ISSN: 1558-0679. DOI: 10.1109/TPWRS.2021.3076629.

[50] Brandon Cortés-Caicedo et al. "Application of the Vortex Search Algorithm to the Phase-Balancing Problem in Distribution Systems". In: *Energies* 14.5 (2021). DOI: 10.3390/en14051282.

[51] Chia-Hung Lin et al. "Optimal Phase Balancing in Electricity Distribution Feeders Using Mixed-Integer Linear Programming". In: *Sustainability* 15.5 (Jan. 2023), p. 4473. ISSN: 2071-1050. DOI: 10.3390/su15054473.

[52] Xueyuan Cui et al. "A Two-Level Coordination Strategy for Distribution Network Balancing". In: *IEEE Transactions on Smart Grid* 15.1 (Jan. 2024). Conference Name: IEEE Transactions on Smart Grid, pp. 529–544. ISSN: 1949-3061. DOI: 10.1109/TSG.2023.3274564.

[53] Q. Gemine, D. Ernst, and B. Cornélusse. "Active network management for electrical distribution systems: Problem formulation, benchmark, and approximate solution". In: *Optimization and Engineering* 18 (2017), pp. 587–629. DOI: 10.1007/s11081-016-9339-9.

[54] L. Zhou et al. "Cost/benefit assessment of a smart distribution system with intelligent electric vehicle charging". In: *IEEE Transactions on Smart Grid* 5 (2014), pp. 839–847. DOI: 10.1109/TSG.2013.2282707.

[55] S. Meunier et al. "Impact of residential low-carbon technologies on low-voltage grid reinforcements". In: *Applied Energy* 297 (2021). DOI: 10.1016/j.apenergy.2021.117057.

[56] W. Zhang et al. "Toward optimal voltage/VAR control with smart PVs in active distribution networks". In: *Electric Power Systems Research* 228 (2024), p. 110076. DOI: 10.1016/j.epsr.2023.110076.

[57] M. R. Alam et al. "Allocation of dynamic operating envelopes in distribution networks: Technical and equitable perspectives". In: *IEEE Transactions on Sustainable Energy* 15 (2024), pp. 173–186. DOI: 10.1109/TSTE.2023.3275082.

[58] K. Petrou et al. "Ensuring distribution network integrity using dynamic operating limits for prosumers". In: *IEEE Transactions on Smart Grid* 12.5 (2021), pp. 3877–3888. DOI: 10.1109/TSG.2021.3081371.

[59] P. P. Vergara et al. "A mixed-integer linear programming model for defining customer export limit in PV-rich low-voltage distribution networks". In: *Journal of Modern Power Systems and Clean Energy* 11.1 (2023), pp. 191–200. DOI: 10.35833/MPCE.2022.000400.

[60] R. K. Gupta, P. Buason, and D. K. Molzahn. "Fairness-aware photovoltaic generation limits for voltage regulation in power distribution networks using conservative linear approximations". In: *2024 IEEE Texas Power and Energy Conference (TPEC)*. 2024, p. 6. DOI: 10.1109/TPEC60005.2024.10472277.

[61] Md Umar Hashmi and Dirk Van Hertem. "Robust Dynamic Operating Envelopes for Flexibility Operation Using Only Local Voltage Measurement". In: *2023 International Conference on Smart Energy Systems and Technologies (SEST)*. 2023, p. 6. DOI: 10.1109/SEST57387.2023.10257504.

[62] Bin Liu and Julio H. Braslavsky. "Robust Dynamic Operating Envelopes for DER Integration in Unbalanced Distribution Networks". In: *IEEE Transactions on Power Systems* 39.2 (2024), pp. 3921–3936. DOI: 10.1109/TPWRS.2023.3308104.

[63] F. Lezama et al. "Local energy markets: Paving the path toward fully transactive energy systems". In: *IEEE Transactions on Power Systems* 34 (2019), pp. 4081–4088. DOI: 10.1109/TPWRS.2018.2833959.

[64] B. Liu, F. Xie, and L. Chai. "A scalable energy management mechanism for peer-to-peer electricity market". In: *IEEE Transactions on Industrial Informatics* 20 (2024), pp. 9255–9265. DOI: 10.1109/TII.2024.3383523.

[65] N. Li. "A market mechanism for electric distribution networks". In: *54th IEEE Conference on Decision and Control (CDC)*. 2015, pp. 2276–2282. DOI: 10.1109/CDC.2015.7402546.

[66] S. H. H. Dolatabadi et al. "A stochastic game-theoretic optimization approach for managing local electricity markets with electric vehicles and renewable sources". In: *Applied Energy* 368 (2024). DOI: 10.1016/j.apenergy.2024.123518.

[67] T. Buisseret et al. "SCOPE project: an innovative market-based solution to deal with injection congestion". In: *CIRED 2025*. 2025. eprint: https://orbi.uliege.be/handle/2268/327367.

[68] M. Imran Azim et al. "Dynamic Operating Envelope-Integrated Cooperative Energy Trading: A Fair Allocation Approach". In: *IEEE Transactions on Power Systems* 40.4 (2025), pp. 2845–2859. DOI: 10.1109/TPWRS.2024.3510673.

[69] F. A. Behringer. "Lexicographic quasiconcave multiobjective programming". In: *Zeitschrift für Operations Research* 21.3 (1977), pp. 103–116. DOI: 10.1007/BF01919766.

[70] S. Chau, K. Elbassioni, and M. Khonji. "Combinatorial optimization of alternating current electric power systems". In: *Foundations and Trends® in Electric Energy Systems* 3 (Jan. 2018), p. 139. DOI: 10.1561/3100000017.

[71] Hannah Moring, Daniel K. Molzahn, and Johanna L. Mathieu. "Exploring the Inexactness of Second-Order Cone Relaxations for Calculating Operating Envelopes". In: *IEEE Transactions on Power Systems* (2026), p. 12. DOI: 10.1109/TPWRS.2026.3657755.

[72] N. Fabra, N. von der Fehr, and D. Harbord. "Designing electricity auctions". In: *The RAND Journal of Economics* 37.1 (2006), pp. 23–46. DOI: 10.1111/j.1756-2171.2006.tb00002.x.

[73] *Directive (EU) 2019/944 of the European Parliament and of the Council of 5 June 2019 on common rules for the internal market for electricity and amending Directive 2012/27/EU (recast)*. https://eur-lex.europa.eu/legal-content/EN/TXT/PDF/?uri=CELEX:02019L0944-20220623.

[74] Sunho Jang, Necmiye Ozay, and Johanna L. Mathieu. "Probabilistic Constraint Construction for Network-Safe Load Coordination". In: *IEEE Transactions on Power Systems* 39.2 (2024), pp. 4473–4485. DOI: 10.1109/TPWRS.2023.3309131.

[75] Talal Alazemi, Mohamed Darwish, and Mohammed Radi. "TSO/DSO coordination for RES integration: a systematic literature review". In: *Energies* 15 (2022), p. 7312. DOI: 10.3390/en15197312.

[76] Younes Zahraoui et al. "Assessment of TSO-DSO coordination to enhance flexible grid operation". In: *Current Sustainable/Renewable Energy Reports* 12 (July 2025). DOI: 10.1007/s40518-025-00269-6.

[77] Stefan Stanković and Lennart Söder. "Probabilistic reactive power capability charts at DSO/TSO interface". In: *IEEE Transactions on Smart Grid* 11 (2020), pp. 3860–3870. DOI: 10.1109/TSG.2020.2992569.

[78] S. Skok. "Transmission power system modeling by using aggregated distributed generation model based on a TSO—DSO data exchange scheme". In: *Energies* 13 (2020). DOI: 10.3390/en13153949.

[79] M Radi et al. "Developing enhanced TSO-DSO information and data exchange based on a novel use case methodology". In: *Frontiers in Energy* (2021). DOI: 10.3389/fenrg.2021.670573.

[80] Mikhail A. Bragin and Y. Dvorkin. "TSO-DSO Operational Planning Coordination through Surrogate Lagrangian Relaxation". In: *ArXiv* (2021). DOI: 10.36227/TECHRXIV.13557242.V1.

[81] Alexander Hermann et al. "A complementarity model for electric power transmission-distribution coordination under uncertainty". In: *European Journal of Operational Research* 299 (2022), pp. 313–329. DOI: 10.1016/j.ejor.2021.08.018.

[82] Jan Ringelstein et al. "A methodology for improved TSO-DSO coordination in grid operation planning". In: *Electric Power Systems Research* 211 (2022), p. 108445. DOI: 10.1016/j.epsr.2022.108445.

[83] Mahdi Habibi, Vahid Vahidinasab, and Mohammad Sadegh Sepasian. "A privacy-preserving approach to day-ahead TSO-DSO coordinated stochastic scheduling for energy and reserve". In: *IET Generation, Transmission & Distribution* 16 (2022), pp. 163–180. DOI: 10.1049/gtd2.12286.

[84] Marcel Sarstedt and Lutz Hofmann. "Monetarization of the feasible operation region of active distribution grids based on a cost-optimal flexibility disaggregation". In: *IEEE Access* 10 (2022), pp. 5402–5415. DOI: 10.1109/ACCESS.2022.3140871.

[85] Moossa Khodadadi Arpanahi, M. E. Hamedani Golshan, and Mohsen Parsa Moghaddam. "Non-cooperative operation of transmission and distribution systems". In: *IEEE Transactions on Industrial Informatics* 18 (2022), pp. 153–162. DOI: 10.1109/TII.2020.3041921.

[86] Till Kolster, Stefan Niessen, and Mathias Duckheim. "Providing distributed flexibility for curative transmission system operation using a scalable robust optimization approach". In: *Electric Power Systems Research* 211 (2022), p. 108431. DOI: 10.1016/j.epsr.2022.108431.

[87] Megha Gupta and Abhijit R. Abhyankar. "Amalgamating TSO and DSO energy markets through minimal data exchange-based framework". In: *IEEE Transactions on Energy Markets, Policy and Regulation* 1 (2023), pp. 173–186. DOI: 10.1109/TEMPR.2023.3277751.

[88] Yu Weng et al. "Asymmetrically reciprocal effects and congestion management in TSO-DSO coordination through feasibility regularizer". In: *IEEE Transactions on Power Systems* 38 (2023), pp. 1948–1962. DOI: 10.1109/TPWRS.2022.3193052.

[89] Merkebu Zenebe Degefa et al. "Challenges of TSO-DSO voltage regulation under real-time data exchange paradigm". In: *IEEE Open Journal of the Industrial Electronics Society* 4 (2023), pp. 75–84. DOI: 10.1109/OJIES.2023.3239946.

[90] Saman Nikkhah et al. "Distributed flexibility to maintain security margin through decentralised TSO–DSO coordination". In: *International Journal of Electrical Power & Energy Systems* 146 (2023), p. 108735. DOI: 10.1016/j.ijepes.2022.108735.

[91] Damian Sieraszewsk et al. "Multi-period hybrid AC/DC-OPF model for flexibility market clearing with seamless TSO-DSO coordination". In: *IEEE Access* 11 (2023), pp. 40093–40106. DOI: 10.1109/ACCESS.2023.3269423.

[92] Xiaotian Sun et al. "Pricing for TSO-DSO coordination: a decentralized incentive compatible approach". In: *IEEE Transactions on Power Systems* 38 (2023), pp. 1869–1882. DOI: 10.1109/TPWRS.2022.3170436.

[93] Hannu Laaksonen, Hosna Khajeh, and Nikos Hatziargyriou. "Advanced distributed energy resources and on-load tap-changer control principles for enhanced flexibility services provision". In: *IEEE Access* 12 (2024), pp. 161768–161785. DOI: 10.1109/ACCESS.2024.3488211.

[94] Maryam Nejadmuri, Afshin Lashkarara, and Jamshid Aghaei. "An uncertainty-aware two-stage optimization framework for coordinating energy and reserve markets in TSO-DSO interface in the presence of energy storage systems". In: *Journal of Energy Storage* 102 (2024), p. 114121. DOI: 10.1016/j.est.2024.114121.

[95] Chenjia Gu, Jianxue Wang, and Lei Wu. "Distributed energy resource and energy storage investment for enhancing flexibility under a TSO-DSO coordination framework". In: *IEEE Transactions on Automation Science and Engineering* 21.3 (July 2024), pp. 2961–2973. ISSN: 1558-3783. DOI: 10.1109/TASE.2023.3272532.

[96] Mohsen Kalantar-Neyestanaki and Rachid Cherkaoui. "Grid-cognizant TSO and DSO coordination framework for active and reactive power flexibility exchange: the Swiss case study". In: *Electric Power Systems Research* 235 (2024), p. 110747. DOI: 10.1016/j.epsr.2024.110747.

[97] Haitham A. Mahmoud and Abdelatty E. Abdelgawad. "A robust unit commitment-based TSO-DSO coordination scheme for optimal generation scheduling". In: *Electric Power Systems Research* 243 (2025). ISSN: 03787796. DOI: 10.1016/j.epsr.2025.111512.

[98] Yilin Wen et al. "Quantifying and optimizing the time-coupled flexibilities at the distribution-level for TSO-DSO coordination". In: *IEEE Transactions on Power Systems* 40 (2025), pp. 5071–5085. DOI: 10.1109/TPWRS.2025.3563041.

[99] Rushuai Han et al. "Unified transmission-distribution coordination for secure and economical frequency support from distributed energy resources". In: *IEEE Transactions on Sustainable Energy* (2026), p. 16. ISSN: 1949-3037. DOI: 10.1109/TSTE.2026.3668374.

[100] Sergio Bruno et al. "Mapping flexibility region through three-phase distribution optimal power flow at TSO-DSO point of interconnection". In: *2021 AEIT International Annual Conference (AEIT)*. 2021, p. 6. DOI: 10.23919/AEIT53387.2021.9627050.

[101] Syed Muhammad Hur Rizvi, Sajan K. Sadanandan, and Tareg Ghaoud. "TDS-CoSim: a static co-simulation tool for integrated T & D snapshot analysis considering large penetration of DERs". In: *2022 IEEE Industrial Electronics and Applications Conference (IEACon)*. 2022, pp. 67–72. DOI: 10.1109/IEACon55029.2022.9951837.

[102] Mohammad Panahazari et al. "A new market-based framework for increasing responsive loads in distribution systems". In: *2023 13th Smart Grid Conference (SGC)*. 2023, p. 6. DOI: 10.1109/SGC61621.2023.10459317.

[103] Andrey Churkin et al. "Impacts of distribution network reconfiguration on aggregated DER flexibility". In: *2023 IEEE Belgrade PowerTech.* 2023, p. 7. DOI: 10.1109/PowerTech55446.2023.10202791.

[104] Mohammad Iman Alizadeh et al. "Uncertainty-aware TSO-DSO coordination methodology for transmission voltages control". In: *2023 IEEE Belgrade PowerTech.* 2023, p. 6. DOI: 10.1109/PowerTech55446.2023.10202827.

[105] Md Sazal Miah et al. "Equivalent network representation for TSO-DSO interaction with present and future DERs, EV charging stations, and storage uptakes". In: *2025 IEEE Kiel PowerTech.* 2025, p. 6. DOI: 10.1109/PowerTech59965.2025.11180571.

[106] Nuran Cihangir Martin and Bruno Fanzeres. "Multi-agent DSO-TSO active and reactive power flow coordination with a two-level decentralised ADMM". In: *2025 IEEE Kiel PowerTech.* 2025, p. 6. DOI: 10.1109/PowerTech59965.2025.11180218.

[107] Burak Dindar et al. "Privacy-preserving flexibility provisioning with an optimization approach for enhanced TSO-DSO interaction in modern power systems". In: *2025 21st International Conference on the European Energy Market (EEM).* 2025, p. 6. DOI: 10.1109/EEM64765.2025.11050293.

[108] SmartNet Project. *TSO-DSO coordination for acquiring ancillary services from distribution grids.* Ed. by Gianluigi Migliavacca. Florence School of Regulation, 2019. URL: https://smartnet-project.eu/wp-content/uploads/2019/05/SmartNet-Booktlet.pdf.

[109] Sergio Potenciano Menci et al. "Functional scalability and replicability analysis for smart grid functions: the InteGrid project approach". In: *Energies* 14 (2021), p. 5685. DOI: 10.3390/en14185685.

[110] I. Losa et al. "PLATONE: towards a new open DSO platform for digital smart grid services and operation". In: *CIRED.* Sept. 2021, pp. 2974–2978. DOI: 10.1049/icp.2021.1880.

[111] V. Mladenov. "A flexibility market platform for electricity system operators using blockchain technology". In: *Energies* 15.2 (2022). ISSN: 1996-1073. DOI: 10.3390/en15020539.

[112] CoordiNet Consortium. *Roadmap towards a new market design including the implementation of standardised products for system services.* Tech. rep. CoordiNet Project (Horizon 2020), 2022. URL: https://www.edsoforsmartgrids.eu/eu-projects/coordinet/.

[113] EU-SysFlex Consortium. *European Flexibility Roadmap.* Tech. rep. 2022. URL: https://ec.europa.eu/research/participants/documents/downloadPublic?documentIds=080166e5e92cd204&appId=PPGMS.

[114] OneNet Project. *Evaluation of OneNet demonstrators' results.* Deliverable D11.1. OneNet Project (Horizon 2020), 2024. URL: https://www.onenet-project.eu/wp-content/uploads/2024/02/OneNet_D11.1_V2.0.pdf.

[115] Zejun Ruan, Dimitris I. Chatzigiannis, and Anthony Papavasiliou. "Application of hierarchical TSO-DSO coordination in European pilot projects". In: *2025 21st International Conference on the European Energy Market (EEM).* 2025, p. 7. DOI: 10.1109/EEM64765.2025.11050314.

[116] BRIDGE Regulation and Data Management Working Groups. *TSO-DSO Coordination*. Tech. rep. Deliverable D3.12.f. Horizon 2020 BRIDGE Initiative. European Commission (BRIDGE Initiative), Dec. 2019. URL: `https://h2020-bridge.eu/wp-content/uploads/2020/01/D3.12.f_BRIDGE-TSO-DSO-Coordination-report.pdf`.

[117] International Renewable Energy Agency. *Innovation landscape brief: co-operation between transmission and distribution system operators*. Tech. rep. International Renewable Energy Agency (IRENA), 2020. URL: `https://www.irena.org/publications/2020/Jul/System-Operation-Innovation-Landscape-briefs`.

[118] B Herndler and ISGAN Annex. "Lessons learned from international projects on TSO-DSO interaction". In: *ISGAN (International Smart Grid Action Network)* (2020). URL: `https://www.iea-isgan.org/wp-content/uploads/2020/12/Lessons-learned-from-international-projects-on-TSO-DSO-interaction.pdf`.

[119] Electric Power Research Institute. *TSO-DSO coordination functions for DER*. Tech. rep. 3002021985. Palo Alto, CA: EPRI, 2022. URL: `https://www.epri.com/research/products/000000003002021985`.

[120] Eric Lambert et al. "Practices and architectures for TSO-DSO data exchange: European landscape". In: *2018 IEEE PES Innovative Smart Grid Technologies Conference Europe (ISGT-Europe)*. 2018, p. 6. DOI: `10.1109/ISGTEurope.2018.8571547`.

[121] Arthur Gonçalves Givisiez, Kyriacos Petrou, and Luis F. Ochoa. "A review on TSO-DSO coordination models and solution techniques". In: *Electric Power Systems Research* 189 (2020), p. 106659. DOI: `10.1016/j.epsr.2020.106659`.

[122] Arsim Bytyqi et al. "A review on TSO-DSO data exchange, CIM extensions and interoperability aspects". In: *Journal of Modern Power Systems and Clean Energy* 10 (2022), pp. 309–315. DOI: `10.35833/MPCE.2021.000770`.

[123] Michael Power et al. "TSO-DSO interaction and coordination". In: *Distributed Energy Resources in Active Distribution Networks*. Ed. by Christine Schwaegerl, Kurt Dedekind, and Ray Brown. CIGRE Green Books. Springer, 2025. ISBN: 978-3-030-91366-3. URL: `https://link.springer.com/book/9783030913663`.

[124] Christian Ziesemann et al. *Challenges and barriers to the implementation of TSO-DSO coordination concepts: discussion paper*. Tech. rep. Aachen, 2023. DOI: `10.18154/RWTH-2022-11734`.

[125] Fatemeh Najibi, Dimitra Apostolopoulou, and Eduardo Alonso. "TSO-DSO coordination schemes to facilitate distributed resources integration". In: *Sustainability* 13.14 (2021). ISSN: 2071-1050. DOI: `10.3390/su13147832`.

[126] Néstor Rodríguez Pérez et al. "ICT architectures for TSO-DSO coordination and data exchange: a European perspective". In: *IEEE Transactions on Smart Grid* 14 (2023), pp. 1300–1312. DOI: `10.1109/TSG.2022.3206092`.

[127] Erica Mourão et al. "Investigating the use of a hybrid search strategy for systematic reviews". In: *2017 ACM/IEEE International Symposium on Empirical Software Engineering and Measurement (ESEM)*. 2017, pp. 193–198. DOI: `10.1109/ESEM.2017.30`.